JPRS L/10644

8 July 1982

USSR Report

EARTH SCIENCES

(FOUO 4/82)

FBIS FOREIGN BROADCAST INFORMATION SERVICE

FOR OFFICIAL USE ONLY

APPROVED FOR RELEASE: 2007/02/09: CIA-RDP82-00850R000500080018-9

NOTE

JPRS publications contain information primarily from foreign newspapers, periodicals and books, but also from news agency transmissions and broadcasts. Materials from foreign-language sources are translated; those from English-language sources are transcribed or reprinted, with the original phrasing and other characteristics retained.

Headlines, editorial reports, and material enclosed in brackets [] are supplied by JPRS. Processing indicators such as [Text] or [Excerpt] in the first line of each item, or following the last line of a brief, indicate how the original information was processed. Where no processing indicator is given, the information was summarized or extracted.

Unfamiliar names rendered phonetically or transliterated are enclosed in parentheses. Words or names preceded by a question mark and enclosed in parentheses were not clear in the original but have been supplied as appropriate in context. Other unattributed parenthetical notes within the body of an item originate with the source. Times within items are as given by source.

The contents of this publication in no way represent the policies, views or attitudes of the U.S. Government.

APPROVED FOR RELEASE: 2007/02/09: CIA-RDP82-00850R000500080018-9

JPRS L/10644

8 July 1982

USSR REPORT

EARTH SCIENCES

(FOUO 4/82)

CONTENTS

OCEANOGRAPHY

UDC 551.466.81:551.465.5

NONLINEAR INTERACTION BETWEEN INTERNAL WAVES AND NEAR-SURFACE SHEAR CURRENT

Moscow IZVESTIYA AKADEMII NAUK SSSR: FIZIKA ATMOSFERY I OKEANA in Russian Vol 18, No 4, Apr 82 (manuscript received 26 Feb 81) pp 383-390

[Article by V. P. Reutov, Institute of Applied Physics, USSR Academy of Sciences]

[Text]

Abstract: A study is made of the absorption (instability) of internal waves in a two-layer model of a stratified fluid with a current near the free surface. Absorption is determined by the critical layer in which the phase velocity of the wave is close to the current velocity. Currents submerged at a depth small in comparison with the thickness of the upper layer are examined. An expression is derived for the increment in a linear approximation and the nonlinear development of a wave with time is described.

A great number of studies have now been published on the linear theory of instability in a stratified medium [1-3]. In very simple cases the nonlinear development of internal waves can be described on the basis of the general approach employed for systems with slight nonlinearity [4, 5]. When the instability is determined by the presence of layers of coincidence (Miles instability mechanism [6-8]) it becomes possible to make an analytical study of highly nonlinear processes of energy exchange between the current and a wave. In this case the analysis is simplified because strong nonlinearity is manifested only in the narrow region of the critical layer (CL) [9-12].

In this article we solve the problem of the nonlinear stage of instability (or absorption of a wave with a finite amplitude) in a two-layer model of a stratified fluid of infinite depth in the presence of a horizontal shear current near the surface. The origin of such a current can be, in particular, related to the directed movement of air over the boundary of the upper layer (wind over the sea surface). An analysis is given for the vertical scales of the velocity profile small in comparison with the thickness of the less dense upper layer. The Miles mechanism of intensification and absorption of internal waves is considered. Within the framework of the theory of a critical layer formulated in [9-12], a study is made of the linear and nonlinear stages in the development of a wave with time.

1. We will take the equations describing the two-dimensional interaction of internal waves with a horizontal current in the near-surface layer of a stratified fluid. We will examine currents penetrating to the depth ℓ, small in comparison with the thickness h of the upper layer, characterizing a slight submergence of the current with the small parameter $\varepsilon = \ell/h \ll 1$. We take flow turbulence into account phenomenologically through the constant coefficient of turbulent viscosity ν. We will use a dimensionless form of writing of the equation for the stream function, as the unit length employing the thickness h of the upper layer, as the velocity unit -- the current velocity at the surface -- u_0, as the time unit -- h/u_0; we normalize the stream function to the value hu_0. The equation with dimensionless variables in this case coincides in form with the initial equation if ν is replaced by $1/R_k$, where $R_k = u_0 h/\nu$ is the Reynolds number. The axes x, z of the coordinate system and records of the dimensionless velocity profile $\bar{u}(z)$ are shown in Fig. 1.

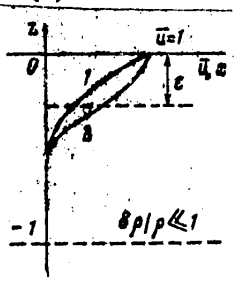

Fig. 1. Illustration of relative positioning of region of current and fluid layers with different density: 1) velocity profile of shear current without flexure point, 2) profile with flexure point.

We will examine sinusoidal waves with an amplitude slowly changing with time. The nonstationarity of the wave, viscosity and nonlinearity cannot be neglected simultaneously in the region of the critical layer situated in the immediate neighborhood of the resonance point $z = z_c$ ($\bar{u}(z_c) = c$, c is the phase velocity of the wave). The characteristic dimensions of the peak of pulsations of vorticity arising with allowance for each of these factors separately, have, accordingly, the form

$$d_t = |\gamma|/k\bar{u}_c', \quad d_\nu = \left[\frac{1}{k\bar{u}_c' R_k}\right]^{1/3}, \quad d_n = (B/\bar{u}_c')^{1/2}, \tag{1}$$

where k is the wave number, B is the amplitude of oscillations of the stream function with $z = z_c$, $\gamma = B^{-1}dB/dt$ is the wave increment; $\bar{u}' = d\bar{u}/dz$, the subscript c here and in the text which follows means that the variable is taken with $z = z_c$. In a general case the scale of the critical layer will be determined by the expression $d_c = \max(d_t, d_\nu, d_n)$. Then we will assume that in the flow there is one critical layer, isolated from the boundary z = 0:

$$d_c \ll |z_c| \sim \varepsilon. \tag{2}$$

Without limiting greater universality of the examination, we will assume that $u_c' > 0$. As limits of the critical layer the weak nonstationarity of the wave, viscosity and nonlinearity in the flow can be regarded as small disturbances.

Neglecting viscosity and nonlinearity, we will write an equation for pulsations of the stream function with $|z-z_c| \gg d_c$ in the form

$$\left(\frac{\partial}{\partial t}+\bar{u}(z)\frac{\partial}{\partial x}\right)\left(\frac{\partial^2\psi}{\partial z^2}+\frac{\partial^2\psi}{\partial x^2}\right)-\frac{\partial^2\bar{u}}{\partial z^2}\frac{\partial\psi}{\partial x}=0. \tag{3}$$

Since $\bar{u} \neq 0$ only at distances $\sim\varepsilon$ from the surface $z = 0$, the linearized conditions at the density jump assume the form

$$\begin{gathered}\psi|_{-i+0}=\psi|_{-i-0},\\ \frac{\partial^2}{\partial t^2}(\psi'|_{-i+0}-\psi'|_{-i-0})+\bar{g}\frac{\delta\rho}{\rho}\frac{\partial^2}{\partial x^2}\psi|_{-i\pm0}=0,\end{gathered} \tag{4}$$

where $\bar{g} = hg/u_0^2$ is a dimensionless analogue of the acceleration of free falling g. For oscillations of the stream function at the boundary we will use the "hard cap" approximation.

$$\psi|_{z=0}=0. \tag{5}$$

When the wind flow creates the shearing stress p_τ at the water surface, the boundary conditions for the mean current will be satisfied with $R_h^{-1}du/dz|_{z=0} p_\tau$. Stipulation of the arbitrary profiles $\bar{u}(z)$ assumes, as usual, a parallelism and stationarity of the current for the considered processes.

2. In the absence of a current ($\bar{u} \equiv 0$) the system (3)-(5) describes internal waves propagating with the phase velocity [13]

$$\bar{c}=c_m\left[\frac{\operatorname{th}k}{k(1+\operatorname{th}k)}\right]^{1/2}, \tag{6}$$

where $c_m = (\bar{g}\delta\rho/\rho)^{1/2}$ is the velocity of infinitely long waves ($c_m \geqslant \bar{c}$). A solution of the problem of weak interaction of an internal wave with a near-surface shear current will be sought using the method of spliced asymptotic expansions [14]. The stream function in the region $|z| \gg \varepsilon$ will be represented in the form

$$\psi=af(z)e^{ik(x-ct)}+\text{к.с.}+\varepsilon\psi^{(1)}+\ldots, \tag{7}$$

where $c = \bar{c} + \varepsilon c^{(1)}$ ($\varepsilon c^{(1)}$ -- phase velocity increment caused by a current), $a(\varepsilon t)$ is the slowly changing complex amplitude of the wave, $f(z)$ describes the form of the profile of an internal wave having the phase velocity $\bar{c}$:

$$f(z)=\begin{cases}2\operatorname{ch}kz, & -1<z<0,\\ (1-\exp 2k)\exp kz, & z<-1.\end{cases}$$

We will examine equation (3) with $\bar{u} \equiv 0$. With $|z| \gg \varepsilon$ such an equation coincides with the initial equation and its solution with $|z| \ll 1$ can be represented in the form

$$\psi=\varepsilon[\psi_0^{(0)'}z_1+\psi_0^{(1)}]+O(\varepsilon^2|a|), \tag{8}$$

where $\psi^{(0)}$ is the first term of the expansion (7), $\psi_0^{(0)'}$ and $\psi_0^{(1)}$ are the values of the variables $\partial\psi^{(0)}/\partial z$ and $\psi^{(1)}$ with $z = 0$; $z_1 = z/\varepsilon$ is an "internal" variable. In the presence of a current the stream function with

$|z| \ll 1$ will be written in the form*

[K. C. = complex conjugate]

$$\psi = \varepsilon \left[\sum_{n=1}^{\infty} \Lambda_n(z_1, \varepsilon t) e^{in\xi} + \text{K. C.} \right] + \ldots, \tag{9}$$

where $\xi = x - ct$, Λ_n are the complex profiles of amplitudes of the harmonics; $n = 1, 2, \ldots$ Substituting (9) into (3), for Λ_n we obtain the Rayleigh equation

$$(\bar{u} - c) \frac{d^2 \Lambda_n}{dz_1^2} - \bar{u}_{1c}'' \Lambda_n = 0, \tag{10}$$

where $\bar{u}_1'' = d^2\bar{u}/dz_1^2 \sim 1$. With $z_1 = 0$ the solution of (10) satisfies the condition $\Lambda_n^1 = 0$. The splicing of the term $\sim z_1$ in (8) with (9) determines the second of the boundary-value conditions for (10): $d\Lambda_n/dz_1 \to 2ak\delta_{1n}$ with $z_1 \to -\infty$ (δ_{1n} is the Kronecker symbol). The effect exerted on a wave by the critical layer can be taken into account by writing the rule for bypassing the singularity in (10) in the form [11]

$$\Lambda_{n+} - \Lambda_{n-} = 0, \quad \left(\frac{\partial \Lambda_n}{\partial z_1}\right)_+ - \left(\frac{\partial \Lambda_n}{\partial z_1}\right)_- = -\int_{-\infty}^{\infty} \zeta_n d\eta. \tag{11}$$

Here the indices ($\pm$) indicate the values of the variables with $z_\pm = z_c \pm 0$, ζ is the deviation of vorticity in the critical layer from the level $\bar{u}_c'$ (here ζ is measured in u_0/h units); $\zeta_n = \langle \zeta \exp(-ikn\xi) \rangle$ are the amplitudes of the Fourier harmonics ζ ($\langle \ldots \rangle$ is the mean for the wave period), $\eta = z - z_c$. The longitudinal and transverse velocity components in the critical layer region have the form [9-12] $u \approx c + u_c' \eta$, $v \approx -\partial \psi_c / \partial \xi$ respectively, where ψ_c is the stream function (9) at the point $z = z_c$. For vorticity in a reading system moving together with the wave it is possible to write the following kinetic equation [12]:

$$\frac{\partial \zeta}{\partial t} + \bar{u}_c' \eta \frac{\partial \zeta}{\partial \xi} - \frac{\partial \psi_c}{\partial \xi} \frac{\partial \zeta}{\partial \eta} = \frac{1}{R_h} \frac{\partial^2 \zeta}{\partial \eta^2} \tag{12}$$

In (11) we use the solutions of (12) undergoing transition into nonviscous solutions in the "wings" of the critical layer:

$$\zeta \to -\bar{u}_c'' \eta + \sum_{n=1}^{\infty} K_n(\xi, t)/\eta^n \quad \text{with} \quad \eta/d_c \to \pm\infty, \tag{13}$$

where the coefficients K_n are found by the substitution of (13) into (12). It follows from the text which follows (see (21)) that the right-hand side of the second expression (11) is a value of the order of $|\Lambda_{1c}|$.

Taking into account that one of the eigenfunctions (10) is $\bar{u}-c$, it is easy to obtain a solution of the boundary-value problem for Λ_n formulated above:

$$\Lambda_n(z_1 > z_{1c}) = M_n(\bar{u} - c) \int_0^{z_1} \frac{dz_1'}{(\bar{u} - c)^2}, \tag{14}$$

---

* Allowance for multiple harmonics of the main wave is necessary in the case of a nonlinear critical layer -- $d_n \geqslant d_{t,v}$.

$$\Lambda_n(z_1<z_{1c})=\frac{\bar{u}-c}{\bar{u}_{1c}'}\int_{-\infty}^{\infty}\zeta_n d\eta+M_n(\bar{u}-c)\times$$
$$\times\left\{\int_0^{z_1}\left[\frac{1}{(\bar{u}-c)^2}-\frac{1}{c^2}\right]dz_1'+\frac{2}{\bar{u}_{1c}''\delta}+\frac{z_1}{c^2}\right\}, \qquad (14)$$

where $\bar{u}_1' = d\bar{u}/dz_1 \sim 1$, $M_n = -2ack\delta_{1n}$; δ is an infinitely small positive value, and the region $z_{1c} - \delta < z_1 < z_{1c} + \delta$ is excluded from the integral. In accordance with (14), with $n \geqslant 2$ the amplitudes $\Lambda_n(z_c) = 0$ and, accordingly,

$$\psi_n = -\frac{M_1}{\bar{u}_{1c}'}e^{ikx} + \text{complex conjugate} \qquad (15)$$

The nonsinusoidal character of the stream function is expressed when $z_1 < z_{1c}$ when the region of the critical layer is greatly nonlinear ($|\zeta_n|$ are values of the same order of magnitude with $n \geqslant 1$). With z_1 tending to $-\infty$, from (14) we obtain

$$\Lambda_n \to F_n - (M_1/c)z_1,$$

where

$$F_n = -\frac{c}{\bar{u}_{1c}'}\int_{-\infty}^{\infty}\zeta_n d\eta - 2ak\delta_{1n}\left\{\int_{-\infty}^{0}\left[\frac{c^2}{(\bar{u}-c)^2}-1\right]dz_1+\frac{2c^2}{\bar{u}_{1c}''\delta}\right\}.$$

Both terms $\sim \varepsilon$ of the expansion (8) are spliced with (9) in the region $1 \ll z_1 \ll 1/\varepsilon$, provided that for equation (3) with $\bar{u} \equiv 0$ there is satisfaction of the effective boundary-value condition in the form

$$\psi_n = \varepsilon F_n|_{z=0}, \qquad (16)$$

where $\psi_n = \langle \psi \exp(-ikn\xi) \rangle$. With formulation of condition (16) the solution in the external region will be the same as in the presence of a current. Thus, the problem of a change in wave amplitude is reduced to solution of an equation with constant coefficients and with an inhomogeneous boundary condition. When the critical layer is nonlinear the variables F_n have an identical order of magnitude with $n \geqslant 1$. However, due to the smallness of the "inhomogeneities" εF_n it is sufficient that there be a small dispersion in order for the internal wave to be close to sinusoidal.

Substituting (7) into equation (3) (where $\bar{u} \equiv 0$) and into the boundary conditions (4), (16), we obtain the boundary-value problem for $\psi^{(1)}$. From the boundedness condition $\psi_1^{(1)} = \langle \psi^{(1)} \exp(ik\xi) \rangle$, using a standard procedure (for example, see [15]), it is possible to obtain the following equation for wave amplitude:

$$\frac{da}{dt} = i\varepsilon\alpha\int_{-\infty}^{\infty}\zeta_1 d\eta, \qquad (17)$$

where $\alpha = c^4k^2/4c_m^2\overline{u}_{ic}'$ sh k. In the derivation of (17) it was assumed that

$$c^{(1)} = \frac{c^4k^2}{2c_m^2 \operatorname{sh}^2 k}\left\{\int_{-\infty}^{0}\left[\frac{c^2}{(\overline{u}-c)^2}-1\right]dz_t + \frac{2c^2}{\overline{u}_{tc}''\delta}\right\}. \tag{18}$$

The increment $c^{(1)}$ determined in this way describes the change in phase velocity c caused by the nonresonance interaction of an internal wave with the flow.

Antisymmetric profiles $\zeta(\xi, \eta)$ satisfy condition (13). As a result, the wave phase is conserved with time. Assuming, without loss of universality, that arg a (0) = 0, we rewrite system (17), (12) in the form

$$\frac{dA}{dt} = -\varepsilon\alpha\int_{-\infty}^{\infty}\langle\zeta \sin k\xi\rangle d\eta, \tag{19}$$

$$\frac{\partial\zeta}{\partial t} + \overline{u}_c'\eta\frac{\partial\zeta}{\partial\xi} + kB\sin k\xi\frac{\partial\zeta}{\partial\eta} = \frac{1}{R_h}\frac{\partial^2\zeta}{\partial\eta^2}, \tag{20}$$

where A = | a |, B = $2\varepsilon|\Lambda_{1c}|$ = $(4ck/\overline{u}_{ic}')\varepsilon$A is the amplitude of oscillations ψ with z = z_c. Using (19), (20) it is easy to obtain expressions (1) for the characteristic scales of the critical layer. In the class of solutions described by the system (19), (20) the rule for bypassing the singularity in the Rayleigh equation can be expressed, as in linear instability theory, through the phase jump of the logarithm entering into one of the Tollmin functions [2]. If it is assumed that with transition through the singularity in the direction of the z-axis the logarithm phase decreases by the value Φ, instead of the second condition (11) we obtain (see [2])

$$\left(\frac{\partial\Lambda_t}{\partial z_t}\right)_+ - \left(\frac{\partial\Lambda_t}{\partial z_t}\right)_- = -i\Phi\frac{1}{2}B_t\frac{\overline{u}_{tc}''}{\overline{u}_{tc}'} \tag{21}$$

(B_t = B/$\varepsilon \sim$ A). Comparing (21) and (11) we find that

$$\Phi = -\frac{2\overline{u}_{tc}'}{\overline{u}_{tc}''B_t}\int_{-\infty}^{\infty}\langle\zeta \sin k\xi\rangle d\eta. \tag{22}$$

As can be seen from (19), (22), the wave increment $\gamma(t) \sim \varepsilon\Phi$.

3. In order to describe the development of a wave with a linear critical layer ($d_{t,v} \gg d_n$) in (20) we must assume here that $\zeta = -\overline{u}_c''\eta + \zeta_\sim$ and linearize the derived equation relative to A and $\zeta_\sim$. It can be shown [11, 12] that the results of the solution of such a linearized problem agree with the conclusions from the linear theory of instability of shear currents. In accordance with the linear theory, the phase jump Φ of the logarithm, found for neutral waves in the presence of viscosity, and from solution of the problem with initial conditions for an ideal fluid, is equal to $-\pi$ [2, 16]. Assuming in (22) that $\Phi = -\pi$, from (19) we immediately obtain an expression for the linear wave increment:

$$\gamma = -\frac{\pi}{2}\varepsilon c_m^2\frac{\overline{u}_{tc}''}{\overline{u}_{tc}'}\frac{k^2}{\operatorname{sh}^2 k}\left(\frac{c}{c_m}\right)^2. \tag{23}$$

As follows from (1) and (23), the scale of the nonstationary critical layer is $d_t \sim \varepsilon^2$ and accordingly, with $\varepsilon \ll 1$ and a sufficiently low viscosity there is satisfaction of the assumption of isolation of the critical layer.

Expression (23) shows that waves with a resonance point situated in the region $\bar{u}''(z) > 0$ attenuate ($\gamma < 0$), whereas waves with $\bar{u}_c'' < 0$ are intensified ($\gamma > 0$). This result, naturally, agrees with the criterion of Miles instability for wind waves [6, 8]. Figure 2 shows the dependence of the normalized increment $\bar{\gamma} = \gamma / \varepsilon c_m^3$ on k, constructed for two model profiles of current velocity*:

$$\bar{u}_1 = \exp(z_1), \quad \bar{u}_2 = \exp[(0{,}2)^2 - (z_1 - 0{,}2)^2].$$

The $\bar{u}_1$ profile, not having a flexure point, can be regarded as a rough model of velocity distribution in the Ekman boundary layer**. In the case of interaction with such a current the internal waves attenuate. When $c_m < 1$ the decrement in the entire wavelength range has the form shown in Fig. 2,a. However, if $c_m > 1$ the lower boundary of the absorption region $k = k_*$ appears; this is determined by the condition $c(k_*) = 1$. With $k < k_*$ the resonance point is absent and $\gamma = 0$. In the region $k > k_*$ the decrement behaves the same as indicated in Fig. 2,a. The increment $\gamma(k)$ with k close to k_* is not described by the theory formulated above because in this case the critical layer region merges with the boundary. The $\bar{u}_2$ profiles having a flexure point evidently can arise when there is a variable wind. If the velocity of the infinitely long waves is less than the velocity flow at the flexure point ($c_m < 0.63$), all the waves attenuate (Fig. 2,b, curve 1). However, when c_m is greater than the velocity at the flexure point an instability arises. With $c_m < 1$ disturbances in the long-wave part of the spectrum are unstable. With a decrease in wavelength the resonance point is displaced downward along the z-axis and after it passes through the flexure point the increment changes sign (Fig. 2,b, curve 2). The behavior of γ with $k \approx k_*$ is shown in Fig. 2,b by a dashed line. In order to determine γ in this region it is necessary to go beyond the framework of approximation of an isolated critical layer.

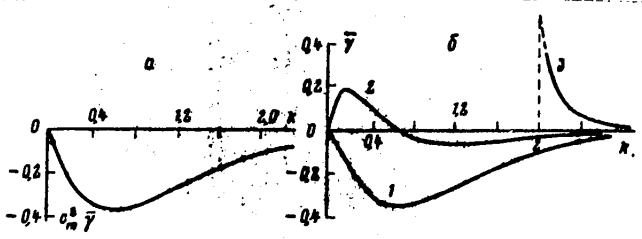

Fig. 2. Dependence of increment of internal waves on dimensionless wave number for two model profiles of velocity of near-surface current: a) attenuation of wave in case of interaction with current $u_1(z) = \exp(z/\varepsilon)$, maximum velocity of internal waves of a lesser flow velocity at the surface $-c_m < \bar{u}(0) = 1$; b) attenuation and intensification of waves in case of interaction with current $u_2(z) = \exp[(0.2)^2 - (z/\varepsilon - 0.2)^2]$; 1-3 -- increments with c_m = 0.5, 0.85, 2.

* The increment $\delta_c^{(1)}$ was not taken into account in determining the resonance point z_{ic}.

** In the Ekman boundary layer the direction of the horizontal velocity changes with depth [17].

System (19), (20) makes it possible to examine such an essentially nonlinear development of internal waves. When $d_v/d_t \gg 1$ it is possible to use the results of solution (20), obtained for stationary critical layers [9, 10]. For such a critical layer the logarithm phase jump is dependent only on the one parameter $\lambda_c = d_v^3/d_n^3$ [10]. The dependence of Φ on the dimensionless amplitude $s = \lambda_c^{2/3}$ is approximated well by a simple formula [12]. After transformation to dimensionless time $\tau = |\gamma| t$, from (19), (20) and (22) we obtain the equation

$$\frac{ds}{d\tau} = (\operatorname{sgn} \bar{u}_{tc}'') \frac{1}{\pi} \Phi(s) s. \tag{24}$$

For the attenuation of waves ($\bar{u}_c'' > 0$) the nonlinearity in the critical layer is manifested in the fact that intensive waves attenuate to a lesser degree than is predicted by linear theory. However, with a decrease in wave amplitude the decrement tends to a "linear" value. When $\bar{u}_c'' < 0$ the increment of increase of a weak wave ($s(0) \ll 1$) decreases smoothly with an increase in amplitude from γ to zero. The scale of the critical layer region in this case increases ($d_n = s^{1/2} d_v$). A violation of the initial assumption (2) of narrowness of the critical layer should lead to a qualitative change in the process of development of instability. The amplitude of the vertical displacement of the density jump in the internal wave $\Delta = 4A \operatorname{sh} k/c$ is related to the normalized amplitude s by the expression

$$\Delta = \left(\frac{d_v}{\varepsilon}\right)^2 \frac{\bar{u}_{tc}'' \operatorname{sh} k}{c^2 k} s. \tag{25}$$

It can be seen from (25) that in the case which we considered of thin critical layers ($d_{n,v} \ll \varepsilon$) the displacements of the jump are small in comparison with the thickness of the upper layer ($\Delta \ll 1$).

The ratio d_v/d_t can be represented in the form

$$\frac{d_v}{d_t} = \frac{(k\bar{u}_{tc}')^{1/3}}{c_m^2} \frac{1}{\varepsilon^{1/2} \sqrt{R_h}}. \tag{26}$$

In accordance with (26), the approximation of a quasistationary critical layer is satisfied with small ε. With sufficiently large ε, when $d_v^3/d_t^3 \ll 1$, viscosity in the critical layer can be neglected. Such a limiting case can be examined within the framework of the theory formulated above if $d_v/d_t = 1$ with $\varepsilon = \varepsilon_* \ll 1$. In the nonviscous critical layer the motion of the fluid is conveniently described in Lagrangian form [11]. After introducing the normalized coordinates of particles

$$X = \xi / 2\pi/k \text{ and } Z = \eta / 2\pi d_t,$$

the amplitudes $N = d_n^2/d_1^2$ and the time τ, from (19), (20) we obtain a system of equations examined in [11]. Its numerical solution shows that in the presence of instability a weak wave ($N(0) \ll 1$) at first increases exponentially with a γ increment. With $N \approx 9.4$ all the fluid particles participating in energy exchange with the wave experience rotations on the plane (X,Z) with the characteristic frequency $|\gamma|$ *. As a result, the instability is stabilized

* The width of the region of resonance particles is numerically great in comparison with d_t: $Z_{max} - Z_{min} \approx 4$ and $z_{max} - z_{min} \approx 25 d_t$ [11].

and weak oscillations of wave amplitude arise. In such a regime the transition corresponds to the amplitude of oscillations of the density jump

$$\Delta = 9{,}4\left(\frac{d_1}{e}\right)^2 \frac{\bar{u}_{1c}''' \operatorname{sh} k}{c^2 k}. \tag{27}$$

As a result of the rotation of fluid particles the vorticity level lines in the critical layer are twisted into spirals and small-scale oscillations arise on the ζ profile. The period of oscillations decreases until viscosity becomes operative, this smoothing the vorticity profile*. The nonlinear regime of wave attenuation ($\bar{u}_c'' > 0$) is realized when $N(0) \gg 1$. In this case resonance particles are immediately captured by a wave, whose amplitude begins to oscillate weakly [12].

Thus, a current localized near the surface, depending on the type of velocity profile, can both absorb and intensify internal waves. The slight submergence of the current makes it possible to speak of an interaction with the flow of internal waves, found in its absence. In this sense the formulated theory for internal waves is similar to that known for wind instability [6, 8]. Interaction with a near-surface current is a strong mechanism of absorption (intensification) of internal waves because the increment is a value of the order of ℓ/h of wave frequency. Instability is possible in the presence of a velocity profile flexure point when the velocities of infinitely long waves are greater than the current velocity at the flexure point. If the velocity of infinitely long waves exceeds the velocity at the surface, the instability is displaced into the short-wave region. The behavior of the wave in the nonlinear stage is greatly dependent on the turbulent viscosity value and on the depth of flow submergence.

BIBLIOGRAPHY

1. Betchov, R. and Kriminale, V., VOPROSY GIDRODINAMICHESKOY USTOYCHIVOSTI (Problems in Hydrodynamic Stability), Moscow, Mir, 1971.

2. Dikiy, L. A., GIDRODINAMICHESKAYA USTOYCHIVOST' I DINAMIKA ATMOSFERY (Hydrodynamic Stability and Atmospheric Dynamics), Leningrad, Gidrometeoizdat, 1976.

3. Gossard, E. and Khuk, U., VOLNY V ATMOSFERE (Atmospheric Waves), Moscow, Mir, 1978.

4. Stewartson, K. and Stuart, J. T., "A Non-linear Instability Theory for a Wave System in Plane Poiseuille Flow," J. FLUID MECH., Vol 48, No 3, pp 529-545, 1971.

5. Craik, A. D. D., "Nonlinear Resonant Instability in Boundary Layers," J. FLUID MECH., Vol 60, No 2, pp 393-413, 1971.

6. Miles, J. W., "On the Generation of Surface Waves by Shear Flows," J. FLUID MECH., Vol 3, No 2, 1957.

* The considered processes have an analogue in the theory of wave-particle interaction in plasma [8, 11].

7. Brooke, Benjamin T., "The Threefold Classification of Unstable Disturbances in Flexible Surface Bounding Inviscid Flows," J. FLUID MECH., Vol 16, No 3, pp 436-450, 1963.

8. Andronov, A. A. and Fabrikant, A. L., "Landau Attenuation, Wind Waves and Whistlers," NELINEYNYYE VOLNY (Nonlinear Waves), Moscow, Nauka, pp 68-104, 1979.

9. Benney, D. J. and Bergeron, R. F., "A New Class of Nonlinear Waves in Parallel Flows," STUD. APPL. MATH., Vol 48, No 3, pp 181-204, 1969.

10. Huberman, R., "Critical Layers in Parallel Flows," STUD. APPL. MATH., Vol 51, No 2, pp 139-161, 1972.

11. Reutov, V. P., "Plasma-Hydrodynamic Analogy and Nonlinear Stage in Instability of Wind Waves," IZV. AN SSSR: FAO (News of the USSR Academy of Sciences: Physics of Atmosphere and Ocean), Vol 16, No 12, pp 1266-1275, 1980.

12. Reutov, V. P., NESTATSIONARNYY KRITICHESKIY SLOY I NELINEYNAYA STADIYA NEUSTOYCHIVOSTI V PLOSKOM TECHENII PUAZEYLYA (Nonstationary Critical Layer and Nonlinear Stage in Instability in a Plane Poiseuille Flow), Preprint No 7, Gor'kiy, IPF AN SSSR, 1980.

13. Phillips, O. M., DINAMIKA VERKHNEGO SLOYA OKEANA (Dynamics of the Upper Layer in the Ocean), Leningrad, Gidrometeoizdat, 1980.

14. Nayfe, A. Kh., METODY VOZMUSHCHENIY (Perturbation Methods), Moscow, Mir, 1976.

15. Reutov, V. P., "Application of the Averaged Variational Principle for Describing Multiwave Interactions of Elastic Surface Waves," IZV. VUZov: RADIOFIZIKA (News of Schools of Higher Education: Radiophysics), Vol 16, No 11, pp 1690-1702, 1973.

16. Lin' Tszya-tszyao, TEORIYA GIDRODINAMICHESKOY USTOYCHIVOSTI (Theory of Hydrodynamic Stability), Moscow, IL, 1958.

17. Kamenkovich, V. M., OSNOVY DINAMIKI OKEANA (Principles of Ocean Dynamics), Leningrad, Gidrometeoizdat, 1973.

5303
CSO: 1865/152

UDC 551.465.5:519.24

MULTIELEMENT FOUR-DIMENSIONAL ANALYSIS OF PRINCIPAL HYDROPHYSICAL FIELDS IN OCEAN

Moscow IZVESTIYA AKADEMII NAUK SSSR: FIZIKA ATMOSFERY I OKEANA in Russian Vol 18, No 4, Apr 82 (manuscript received 5 May 81) pp 391-398

[Article by V. V. Knysh, Marine Hydrophysical Institute, Ukrainian Academy of Sciences]

[Text]

Abstract: Equations for optimum evaluations of the principal hydrophysical fields in the ocean and for the covariational matrix of errors in the evaluations are given. Approximate methods are proposed for computing the the cross-covariational functions of errors of functionally related fields. The results of model numerical experiments for evaluation of "measurements" of both individual parameters and combinations of parameters in a four-dimensional analysis of ocean fields are given.

In the continuous four-dimensional analysis of hydrophysical fields in the ocean use is made of the following sequence of operations [1]: determination of initial fields; prediction of fields and statistical characteristics on the basis of a thermohydrodynamic model; correction of prediction by observational data (obtaining initial data for further prediction). Independently it is possible to carry out an analysis of several fields (density, horizontal components of current velocity), in computing the field of any parameter proceeding solely on the basis of the measured values of this parameter [1, 2]. Another approach involves computation of each hydrophysical element on the basis of information on the combination of such elements; the computation element may or may not be included in this combination. Such an approach can be called multielement four-dimensional analysis of hydrophysical fields in the ocean [3].

In this article we give equations for multielement four-dimensional analysis of the principal hydrophysical fields in the ocean. We also give methods for computing the cross-covariational functions of errors of functionally related

fields. Also given are model numerical experiments for evaluating the contribution of "measurements" of specific hydrophysical parameters to their analysis and the possibilities of reconstructing fields on the basis of measurement data for elements of other fields.

1. We will write equations for the optimum evaluation (in the sense of a minimum mean square error) of the vector of state $\hat{U}(x,t)$ of the dynamic system (ocean) and covariation function $P(x, x', t) = E\{\delta U(x,t) \cdot \delta U^T(x', t)\}$ of errors $\delta U(x,t) = U(x, t) - \hat{U}(x,t)$ in the form [4-6]

$$\begin{aligned}\partial\hat{U}(x, t) / \partial t = L_x\hat{U}(x, t) + P_N(x, t_l^-)\theta^T(t_l^+)\times\\ \times[\theta(t_l^+)P_N(x_r, t_l^-)\theta^T(t_l^+) + R(t_l^+)]^{-1}\times\\ \times[\varphi(t_l^+) - \theta(t_l^+)\hat{U}(t_l^-)]\delta(t - t_l),\end{aligned} \tag{1}$$

$$\begin{aligned}\partial P(x, x', t) / \partial t = L_x P(x, x', t) + [L_{x'} P(x', x, t)]^T - P_N(x, t_l^-)\theta^T(t_l^+)\times\\ \times[\theta(t_l^+)P_N(x_r, t_l^-)\theta^T(t_l^+) + R(t_l^+)]^{-1}\times\\ \times\theta(t_l^+)[P_N(x', t_l^-)]^T\delta(t - t_l) + \theta_\omega(x, x', t)\end{aligned} \tag{2}$$

with the boundary and initial conditions

$$\begin{aligned}F(\xi)\hat{U}(\xi, t) + \partial\hat{U}(\xi, t) / \partial\tau = \bar{U}(\xi, t), \quad \hat{U}(x, t_0) = \bar{U}_0(x),\\ F(\xi)P(\xi, x', t) + \partial P(\xi, x', t) / \partial\tau = Q_\theta(\xi, x', t) / 2,\end{aligned} \tag{3}$$

$$P(x, x', t_0) = P_0(x, x'). \tag{4}$$

In equations (1), (2) and conditions (3), (4) $x = (x,y,z)$; ξ is a point belonging to the boundary of the region; L_x, $L_{x'}$ are matrix linear differential operators; $\varphi(t_l^+) = \theta(t_l^+)U_N(t_l^+) + \lambda(t_l^+)$ is the vector of measurements at discrete moments in time t_l, the matrices $\theta(t_l^+)$, $R(t_l^+)$ are the characteristics and covariations of errors $\lambda(t_l^+)$ of the measuring instrument respectively; $\theta_\omega(x, x', t)$, $\theta_\beta(\xi, x', t)$ are the covariations of errors in the hydrodynamic modeling of the vector of state $U(x, t)$ of the Gaussian distribution:

$$U(x, t) = \begin{Vmatrix} u^1(x, t) \\ u^2(x, t) \\ \vdots \\ u^m(x, t) \end{Vmatrix}, \quad U_N(t_l^+) = \begin{Vmatrix} U(x_1, t_l^+) \\ U(x_2, t_l^+) \\ \vdots \\ U(x_N, t_l^+) \end{Vmatrix},$$

$$P_N(x, t_l^-) = [P(x, x_1, t_l^-), \ldots, P(x, x_N, t_l^-)];$$

$r = 1, 2, \ldots, N$ are points in the region where there are measurement data $U(x, t)$ at the measurement time t_l; $F(\xi)$ is a known function; τ is the normal to the boundary of the region; the indices T and -1 denote the transposition and inverse operators respectively; $\bar{U} = E\{U(x,t)\}$, E is the averaging operator; $f(t_l^-)$ and $f(t_l^+)$ are the values of the function without allowance for measurement data arriving with $t = t_l$ and with them taken into account respectively; δ is the Dirac delta function.

Assume now that the vector of state of the ocean includes the components u, v -- the horizontal components of the current velocity vector, ρ is the sea water density anomaly:

$$\mathbf{U}(x,t)=\begin{Vmatrix} u(x,t) \\ v(x,t) \\ \rho(x,t) \end{Vmatrix}. \tag{5}$$

The u, v, ρ fields are measured in the ocean by means of known measurement instruments [7].

We will use the hydrodynamic model set forth in [8]. Numerical experiments carried out within the framework of this model indicated [9] that it describes well the interaction between eddies of a synoptic scale and large-scale circulation. In the equations of motion of the model described in [8] we will neglect the nonlinear terms and horizontal turbulent viscosity and in the equation for the total flows function we will neglect lateral exchange. With equation (1) taken into account, the equations for the optimum evaluations of the components of the vector of state (5) in a small time interval $t_n \leqslant t \leqslant t_{n+1}$ between the moments of assimilation of measurement data have the form

$$\frac{\partial \hat{u}}{\partial t}=f\hat{v}+\nu\frac{\partial^2\hat{u}}{\partial z^2}-\frac{f}{H}\frac{\partial\hat{\psi}}{\partial x}+\frac{g}{H\rho_0}\int_0^H(H-z)\frac{\partial\hat{\rho}}{\partial x}dz-\frac{g}{\rho_0}\int_0^z\frac{\partial\hat{\rho}}{\partial x}d\mu+\frac{\tau_x}{H}, \tag{6}$$

$$\frac{\partial \hat{v}}{\partial t}=-f\hat{u}+\nu\frac{\partial^2\hat{v}}{\partial z^2}-\frac{f}{H}\frac{\partial\hat{\psi}}{\partial y}+\frac{g}{H\rho_0}\int_0^H(H-z)\frac{\partial\hat{\rho}}{\partial y}dz-\frac{g}{\rho_0}\int_0^z\frac{\partial\hat{\rho}}{\partial y}d\mu+\frac{\tau_y}{H} \tag{7}$$

$$\frac{\partial\hat{\rho}}{\partial t}=-\hat{u}_n\frac{\partial\hat{\rho}}{\partial x}-\hat{v}_n\frac{\partial\hat{\rho}}{\partial y}-\hat{w}_n\frac{\partial\hat{\rho}}{\partial z}+\varkappa\frac{\partial^2\hat{\rho}}{\partial z^2}+A\Delta\hat{\rho}. \tag{8}$$

The equation for evaluating the total flows function and evaluating the vertical component of current velocity has the form

$$\begin{aligned}
&\frac{\partial\Delta\hat{\psi}}{\partial t}+\frac{f}{2\alpha H}\Delta\hat{\psi}+\frac{f}{H}J(H,\hat{\psi})+\beta\frac{\partial\hat{\psi}}{\partial x}=\frac{1}{\rho_0}\operatorname{rot}_z\tau+\frac{1}{H\rho_0}\left(\frac{\partial H}{\partial x}\tau_y-\frac{\partial H}{\partial y}\tau_x\right)-\\
&-\frac{g}{2\alpha\rho_0}\int_0^H\frac{z}{H}\Delta\hat{\rho}dz-\frac{g}{\rho_0}\int_0^H\frac{z}{H}J(H,\hat{\rho})dz-\frac{\beta}{f\rho_0}\tau_x-\\
&-\frac{\partial}{\partial x}\int_0^H\left[\frac{\partial(\hat{u}\hat{v})_n}{\partial x}+\frac{\partial\hat{v}_n^2}{\partial y}\right]dz+\frac{\partial}{\partial y}\int_0^H\left[\frac{\partial\hat{u}_n^2}{\partial x}+\frac{\partial(\hat{u}\hat{v})_n}{\partial y}\right]dz,\\
&\hat{w}=\frac{1}{f}\left\{\beta\int_0^z\hat{v}d\mu+\frac{1}{\rho_0}\operatorname{rot}_z\tau+\int_0^z\left[\frac{\partial\hat{\xi}}{\partial t}+\frac{\partial(\hat{u}\hat{\xi})_n}{\partial x}+\frac{\partial(\hat{v}\hat{\xi})_n}{\partial y}\right]d\mu\right\},
\end{aligned} \tag{9}$$

$$\xi = \frac{\partial \hat{v}}{\partial x} - \frac{\partial \hat{u}}{\partial y}. \tag{10}$$

The boundary and initial conditions are as follows:

with z = 0

$$\nu \partial \hat{u}/\partial z = -(1/\rho_0)\tau_x, \quad \nu \partial \hat{v}/\partial z = -(1/\rho_0)\tau_y, \quad \varkappa \partial \hat{\rho}/\partial z = \gamma_1(\hat{\rho} + \gamma_2 T_a), \tag{11}$$

at the bottom z = H(x,y)

$$\hat{u} = \hat{v} = 0, \quad \hat{\rho} = \rho_3, \tag{12}$$

at the lateral boundaries

$$\hat{\psi} = -\frac{g}{f\rho_0}\int_0^z z\hat{\rho}\,dz, \quad \hat{\rho} = \rho_3, \tag{13}$$

$$\hat{\rho}|_{t=t_0} = \rho^0, \quad (\hat{u}, \hat{v})|_{t=t_0} = (u^0, v^0), \quad \hat{\psi}|_{t=t_0} = \psi^0. \tag{14}$$

In equations (6)-(9), formula (10) and conditions (11)-(14) the notations are the same as in [8]. We note that the form of the equations for the optimum evaluations between the moments of assimilation of observational data is the same as for the equations of the hydrodynamic model [8].

At the times t_l of measurements of the components of the vector of state (5) (t_l coincides with t_n and $t_{l+1} - t_l \geqslant \Delta t$, where Δt is the time interval in the numerical scheme) the optimum evaluations $\hat{u}(x, t_l^-)$, $\hat{v}(x, t_l^-)$, $\hat{\rho}(x, t_l^-)$, found at this time from a solution of equations (6)-(8), are corrected by measurements on the basis of formulas [2, 6]:

$$\hat{u}(\mathbf{x}, t_l^+) = \hat{u}(\mathbf{x}, t_l^-) + \sum_{r=1}^{N} [\Delta_r^{1u}(\mathbf{x}, t_l^-)\delta u(\mathbf{x}_r, t_l^+) + \Delta_r^{1v}(\mathbf{x}, t_l^-) \times \tag{15}$$

$$\times \delta v(\mathbf{x}_r, t_l^+) + \Delta_r^{1\rho}(\mathbf{x}, t_l^-)\delta\rho(\mathbf{x}_r, t_l^+)],$$

$$\hat{v}(\mathbf{x}, t_l^+) = \hat{v}(\mathbf{x}, t_l^-) + \sum_{r=1}^{N} [\Delta_r^{2u}(\mathbf{x}, t_l^-)\delta u(\mathbf{x}_r, t_l^+) + \tag{16}$$

$$+ \Delta_r^{2v}(\mathbf{x}, t_l^-)\delta v(\mathbf{x}_r, t_l^+) + \Delta_r^{2\rho}(\mathbf{x}, t_l^-)\delta\rho(\mathbf{x}_r, t_l^+)],$$

$$\hat{\rho}(\mathbf{x}, t_l^+) = \hat{\rho}(\mathbf{x}, t_l^-) + \sum_{r=1}^{N} [\Delta_r^{3u}(\mathbf{x}, t_l^-)\delta u(\mathbf{x}_r, t_l^+) + \tag{17}$$

$$+ \Delta_r^{3v}(\mathbf{x}, t_l^-)\delta v(\mathbf{x}_r, t_l^+) + \Delta_r^{3\rho}(\mathbf{x}, t_l^-)\delta\rho(\mathbf{x}_r, t_l^+)],$$

where

$$\delta u(x_r,\ t_l^+)=u(x_r,\ t_l^+)-\hat{u}(x_r,\ t_l^-),\quad \delta v(x_r,\ t_l^+)=v(x_r,\ t_l^+)-\hat{v}(x_r,\ t_l^-),$$
$$\delta\rho(x_r,\ t_l^+)=\rho(x_r,\ t_l^+)-\hat{\rho}(x_r,\ t_l^-)$$

are the prediction errors; $\Delta_r^{ju}-\Delta_r^{j\rho}$ are the weighting factors (j = 1, 2, 3). Formulas (15)-(17) were written for the case of point error-free measurements of the components of the vector (5); the $\Theta(t)$ matrix is a unit matrix and $\lambda(t)=0$. Then, taking into account the form of the factor on $\delta(t-t_l)$ in the last term on the right-hand side of equation (1), for determining the weighting coefficients we obtain the formulas

$$\begin{aligned}\Delta_r^{1u}(x,\ t_l^-)&=\|P(x_r,\ x_p,\ t_l^-)\|^{-1}\cdot P_{uu}(x,\ x_r,\ t_l^-),\\ \Delta_r^{2u}(x,\ t_l^-)&=\|P(x_r,\ x_p,\ t_l^-)\|^{-1}\cdot P_{vu}(x,\ x_r,\ t_l^-),\\ \Delta_r^{3u}(x,\ t_l^-)&=\|P(x_r,\ x_p,\ t_l^-)\|^{-1}\cdot P_{\rho u}(x,\ x_r,\ t_l^-),\end{aligned}\tag{18}$$

where

$$\Delta_r^{ju}(x,\ t_l^-)=\left\|\begin{matrix}\Delta_r^{ju}(x,\ t_l^-)\\ \Delta^{jv}(x,\ t_l^-)\\ \Delta_r^{j\rho}(x,\ t_l^-)\end{matrix}\right\|,\quad P_{uu}(x,\ x_r,\ t_l^-)=\left\|\begin{matrix}P_{uu}(x,\ x_r,\ t_l^-)\\ P_{uv}(x,\ x_r,\ t_l^-)\\ P_{u\rho}(x,\ x_r,\ t_l^-)\end{matrix}\right\|,\tag{19}$$

$$j=1,\ 2,\ 3;\ \ r=1,\ \ldots,\ N,$$

$$P(x_r,\ x_p,\ t_l^-)=\left\|\begin{matrix}P_{uu}(x_r,x_p,t_l^-) & P_{vu}(x_r,x_p,t_l^-) & P_{\rho u}(x_r,x_p,t_l^-)\\ P_{up}(x_p,x_r,t_l^-) & P_{vv}(x_r,x_p,t_l^-) & P_{\rho v}(x_r,x_p,t_l^-)\\ P_{u\rho}(x_p,x_r,t_l^-) & P_{vp}(x_p,x_r,t_l^-) & P_{\rho\rho}(x_r,x_p,t_l^-)\end{matrix}\right\|,\tag{20}$$

$$p=1,\ \ldots,\ N.$$

The vectors $P_{vu}(x,\ x_r,\ t_l^{-1})$ and $P_{\rho u}(x,\ x_r,\ t_l^-)$ have a form similar to the vector $P_{uu}(x,\ x_r,\ t_l^-)$. The covariational and cross-covariational functions in formulas (18) and the notations (19), (20) form a matrix P(x, x', t) of the type (20), in the small time interval $t_n\leqslant t\leqslant t_{n+1}$ between the times of assimilation of measurement data satisfying equation (2) without the next-to-the-last term on its right-hand side. The operators L_x and L_x, in this case are linear and are determined by the form of the equations (6)-(8). At the time t_l of measurements the covariation matrix P is corrected using the formula [2, 6]

$$P(x,x',t_l^+)=P(x,x',t_l^-)-\sum_{p=1}^{N}\sum_{r=1}^{N}P(x,x_r,t_l^-)\times\tag{21}$$
$$\times[P(x_p,x_r,t_l^-)]^{-1}P(x',x_p,t_l^-).$$

Due to the great dimensionality of both the system of equations (2) and the covariation functions its solution without simplifications is virtually impossible. We will proceed in the following way.

From the system of differential equations (2) we will write an equation for the covariational function of the errors in evaluating density $P_{\rho\rho}(x,\ x',\ t)$. Between the times of measurements in the small time interval $t_n\leqslant t\leqslant t_{n+1}$ we have

Table 1

Mean $\overline{\delta}$, Mean Square σ and Maximum σ_{max} Errors of Current Velocity Components u, v (cm/sec) and Nominal Density $\sigma_t \cdot 10^2$ (g/cm^3) in Numerical Experiments for the Assimilation of Measurement Data

Horizon	Experiment	Type of assimilation of observational data	$\overline{\delta}$			σ			δ_{max}		
			u	v	$\sigma_t \cdot 10^2$	u	v	$\sigma_t \cdot 10^2$	u	v	$\sigma_t \cdot 10^2$
400	PE		1,440	1,466	0,655	2,020	2,093	0,819	7,598	10,760	2,610
	I	u, v	1,385	1,345	0,664	1,981	2,009	0,823	7,765	10,760	2,620
			(3,8)	(8,3)	(−1,3)	(2)	(4,1)	(−0,5)	(−2,2)	(0)	(−0,4)
	II	u, v	1,358	1,306	0,623	1,950	1,970	0,778	7,668	10,619	2,580
			(5,7)	(11)	(4,9)	(3,5)	(5,9)	(5)	(−0,9)	(1,3)	(1,1)
	III	Correction ρ	1,025	1,071	0,402	1,364	1,422	0,522	4,302	4,658	2,130
			(28,8)	(26,9)	(38,6)	(52,5)	(32,1)	(36,3)	(43,4)	(56,7)	(18,8)
	IV	ρ	1,023	1,055	0,400	1,361	1,406	0,522	4,397	4,801	2,150
			(30)	(28,1)	(38,9)	(32,6)	(32,8)	(36,3)	(42,1)	(55,4)	(17,6)
	V	Correction u, v, ρ	0,964	0,981	0,399	1,291	1,326	0,516	4,450	4,756	2,060
			(33,1)	(33,1)	(39,1)	(36,1)	(36,6)	(37)	(41,4)	(55,8)	(21,1)
800	PE		0,743	0,741	0,856	1,100	1,164	1,280	4,496	6,129	9,420
	I	u, v	0,710	0,685	0,876	1,081	1,121	1,300	4,422	6,032	9,420
			(4,4)	(7,5)	(−2,3)	(2)	(3,7)	(−1,6)	(1,6)	(1,6)	(0)
	II	u, v	0,702	0,676	0,853	1,072	1,115	1,270	4,386	6,009	9,300
			(5,5)	(8,8)	(0,4)	(2,5)	(4,2)	(0,8)	(2,4)	(2)	(1,3)
	III	Correction ρ	0,579	0,693	0,530	0,773	0,940	0,798	2,831	3,757	3,360
			(22,1)	(6,4)	(38,1)	(29,7)	(19,2)	(37,7)	(37)	(38,7)	(64,3)
	IV	ρ	0,577	0,686	0,530	0,766	0,921	0,794	2,605	3,741	3,370
			(22,3)	(7,4)	(38,1)	(30,4)	(20,9)	(38)	(42,1)	(39)	(64,2)
	V	Correction u, v, ρ	0,554	0,659	0,530	0,746	0,902	0,796	2,694	3,580	3,480
			(25,4)	(11,1)	(38,1)	(32,1)	(22,5)	(37,8)	(40,1)	(41,6)	(63,1)

$$(\partial/\partial t)P_{\rho\rho}(x, x', t) = L_x P_{\rho\rho}(x, x', t) + L_{x'} P_{\rho\rho}(x', x, t) + Q_{\rho\rho}(x, x', t),$$
$$L_x = A\Delta + \varkappa\partial^2/\partial z^2 - \hat{u}(x, t_n)\partial/\partial x - \hat{v}(x, t_n)\partial/\partial y - \hat{w}(x, t)\partial/\partial z. \quad (22)$$

At the measurement time t_l the covariational function $P_{\rho\rho}(x, x', t_l^-)$, found at this time from solution of equation (22), is corrected using the formula [2]:

$$P_{\rho\rho}(x, x', t_l^+) = P_{\rho\rho}(x, x', t_l^-) - \sum_{r=1}^{N} [\Delta_r^{\rho\rho}(x, t_l^-) P_{\rho u}(x', x_r, t_l^-) + \Delta_r^{\rho v}(x, t_l^-) P_{\rho v}(x', x_r, t_l^-) + \Delta_r^{\rho\rho}(x, t_l^-) P_{\rho\rho}(x', x_r, t_l^-)]. \quad (23)$$

The authors of [2] proposed an approximate method for computing the covariational functions P_{uu}, P_{uv}, P_{vu}, P_{vv} through the covariation function $P_{\rho\rho}$. In order to obtain formulas for computing the cross-covariational functions $P_{u\rho}$, $P_{v\rho}$, $P_{\rho u}$ and $P_{\rho v}$ through the function $P_{\rho\rho}$ we will use geostrophic expressions and a formula for the approximate determination of the ocean level by the dynamic method [10]. Then the cross-covariational function of the errors of the u-component of velocity and the density anomaly is determined as follows:

$$P_{u\rho}(x, x', t) = E\{\delta u(x, t)\delta\rho(x', t)\} = E\left\{\left(\frac{g}{f\rho_0}\int_z^H \frac{\partial[\delta\rho(x, t)]}{\partial y} \times d\mu\right)\delta\rho(x', t)\right\} = -\frac{g}{f\rho_0}\frac{\partial}{\partial y}\int_z^H P_{\rho\rho}(x, x', t)\, d\mu. \quad (24)$$

Similarly we obtain formulas for computing the remaining cross-variational functions

$$P_{v\rho}(x, x', t) = -\frac{g}{f\rho_0}\frac{\partial}{\partial x}\int_z^H P_{\rho\rho}(x, x', t)\, d\mu, \quad (25)$$

$$P_{\rho u}(x, x', t) = \frac{g}{f\rho_0}\frac{\partial}{\partial y'}\int_{z'}^H P_{\rho\rho}(x, x', t)\, d\mu, \quad (26)$$

$$P_{\rho v}(x, x', t) = -\frac{g}{f\rho_0}\frac{\partial}{\partial x'}\int_{z'}^H P_{\rho\rho}(x, x', t)\, d\mu. \quad (27)$$

In the derivation of formulas (24)-(27) the density anomaly at the bottom was neglected.

Thus, all the elements of the covariation matrix P(x, x', t) can be computed, which makes it possible to carry out a four-dimensional analysis of the main fields in the ocean with the presence of their measurement data at discrete moments in time t_l.

2. Model computations were made in a grid region measuring 13 x 15 x 9 points with a spatial interval $\Delta x = \Delta y = 17$ miles, $\Delta z = 200$ m. The principal parameters in the numerical model used were as follows [9, 11]: $\tau_x = -0.00547$; $\tau_y = 0.03648$ N/m^2; A = 10; $f = 10^{-4}$, $\nu = 10^{-3}$ m^2/sec, $\beta = 0.2\cdot10^{-10}$ m$^{-1}\cdot$sec^{-1}, $\gamma_1 = 0.712\cdot10^{-5}$ m/sec, $\gamma_2 = 0.735\cdot10^{-1}$ kg/K, $\Delta t = 8.64\cdot10^4$ sec, $T_a = 29°C$.

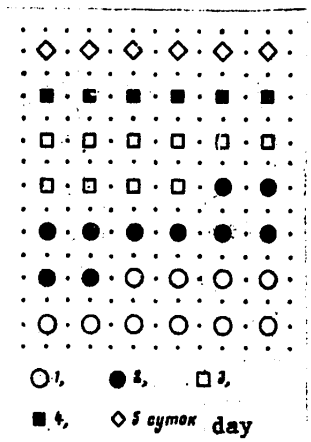

Fig. 1. Sequence and number of observation stations for density and current velocity fields on each day of model time.

As the true fields we used the hydrophysical fields computed in an inertial forecast (with constant lateral boundary values $\hat{\rho}$) for five days of model time. We used equations (6)-(10) with the boundary conditions (11)-(13). As the initial equations we took the fields corresponding to the initial density field, obtained on the basis of observational data from the second density survey carried out in the POLYMODE polygon [11]. Observational data were generated from this true state each 24 hours (see Fig. 1).

In subsequent computations as the initial density field we used the initial field $\hat{\rho}$ averaged on the basis of the nearest four points within the region and two at the lateral boundaries. At the lateral boundaries the density changed linearly from the smoothed value on the first day to the true value on the last day. The following variants of computations for five days of model time were used.

In the preliminary experiment (PE) a purely hydrodynamic prediction of field evaluations was made. In the first experiment (I), in addition to a prediction of evaluations of the fields for each day there was assimilation of data from observations of the u, v components of current velocity. In this procedure in formulas (15), (16) beneath the summation symbol we keep the first two terms and in formula (17) the last term on the right-hand side is neglected. In the second experiment (II) the density evaluation was corrected using observational data on velocity in explicit form (the indicated term was taken into account in (17)). In variants I, II there was a two-element four-dimensional analysis of oceanic fields. In the third (III) and fourth (IV) experiments there was a single-element four-dimensional analysis using measurement data only for the density field.

The fifth experiment (V) was carried out with simultaneous allowance for observational data on the velocity and density fields. The covariation matrix $P_{\rho\rho}(x, x', t)$ was computed as in [2].

We will introduce the following notations:

[И = true; Э = exp]

$$\delta(z)=\frac{1}{\Sigma}\int|\varphi_{\text{и}}-\varphi_{\text{о}}|dS,$$

$$\delta_{\text{макс}}(z)=\max_{(x,y)\in S}|\varphi_{\text{и}}-\varphi_{\text{о}}|,\quad \sigma(z)=\left\{\frac{1}{\Sigma}\int_{S}[|\varphi_{\text{и}}-\varphi_{\text{о}}|-\delta(z)]^2dz\right\}^{1/2},$$

S is the surface of the polygon, Σ is the surface area, φ_{true} is the true value of the field on the fifth day of model time; φ_{exp} is the field value obtained in the course of an experiment in this same time period. The table gives the results of the numerical experiments. The figures in the parentheses indicated by what percent the considered values of the errors $\bar{\delta}$, $\delta_{\max}$ and σ were improved relative to the similar errors in the PE.

It can be seen that the assimilation of measurement data only for the velocity field leads to an insignificant improvement in the results of four-dimensional analysis of the velocity and density fields. At the same time experiment III shows that with the assimilation of information on the density field the errors $\bar{\delta}$, $\delta_{\max}$ and σ for the velocity and density fields decrease significantly. This is also confirmed by experiments IV and V. The conclusion can be drawn that the principal factor in the process of reconstruction of the principal hydrophysical fields in the ocean in the case of their four-dimensional analysis is the density field. Within the framework of the conducted model experiments the correction to a field, information on whose measurements is lacking, by measurement data for other fields in explicit form on the average is insignificant (see experiments II, IV). In individual regions of the polygon, as indicated by an analysis of the results of computations, it can be substantial. Minimum values of the errors $\bar{\delta}$, $\delta_{\max}$ and σ are observed with the simultaneous assimilation of measurement data for the density and velocity fields (experiment V).

BIBLIOGRAPHY

1. Knysh, V. V., Nelepo, B. A., Sarkisyan, A. S. and Timchenko, I. Ye., "Dynamic-Stochastic Approach to Analysis of Observations of the Density Field in Hydrophysical Polygons," IZV. AN SSSR: FAO (News of the USSR Academy of Sciences: Physics of the Atmosphere and Ocean), Vol 14, No 10, pp 1079-1093, 1978.

2. Knysh, V. V., Moiseyenko, V. A., Sarkisyan, A. S. and Timchenko, I. Ye., "Multisided Use of Measurements in Hydrophysical Polygons in the Ocean in Four-Dimensional Analysis," DOKL. AN SSSR (Reports of the USSR Academy of Sciences), Vol 252, No 4, pp 832-836, 1980.

3. Mashkovich, S. A., "Multielement Objective Analysis of Meteorological Fields," METEOROLOGIYA I GIDROLOGIYA (Meteorology and Hydrology), No 5, pp 5-14, 1980.

4. Sakeva, Y., "Optimal Filtering in Linear Distributed Parameter Systems," INT. J. CONTROL., Vol 16, No 1, pp 115-127, 1972.

5. Brayson, A. and Kho Yu Shi, PRIKLADNAYA TEORIYA OPTIMAL'NOGO UPRAVLENIYA (Applied Theory of Optimum Control), Moscow, Mir, 1972, 544 pages.

6. Colantuoni, G. and Padmanabhan, L., "Optimal Sensor Selection in Sequential Estimation Problems," INT. J. CONTROL, Vol 28, No 6, pp 821-845, 1978.

7. Paramonov, A. N., Kushnir, V. M. and Zaburdayev, V. I., SOVREMENNYYE METODY I SREDSTVA IZMERENIYA GIDROLOGICHESKIKH PARAMETROV OKEANA (Modern Methods and Instrumentation for Measuring Hydrological Parameters in the Ocean), Kiev, Naukova Dumka, 1979, 246 pages.

8. Knysh, V. V. and Demyshev, S. G., "Hydrothermodynamic Model for Investigating Synoptic Variability and Energetics of the Ocean," MORSKIYE GIDROFIZICHESKIYE ISSLEDOVANIYA (Marine Hydrophysical Research), No 3, pp 97-109, 1980.

9. Demyshev, S. G. and Knysh, V. V., "Numerical Modeling of Synoptic and Macroscale Currents in the Ocean," STRUKTURA, KINEMATIKA I DINAMIKA SINOPTICHESKIKH VIKHREY (Structure, Kinematics and Dynamics of Synoptic Eddies), Sevastopol', MGI AN UkSSR, pp 46-58, 1980.

10. Perederey, A. I., "Computation of Surface and Deep Currents in the Southern Part of the Pacific Ocean," MORSKIYE GIDROFIZICHESKIYE ISSLEDOVANIYA, No 1, pp 76-87, 1972.

11. Nelepo, B. A., Bulgakov, N. P., et al., SINOPTICHESKIYE VIKHRI V OKEANE (Synoptic Eddies in the Ocean), Kiev, Naukova Dumka, pp 223-248, 1980.

5303
CSO: 1865/152

UDC 551.446.82

CORRELATION BETWEEN TRAINS OF SHORT-PERIOD INTERNAL WAVES AND THERMOCLINE RELIEF IN OCEAN

Moscow IZVESTIYA AKADEMII NAUK SSSR: FIZIKA ATMOSFERY I OKEANA in Russian Vol 18, No 4, Apr 82 (manuscript received 3 Apr 81, after revision 14 Jul 81) pp 416-425

[Article by K. D. Sabinin, A. A. Nazarov and A. N. Serikov, Acoustics Institute, USSR Academy of Sciences]

[Text]

Abstract: Measurements of internal waves by means of drifting and towed arrays of distributed temperature sensors are described. The work was carried out in the POLYMODE polygon in September 1977. The correlation between the directions of waves in trains of short-period waves and thermocline slopes is indicated. It is postulated that the refraction of internal waves and nonlinear effects arising during the propagation of waves over the sloping thermocline play an important role in the generation of trains of short waves similar to those appearing during the nonlinear decay of an internal tidal wave arriving in shallow waters.

Arrays of distributed temperature sensors in drifting [1] and towed variants have been used in studying the spatial structure of trains of short-period internal waves frequently encountered in the upper thermocline and their correlation with synoptic variability of the ocean. The studies were carried out in the POLYMODE polygon during the period 6-9 September 1977 simultaneously on the scientific research ships "Petr Lebedev" (drifting array) and "Sergey Vavilov" (towed array).

The principal element of the array -- the distributed temperature sensor -- was made of a cable with steel strands whose resistance varied proportionally to the mean temperature of the water layer intercepted by the sensor. As a result of such averaging properties the distributed temperature sensor is insensitive to the distorting influence of the fine structure of the vertical distribution of temperature in the ocean [2] and this makes it possible

to carry out both phase and amplitude comparisons of the readings of spatially separated sensors, that is, to use array methods for evaluating the spatial-temporal spectrum of waves [3]. The readings of the distributed temperature sensors were converted into the vertical displacements relative to the thermocline by means of the experimentally evaluated response of the distributed temperature sensors to the known vertical displacement, as a rule stable during the entire course of the measurements.

The drifting array, consisting of four 100-m distributed temperature sensors, spaced horizontally, was supplemented by a "stepped" sensor of four 20-m distributed temperature sensors for evaluating the vertical variability of the waves and three BPV-2 current meters for determining movements of the array relative to the water (Fig. 1).

The towed array included three 40-m distributed temperature sensors, at whose ends there were hydrodynamic deepeners of the lattice type. One sensor (C) was submerged from the stern, and the other two were deflected by means of torpedo-shaped floats along the wake (K) and in a direction away from the ship (B) (Fig. 2). In the latter case the float was supplied with a special line ensuring deflection under the influence of the oncoming flow.

Figure 3 shows the position of the runs which were carried out against the background of relief of the 15° isotherm, characterizing the position of the synoptic eddies during the course of the experiment (the map was compiled on the basis of data from a temperature survey carried out during the period 9-11 September 1977). The track of the scientific research ship "Petr Lebedev" with a drifting array is also shown here. Figure 3 shows that the region of the measurements was situated for the most part in a transition region between cyclonic and anticyclonic eddies and only run V intercepted an anticyclonic formation. The discreteness of the measurements was 30 sec and was equal to the time constant of the distributed temperature sensor at the 0.7 level. The basic information on the towing runs is given in Table 1.

Pressure sensors of the vibrotron type with a sensitivity of $\sim$10 cm were mounted at the ends of the distributed pressure sensor. These made possible a reliable checking of the change in depth and choice of sectors with small depth variations. Substantial changes in depth (up to 5 m) during towing were observed only during changing of the runs, but some increase in coherence between the readings of the distributed temperature detectors and the depth of its lower end at frequencies of 12-15 cycles/hour made it necessary to use caution in examining data for this frequency range (in the subsequent processing the data were smoothed by moving averaging in six ordinates, that is, with a smoothing interval of 3 min). At frequencies from 0.51 to 10-12 cycles/hour the coherence was close to zero and the spectral density of oscillations of the end of the distributed temperature sensor was 1-1.5 orders of magnitude less than the spectral density of readings of the distributed temperature sensor.

The situation is different with respect to fluctuations in the depth of the drifting array, when sporadic squalls have led to sharp intensifications of drift and a decrease in the depth of the distributed temperature sensor.

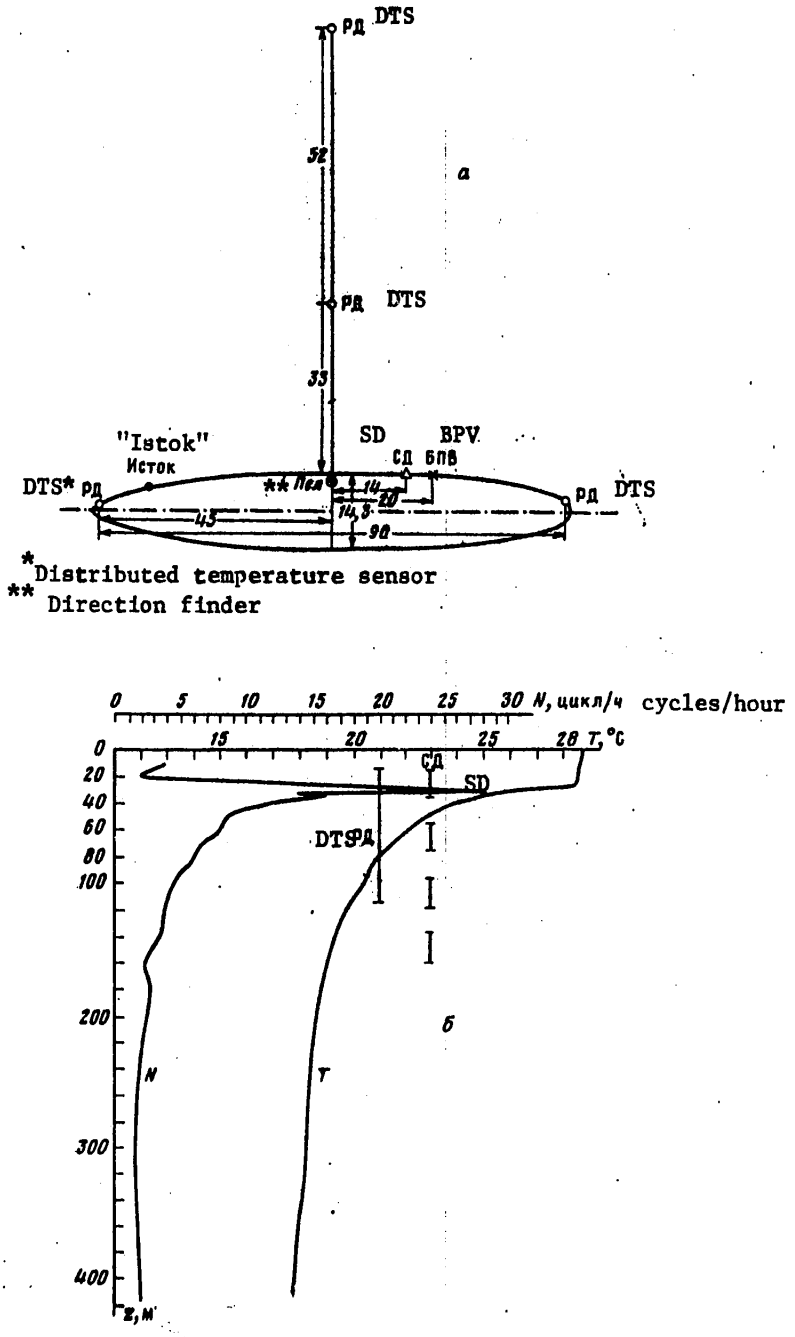

Fig. 1. Drifting array of distributed temperature sensors: a) appearance from above; b) position of sensors relative to thermocline (T is temperature, N is buoyancy frequency).

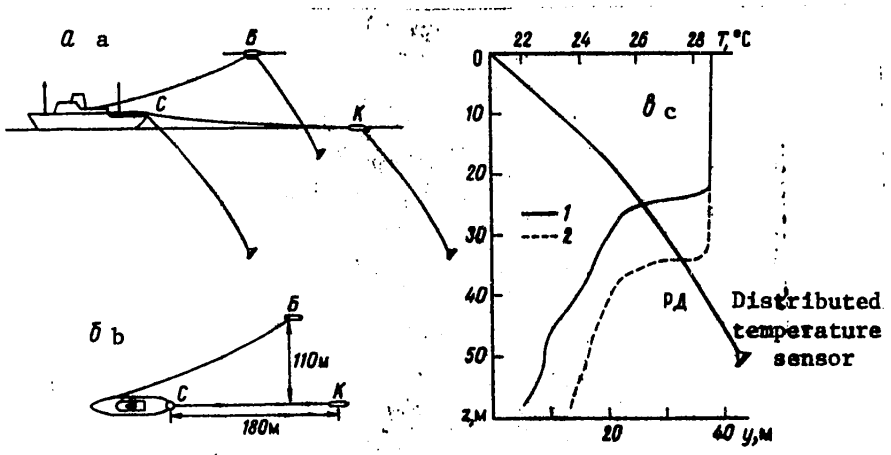

Fig. 2. Towed array of distributed temperature sensors: a) general view, b) appearance from above, c) position of sensors relative to thermocline (positions of the thermocline close to extremal are indicated: 1) STD station No 25, 7 September 1977, 2) KhVT station No 61, 9 September 1977).

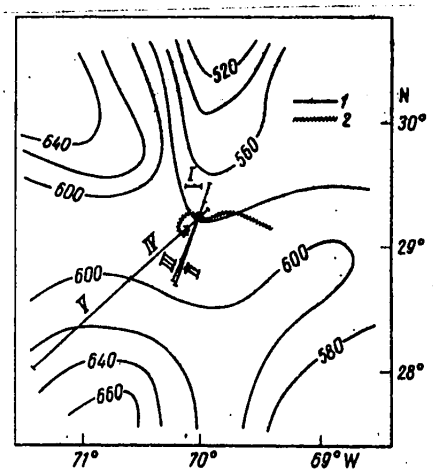

Fig. 3. Thermal trawling runs (1) and drift of scientific research ship "Petr Lebedev" (2) against background of isobaths of 15° isotherm. The depths of the isobaths are given in meters.

The exclusion of the corresponding parts of the record from processing, as well as sectors with a changing direction of drift and relative positioning of array elements in space, resulted in a marked reduction in the informational material; from the entire 2.5-day record it was possible to select only one one-hour (I) and four two-hour segments (II-IV) reproachless in all respects. Samples of the corresponding records and frequency spectra are shown in

Fig. 4,a and b. The spectra were computed on the basis of segments (overlapping by 98%) of 256 (for the first segment - 128) ordinates with subsequent averaging for all segments and 5 frequencies. "Prewhitening" was used (filter of the first differences with subsequent reconstruction of the spectrum by means of dividing the resulting evaluation by the filter transmission function).

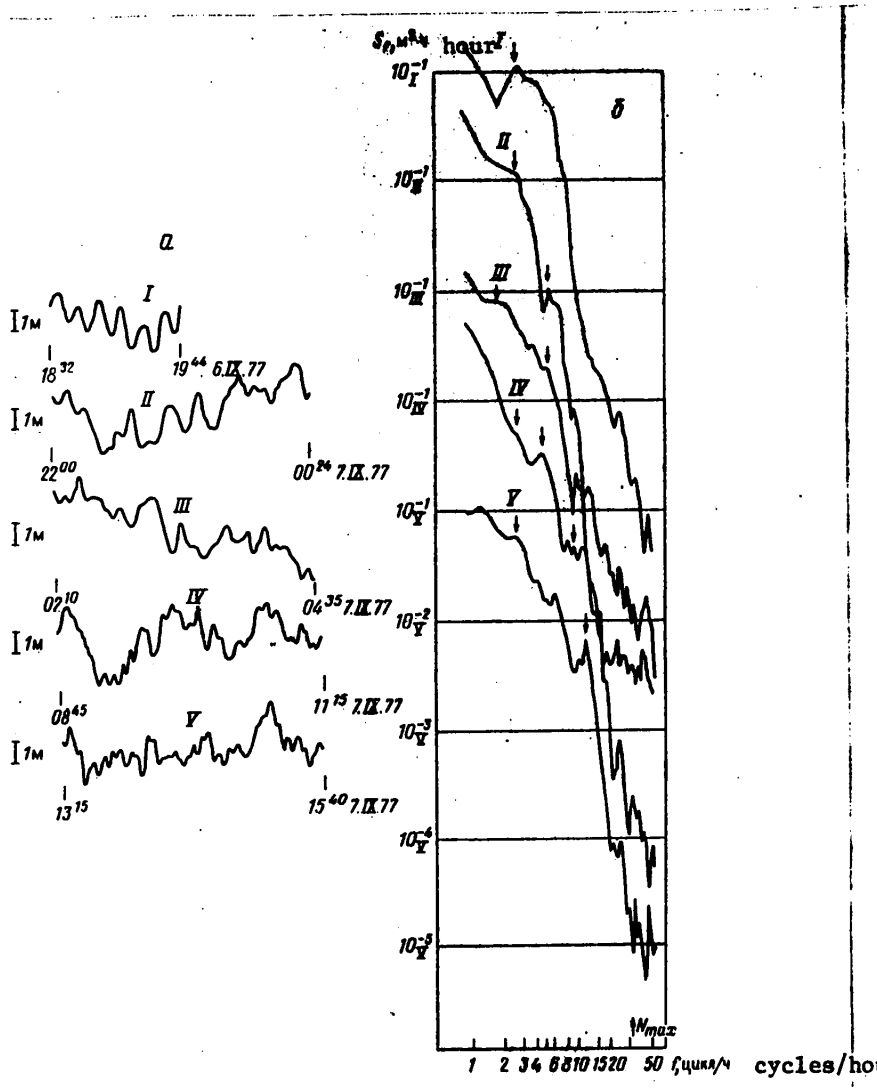

Fig. 4. Samples of records (a) and frequency spectra (b) of drifting array. The scale along the y-axis is given for segment V (lower spectrum). For other segments the scales are given with successive displacements by one order of magnitude. The arrows indicate segments of the spectra subjected to spatial and temporal analysis.

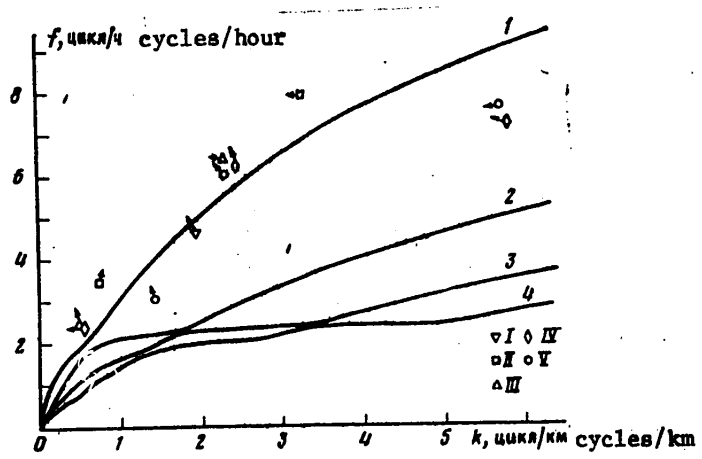

Fig. 5. Position of peaks of evaluations of spatial-temporal spectrum in plane of frequencies f and wave numbers k against background of dispersion curves. (The figures indicate the numbers of the modes.) The arrows indicate the direction of the waves (Of coincides with a direction to the north, Ok -- to the east).

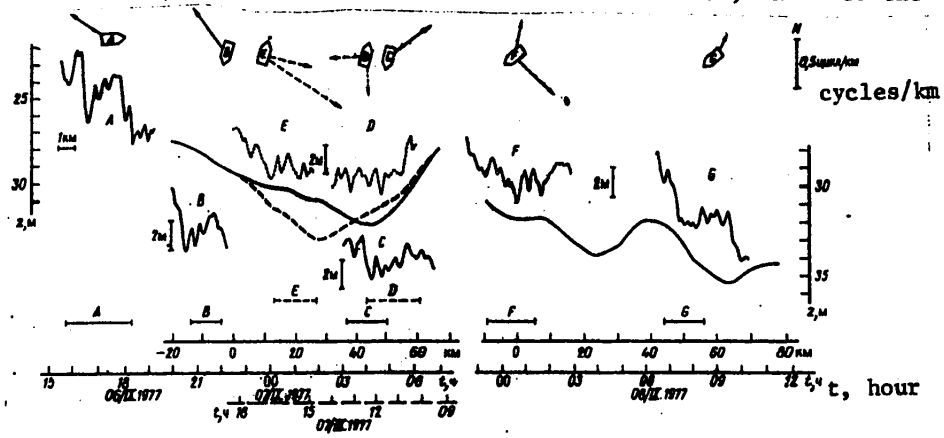

Fig. 6. Smoothed change in depth of thermocline on runs II, IV (solid curves) and III (dashed curve) and trains of internal waves. The arrows on the symbols for the ship indicate the wave vectors of the trains.

Figure 4 shows that only in the first segment was there a train of quasisinusoidal oscillations with a period of $\sim$15 m; nevertheless the remaining segments do not exhibit an appreciable predominance of any one periodicity. However, against the general decreasing background of the corresponding spectra it is possible to discriminate individual insignificant plateaus and peaks for which we obtained evaluations of the spatial-temporal spectrum by the traditional method and by the maximum similarity method [3]; these usually agree well with one another and are characterized by a single-peak structure. The determined value of the wave vector of waves predominating at a given frequency f_g

k $\{k_x, k_y\}$ (k_x, k_y are the stipulated coordinates of the peak of the spectral evaluation in the plane of wave numbers) was used for finding the true frequency f on the basis of the known velocity of motion of the array relative to the water v $\{u, v\}$:

$$f=f_g+\mathbf{kv}=f_g+uk_x+vk_y,$$

where u and v are the velocity components along OX and OY.

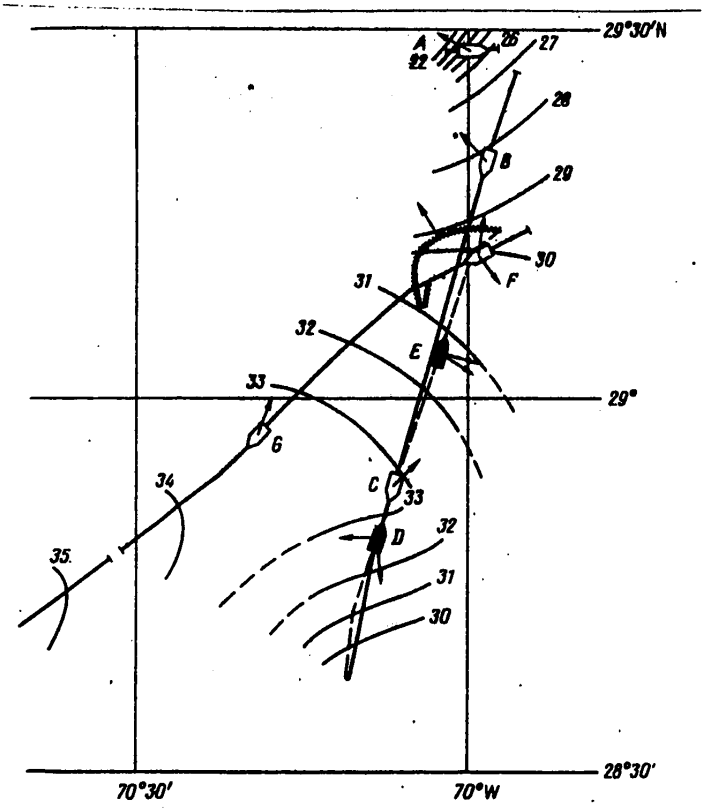

Fig. 7. Isobaths of thermocline and direction of waves in trains on the basis of data from towed (the arrows on the symbols for the ship, placed at the sites where the trains were encountered) and drifting arrays (arrow on the wavy line denoting the drift of the scientific research ship "Petr Lebedev").

The results are summarized in Fig. 5, showing the k, f- coordinates of the peaks of the spatial-temporal spectrum of individual segments against the background of the dispersion curves of the different modes, computed on the basis of data from the "ISTOK" temperature and salinity meter. The direction of the corresponding waves is indicated by the arrows at the k, f- points; the direction to the north coincides with Of, to the east -- with Ok. Most of the points are grouped near the curve of the lower mode, which agrees well with the readings of the stepped sensor, indicating the in-phase character of

the oscillations at different depths. The latter circumstance very convincingly confirms the fact of a predominance of the lower mode because a distributed temperature sensor with a length of 100 m, by virtue of averaging in a thick layer, filters out oscillations of the higher modes and creates the illusion of a predominance of a lower mode in places where this is not actually the case. However, the fact of a dominance of the first mode of high-frequency oscillations in the upper thermocline is not new and is easily explained, since the higher modes attenuate rapidly due to the small thickness of the waveguide.

Table 1

Information on Towing Runs

Run	Time (zone -IV), 1977		Length, km	Means		Mean depth of lower end of DTS, m
	Beginning	End		velocity*, km/hour	course, degrees	
I	1545, 6 Sep	1804, 6 Sep	5.1	2.3	86	61
II	1915, 6 Sep	0746, 7 Sep	97.3	7.9	196	47
III	0903, 7 Sep	1848, 7 Sep	69.0	7.3	18	49
IV	2300, 7 Sep	1209, 8 Sep	94.3	7.2	232	51
V	1231, 8 Sep	0549, 9 Sep	116.8	6.8	226	52

Another fact of interest is that in the entire analyzed frequency range and in all the above-mentioned segments the observed directions of the indicated waves waves are limited to the northwest quadrant. Such a unidirectionality of the wave spectrum, registered with a drifting array, is all the more meaningful in that it contrasts sharply with the broad scatter of directions of waves in trains encountered during the towing of the distributed temperature sensor. In Fig. 6 we illustrate these trains; the smoothed change in depth of the thermocline on runs II, III and IV is illustrated; sectors with trains to which the entire run I is related (train A) are shown at a somewhat enlarged scale. Their position in time and space is represented by segments of a straight line over the axis of time and distances in Fig. 6 and by the ship symbols in Fig. 7. The smoothed curves of change in the depth of the thermocline along the ship's course on the counterruns II and III were matched so that the time axis of run III was directed from right to left (dashed line) and the distance zero corresponds to the point of intersection of runs II, III and IV (see Figures 3 and 7). The absolute depth scale is related to the smoothed curves and to the train A (run 1); only the vertical scale is indicated for the remaining trains. On run V, being a continuation of run IV and not shown in Fig. 6, there was a further deepening of the thermocline to 39 m with some rising (to 35 m) toward the end of the run. A peculiarity of run V was the absence of clearly expressed trains and a general decrease in the dispersion of the high-frequency oscillations.

A comparison of counterruns II and III makes it possible to evaluate the time variability of the smoothed depth of the thermocline. The characteristic flexure of the thermocline, observed on both runs, was displaced to the north

* The table gives the velocity of antenna motion relative to the water since it, and not absolute velocity, is important for excluding the Doppler effect.

Table 2

Data From Analysis of Trains

Train	Time of segment beginning - end (1977)	Computation parameters				f_g, cycles/hour	k, cycles/km	α,°	f, cycles/hour
		M	N	ΔN	n				
A	1545-1722, 6 September	194	64	-	3	3.8	0.45	296	2.9
B	2056-2203, 6 September	136	128	127	9	3.8	0.57	320	1.0
C	0339-0448, 7 September	140	128	127	13	3.8	0.46	52	1.5
D	1013-1206, 7 September	226	128	118	10	2.8 3.8	0.37 0.39	270 175	2.1 1.0
E	1442-1607, 7 September	170	128	124	11	2.8 3.8	0.91 0.64	118 110	1.4 1.0
F	2340-0125, 7 September	211	128	119	10	3.8 2.8	0.37 0.54	13 133	1.7 2.1
G	0700-0820, 8 September	160	128	126	17	2.8	0.31	30	2.5

Note. M is the total number of ordinates in the segment (Δ t = 30 sec), N is the number of ordinates in the segment; Δ N is the overlapping of adjacent segments; n is the number of overlapping segments; f_g and f are the Doppler and true frequencies; α is wave direction. "Prewhitening" was used; averaging was carried out only by segments.

during the time between runs at a mean rate of 0.5 m/sec, which is too small for internal waves of such a length (100 km), which could be considered the reason for the detected variability. Evidently here there are synoptic inhomogeneities of the thermocline transported by the current. Assuming that all the other smoothed changes observed on runs I-V were caused by relatively slowly moving synoptic inhomogeneities, we attempted to construct the pattern of depth of the thermocline with time and at the place of towing, shown in Fig. 7.

We will now return to the trains of short waves A-G encountered during towing and shown in Fig. 6. A common feature of these trains, consisting of several waves, is the close affinity with a marked deepening of the thermocline, which resembles the situation arising during the nonlinear decay of waves over shallow water [4]. The highest waves (up to 3 m) were discovered on run I (train A); the height of the waves in the remaining trains did not exceed 1.5-2 m. (In a comparison of the apparent periods of the waves in different trains it must be taken into account that the rate of towing on run I was 3-4 times lower than on the remaining runs.)

General information on the trains and parameters of the waves, determined by means of spatial-temporal spectral analysis by the maximum probability method, is given in Table 2 and the corresponding wave vectors k are shown in the form of arrows near the schematic representations of the ship in Fig. 6. As a comparison, at the upper right we have shown a vector directed to the north whose length corresponds to $|k| = 0.5$ cycle/km. In those cases when the time periodogram of the train contained not one, but two peaks close in value, as was the case in trains D, E and F, two wave vectors have been shown, this reflecting the complex spatial-temporal structure of the train.

The lengths of the waves in the trains for the most part vary about 2 km; the true periods on the average were close to a half-hour*. No direction can be called predominant, in contradiction to the observations in the case of a drifting array. The reason for such an inconsistency in the results must evidently be sought in the spatial variability of the directions since the measurements with the drifting array were carried out in a localized region, whereas towing was carried out over a relatively great area (see Fig. 7). In particular, this is indicated by the good agreement between the directions of the waves in trains B and F encountered during the time of towing near the place of drift of the scientific research ship "Petr Lebedev" and measurement data from the latter.

The directions of the waves in different trains, registered with the towed distributed temperature array, can be explained by a comparison of the observed pattern with the relief of the thermocline (Fig. 7). In actuality, when waves of any direction run onto a sloping thermocline their direction under the influence of refraction will approach the normal to the thermocline isobaths, much as is the case with surface waves in the coastal zone. Refraction

* The high rate of towing (in comparison with the phase velocity of the waves) is responsible for the low accuracy in evaluating the true frequency; this evidently also explains the great scatter of the determined periods and phase velocities.

occurs because the phase velocity C of the considered waves for all practical purposes is determined only by the depth of the thermocline, and not by the total depth of the ocean. (In a two-layer case, for example, $C \approx \sqrt{gh\Delta\rho/\rho}$, where g is the acceleration of gravity, h is the depth of the interface between layers with the densities ρ_1 and ρ_2, $\Delta\rho = \rho_2 - \rho_1$, $\rho \approx \rho_1$, ρ_2. With the observed differences in the depth of the thermocline the phase velocity changes by 20%. This evidently also explains the stable predominance of the northwesterly moving waves discovered by the scientific research ship "Petr Lebedev," which drifted near the steep slope of the thermocline, rising in this direction.

If the height of the oncoming waves is not negligible in comparison with the depth of the thermocline the nonlinear effects determined by the nonlinearity parameter $\varepsilon = a/h$, where a is wave amplitude, become important. This parameter, in essence, determines the difference in velocities at the crest and in the trough of an internal wave traveling along a shallow thermocline. Since, in contrast to a surface wave in shallow waters, an internal wave is not "braked" by the bottom, but by the ocean surface, its trough, more distant from the surface, travels with the velocity C_{tr}, greater than the velocity of the crest C_{cr}, $C_{tr} = \sqrt{g\Delta\rho(h+a)/\rho} > C_{cr} = \sqrt{g\Delta\rho(h-a)/\rho}$, and overtakes the crest, increasing the steepness of the rear slope of the wave. Finally, the rear slope of the wave acquires the character of an internal front (bora), accompanied by a singular train of short waves which are "released" by the bora as it moves and gradually lag behind it due to dispersion. A similar phenomenon over a sloping shallow bottom was examined in [4] and has been observed repeatedly in nature (for example, see [5, 6]).

It is understandable that the described effects are the stronger the shallower the thermocline and possibly precisely for this reason the trains were not observed on run V, where the thermocline depths were maximum (35-39 m) and the slopes were minimum. Assuming the amplitude of the bora-forming waves to be 3 m, we obtain $\varepsilon_{max} = 3/22 = 0.14$ (at the beginning of run I) and $\varepsilon_{min} = 3/39 = 0.08$ (in the middle of run V), that is, the nonlinearity parameter changes by almost a factor of 2 with a rather significant mean value. A definite role is evidently also played by the decrease in the slopes of the thermocline because the narrowing of the angular spectrum of waves, as a result of refraction, is the weaker the lesser the slope of the thermocline and therefore whereas large slopes of the thermocline lead to a refraction concentration of waves along one direction (upslope) and thereby lead to an increase in the height of bora-forming waves, in the case of small slopes these effects are expressed to a lesser degree, that is, nonlinear phenomena also attenuate.

In general, the following picture is observed: running onto a sloping thermocline, the waves, under the influence of refraction, acquire a direction upslope and experience a nonlinear transformation, leading to the formation of a bora and accompanying trains of short waves. Naturally, the direction of the waves in these trains is close to the direction of the bora-forming waves propagating upslope. Such bora-forming waves can be present also in the background, possibly quasi-isotropic field of internal waves, which becomes anisotropic, being refracted over irregularities of the thermocline. Precisely the anisotropization of the background field over the thermocline, rising

toward the northwest, evidently also explains the observed stable predominance of northwesterly directions of the waves in a broad frequency range of a more or less monotonically decreasing spectrum (see Figures 4 and 5). The simultaneous existence of two systems of waves in some trains (D, E, F) agrees with the earlier observed facts of a complex structure of the trains accompanying the bora [5].

The proposed hypothesis of a correlation of the trains of short-period internal waves frequently encountered in the upper layer of the ocean and the relief of the thermocline finds indirect confirmation in the well-known facts of intensification of such waves near fronts (for example, see [7]). It is interesting that the considered mechanism even explains such earlier-noted peculiarities of short-period internal waves as the possibility of their quasi-standing character, even under the conditions prevailing in the open ocean [1], to which must be added the refraction of background isotropic waves on extended rises of the thermocline.

Thus, the phenomenon of formation of trains of powerful waves (related to the shelf), in the case of nonlinear decay of an internal tidal wave in shallow water, possibly has its analogy in the open ocean in the form of formation of trains over the thermocline with a changing depth. Since synoptic nonuniformities of depth of the upper thermocline occur widely, the development of more or less significant trains of short-period internal waves, directed up the slope of the thermocline, can be a frequently encountered phenomenon in the ocean.

BIBLIOGRAPHY

1. Sabinin, K. D. and Serikov, A. N., "Spatial-Temporal Parameters of Short-Period Internal Waves in the Indian Ocean," GIDROFIZICHESKIYE I OPTICHESKIYE ISSLEDOVANIYA V INDIYSKOM OKEANE (Hydrophysical and Optical Investigations in the Indian Ocean), Moscow, Nauka, pp 13-27, 1975.

2. Sabinin, K. D., "Use of Distributed Temperature Sensors for Measuring Internal Waves," POVERKHNOSTNYYE I VNUTRENNIYE VOLNY (Surface and Internal Waves), Sevastopol', MGI AN UkSSR, pp 134-145, 1978.

3. Kozubskaya, G. I. and Konyayev, K. V., "Adaptive Spectral Analysis of Random Processes and Fields," IZV. AN SSSR: FAO (News of the USSR Academy of Sciences: Physics of the Atmosphere and Ocean), Vol 13, No 1, pp 61-71, 1977.

4. Lee, C. Y. and Beardsley, R. C., "The Generation of Long Nonlinear Internal Waves in a Weakly Stratified Shear Flow," J. GEOPHYS. RES., Vol 79, No 3, pp 453-462, 1974.

5. Ivanov, V. A. and Konyayev, K. V., "Bora in the Thermocline," IZV. AN SSSR: FAO, Vol 12, No 4, pp 416-423, 1976.

6. Apel, J. R., Byrn, H. M., Proni, J. R. and Harnell, R. L., "Observations of Oceanic Internal and Surface Waves From Earth Resources Technology Satellite," J. GEOPHYS. RES., Vol 80, No 6, pp 865-881, 1975.

7. Beckerly, J. C., "Doppler Shifted Internal Waves Relative to a Tower Sensor in a Thermal Front Region," DEEP SEA RES., Vol 22, No 3, pp 197-200, 1975.

5303
CSO: 1865/152

UDC 551.461

EFFECT OF SELF-ENHANCEMENT OF GRAVITATIONAL ANOMALIES IN GRADIENT MEDIA

Moscow DOKLADY AKADEMII NAUK SSSR in Russian Vol 263, No 5, Apr 82 (manuscript received 22 Oct 81) pp 1092-1094

[Article by S. S. Ivanov, Institute of Oceanology imeni P. P. Shirshov, USSR Academy of Sciences, Moscow]

[Text] One of the promising directions in the development of marine geophysics at the present time is the study and allowance for the influence of some fine effects arising due to different processes in the water layer of the ocean. This direction can also be traced in such methods as magnetometry [1] and gravimetry [2, 3] which in the past have traditionally not taken the influence of the water layer into account. In this article we wish to note one effect not described earlier associated with the restructuring of the density structure of the ocean water layer in the anomalous gravitational field.

We will visualize that in a homogeneous gravitational field characterized by a constant vertical potential gradient ($\partial U/\partial z = \text{const} = \gamma$) and, accordingly, by parallel and equidistant equipotential surfaces, there is some inhomogeneous medium of a low viscosity in which for some reasons (thermal factors, compressibility in the gravity field, etc.) there is a vertical density gradient whose value will also be considered constant ($d\sigma/dz = \text{const}$). Surfaces of equal densities (isopycnic surfaces) will coincide with the isopotential surfaces, that is, in this case will be represented by horizontal planes (Fig. 1). At some point in this medium we will place the origin of coordinates (the z-axis is directed vertically downward) and at this point we will place the values of the gravitational potential and density respectively U_0 and σ_0. Then for each point in the medium these values will be expressed as

$$U = U_0 + \gamma z, \quad \sigma = \sigma_0 + (d\sigma/dz)z.$$

We will examine what will occur if at the origin of coordinates we place some point mass M, which we call an anomaly. Its appearance gives rise to an anomalous gravitational field having the potential $W_a = fM/r$ (where f is the gravitational constant, r is the distance to the origin of coordinates) and the gravitational acceleration $\Delta g_a = -fMz/r^3$. In turn, the appearance of anomalous potential leads to the vertical displacement of isopotential surfaces by the value $\zeta = -W_a/(\gamma+\Delta g_a)$. The isopycnic surfaces are displaced by the same value, due to the low viscosity of the medium following the isopotential surfaces. As a result of this, at each point in the medium there will be an increase in density caused by displacement of the isopycnic line by the value

$\Delta\sigma = -\zeta\,(d\sigma/dz)$ and accordingly there will be an elementary additional mass $dm = \Delta\sigma dv$. The total additional mass will be determined by integration in a volume bounded by a sphere of some finite radius R. Introducing the natural assumption that $\Delta g_a \ll \gamma$, we obtain

$$m = \iiint_{v_R} \Delta\sigma dv = \frac{fM}{\gamma}\frac{d\sigma}{dz}\iiint_{v_R}\frac{1}{r}dv = \frac{fM}{\gamma}2\pi R^2\frac{d\sigma}{dz}. \qquad (1)$$

Expression (1) shows that the appearance of the anomalous mass M in the gradient medium causes a restructuring of the density field and the formation because of this of the additional mass m, whose value is dependent on the M parameter, and also on the extent of the region occupied by the medium, as well as the value of its density gradient. The influence of this additional mass is expressed in the appearance of an additional gravitational field, spherically symmetric and concentric with the anomalous field of the mass M and having the potential $W_{add} = fm/R$ and the acceleration $\Delta g_{add} = -fmz/R^3$.

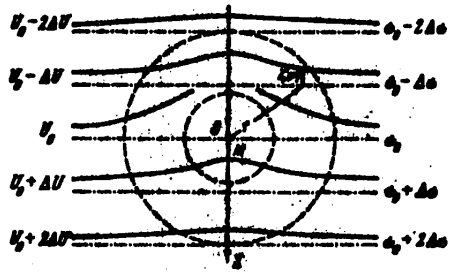

Fig. 1. Vertical section of gradient density medium in gravitational field. The dot-dash lines represent isopotential (and isopycnic) surfaces corresponding to a homogeneous field; the solid lines represent the same in the presence of an anomalous mass M; the dashed lines represent isolines of anomalous potential.

Thus, it appears that the gravitational field of an anomalous mass (potential and its derivatives) in a gradient medium somewhat exceeds in its intensity a field of the same mass in a medium homogeneous in density. Since this effect arises due to a corresponding organization of the medium occurring under the influence of the anomalous mass itself, we called it the effect of self-enhancement of gravitational anomalies in gradient media.

Two circumstances should be emphasized. First, the noted effect arises in both gradient and in density-stratified media, in a limiting case -- in a two-layer medium. The sole condition for the appearance of the effect in this case is that the viscosity of matter must be sufficiently small that the density boundaries will adhere to the equipotential surfaces of the gravity field. Second, this effect also arises in a case when the anomalous mass is situated outside the gradient medium. In other words, the additional mass in the gradient or stratified medium arises under the influence of any gravitating object disrupting the homogeneity of the field in this medium.

It follows from the cited computations that the following expression will be correct at the boundary of the spherical region

[ДОП = add]

$$\frac{W_{доп}}{W_0} = \frac{\Delta g_{доп}}{\Delta g_0} = \frac{m}{M} = \frac{2\pi f}{\gamma} \frac{d\sigma}{dz} R^2.$$

This expression makes it possible to evaluate the described effect in some specific cases. In particular, we will examine its possible manifestation in an ocean whose water thickness can be represented as a gradient medium in density respects.

Assuming for $d\sigma/dz$ a value $1 \cdot 10^{-6}$ g·cm^{-4} (frequently observed in the ocean, although somewhat exaggerated for the water layer as a whole) [4], we find that for R = 5 km the relative self-enhancement of gravitational anomalies at the ocean surface should be about $1 \cdot 10^{-4}$, that is, 0.01% (an anomaly of 100 mgal is intensified by 0.01 mgal). This value, to be sure, is too small to be of importance for experimental gravimetric investigations in the ocean. However, for oceanological practice another aspect of the described effect can be important, specifically, the increase in the density of sea water horizontally in the direction of greater values of the anomalous gravitational field necessary for its appearance.

Elementary computations show that the free-air anomalies observed at the ocean surface with a characteristic amplitude of 50 mgal [5] correspond to an increment of gravity potential in the water layer of about $1 \cdot 10^5$ sec^{-2}, that is, the magnitude of displacement of the isopotential (and isopycnic) surfaces is about 10^2 cm. With the above-mentioned sea water density gradient (vertically) this gives a density increment (horizontally) of about $1 \cdot 10^{-4}$ g·cm^3 or in the first place after the decimal point in the so-called nominal density of sea water (a parameter adopted in oceanology and equal to $\sigma_y = (\sigma - 1) \cdot 10^3$ g·cm^{-3}). Such changes are extremely significant and without question can be detected during hydrophysical measurements in the ocean and taken into account in computing currents by the dynamic method [6, 7]. It should be noted that there are some still unpublished data on the presence of a quite close correlation between the density values for sea water at different horizons and gravity anomalies (A. M. Boyarinov, S. V. Protsayenko, personal communication); these can serve as unquestionable support in favor of the existence of the self-enhancement effect for gravitational anomalies in the ocean.

An important feature in the appearance of the described effect in the ocean is that gravitating objects, including those situated deep beneath the ocean floor, lead to the forming of an inhomogeneous structure of isopycnic (and accordingly, isobaric) surfaces in the water layer, as a result of which there are unequal conditions for the passage of water masses associated with gravitational anomalies. It is easy to see that more favorable conditions for this prevail in regions where the distance between these surfaces is maximum, that is, in places where the additional gravitational potential is minimum. In this connection it can be expected that ocean currents in principle should gravitate toward regions of negative gravitational anomalies. This effect probably should be manifested more strongly for weak currents having a relatively small kinetic energy and most strongly for the trajectories of movements of isolated

water masses, such as individual ocean eddies.

It follows from what has been said that the effect of self-enhancement of gravitational anomalies must be manifested most clearly in the ocean. A study of this effect and its corollaries by hydrophysical methods will be of great importance for dynamic oceanology.

BIBLIOGRAPHY

1. Sochel'nikov, V. V., OSNOVY TEORII YESTESTVENNOGO ELEKTROMAGNITNOGO POLYA V MORE (Principles of the Theory of the Natural Electromagnetic Field in the Sea), Leningrad, Gidrometeoizdat, 1979.

2. Ivanov, S. S., DAN (Reports of the USSR Academy of Sciences), Vol 253, No 2, p 312, 1980.

3. Demenitskaya, P. M., Ivanov, S. S. and Litvinov, E. M., YESTESTVENNYYE FIZICHESKIYE POLYA OKEANA (Natural Physical Fields in the Ocean), Leningrad, Nedra, 1981.

4. OKEANOLOGIYA. FIZIKA OKEANA. GIDROFIZIKA OKEANA (Oceanology. Ocean Physics. Ocean Hydrophysics), Moscow, Nauka, 1978.

5. Dehlinger, P., MARINE GRAVITY, Amsterdam, Oxford, N. Y., 1978.

6. Zubov, H. H. and Mamaev, O. I., DINAMICHESKIY METOD VYCHISLENIYA ELEMENTOV MORSKIKH TECHENIY (Dynamic Method for Computing the Elements of Sea Currents), Leningrad, Gidrometeoizdat, 1956.

7. Burkov, V.A., OBSHCHAYA TSIRKULYATSIYA MIROVOGO OKEANA (General Circulation of the World Ocean), Leningrad, Gidrometeoizdat, 1980.

5303
CSO: 1865/147

UDC 550.348.432

SEISMIC NOISE AT OCEAN FLOOR

Moscow DOKLADY AKADEMII NAUK SSSR in Russian Vol 263, No 5, Apr 82 (manuscript received 14 Dec 81) pp 1098-1101

[Article by Yu. P. Neprochnov, V. V. Sedov and A. A. Ostrovskiy, Institute of Oceanology imeni P. P. Shirshov, USSR Academy of Sciences, Moscow]

[Text] Recently seismic investigations in the ocean have been requiring use of increasingly more complex observation systems, including up to 10 or more bottom seismographs. The rational planning of these extremely costly experiments requires information on the level and spectral composition of bottom seismic noise, limiting the effective response of receiving-recording apparatus situated at the ocean floor or near it. The vigorous development of technology and the method for seismic investigations with bottom seismographs during the last 20 years has favored the registry of bottom noise phenomena in the USSR and abroad [1-5]. However, this information, obtained by the scientists of different countries with the use of various kinds of apparatus, with the use of different processing methods and forms of representation of the noise spectra, is difficult to compare and is frequently contradictory.

At the Institute of Oceanology, USSR Academy of Sciences, seismic investigations with bottom seismographs have been carried out since 1965. Although the principal purpose of these studies was deep seismic sounding of the earth's crust and upper mantle, incidentally extensive material on bottom noise was obtained in the frequency range 2-20 Hz. The investigations covered all the principal tectonic structures of the floor of the world ocean -- internal and marginal seas, ocean basins and major rises within their limits, mid-oceanic ridges and the areas surrounding them, and block ranges. The observations were made under the most diversified hydrometeorological conditions. Noise was registered using instruments of the same type (bottom seismographs designed at the Physics Faculty of Moscow State University and the Institute of Oceanology, USSR Academy of Sciences) and processed by the same method, making it possible to carry out a joint analysis and statistical processing of the experimental spectra.

The analysis was made using the 59 most representative magnetic records of seismic noise obtained on expeditions of the Institute of Oceanology, USSR Academy of Sciences, during the period from 1973 through 1979. The distribution of these records by research regions is shown in Table 1. The bottom seismographs were placed at depths from 210 to 6520 m. The duration of the continuous registry at the bottom varied from 1 to 10 days, depending on the purpose of the experiment

Table 1

Regions of Seismic Investigations in Which Records of Bottom Noise Were Obtained

Region	Depth, m	Number of records	Scientific research ship (number of voyage)	Year
Black Sea	1600	1	"Akademik Vavilov"	1973
	2200	3		
Caspian Sea	287	1	"Bakuvl"	1974
	357	1		
Barents Sea	960	1	"Akademik Kurchatov" (23)	1976
Norwegian Sea	1200	1	Same	1976
Sea of Okhotsk	210	1	"Dmitriy Mendeleyev" (17)	1976
	3200	1		
East Indian Ocean Ridge	1800-4000	13	"Vityaz'" (58)	1976
Mid-Atlantic Ridge	3600-3900	3	"Akademik Kurchatov" (20)	1975
Region of Vema fault				
Mid-Atlantic Ridge	4220-4420	2	"Akademik Kurchatov" (24)	1977
Region of Cane fault				
Mid-Atlantic Ridge,	4200	2	Same	1977
slope, region of Atlantis fault	5500	2		
East Pacific Ocean Rise	3240-6520	7	Same	1977
Shatskiy Rise	4170-5100	4	"Dmitriy Mendeleyev" (21)	1978
Hess Rise	2190-2770	5	"Dmitriy Mendeleyev" (23)	1979
Northwestern Basin of Pacific Ocean	5400-5650	4	"Dmitriy Mendeleyev" (21, 23)	1978-1979
Emperor fault	5035-5240	4	"Dmitriy Mendeleyev" (23)	1979
Northeastern Basin of Pacific Ocean	5100	2	Same	1979
East Carolines Basin	3800	1	"Dmitriy Mendeleyev" (21)	1978

and the method used. The seismic noise was analyzed on segments of the records of bottom seismographs with an extent of about 3 minutes, free of seismic waves caused by known artificial and natural sources (shots, pneumatic radiations and ship's noise during deep seismic sounding in the region of the experiment, earthquakes).

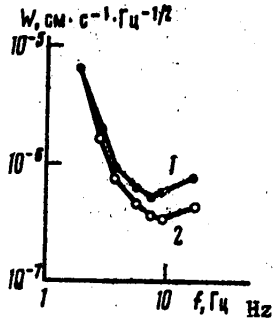

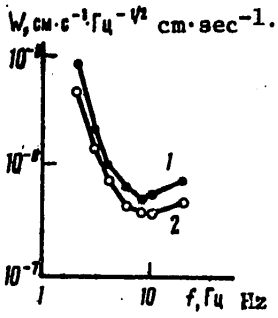

Fig. 1. Fig. 2. Fig. 3.

Fig. 1. Statistically mean (1), maximum (2) and minimum (3) spectra of bottom seismic noise in frequency range 2-20 Hz; 4) spectrum of bottom seismograph amplifier noise.

Fig. 2. Dependence of mean level of bottom seismic noise on thickness of uncompacted sediments in neighborhood of placement of bottom seismograph. 1) thickness greater than 300 m; 2) thickness less than 300 m.

Fig. 3. Dependence of mean level of bottom seismic noise on measurement season; 1) spring and autumn; 2) summer.

The spectra of bottom seismic noise were obtained using an analog 1/3-octave spectrum analyzer, type NR-8054A, which makes it possible to obtain the square root of the spectral density of intensity of the investigated signal W in the frequency range 1-60 Hz. The relative error in computing W averaged $\sim$30% with a reliability coefficient 0.95, which was adequate for the purposes of this study.

Most of the registry points constituted a group of bottom seismographs situated in a particular research region, but the groups themselves were spaced quite widely, which makes it possible to judge the characteristics of bottom noise

not only of individual parts, but also of the entire world ocean.

Figure 1 shows the statistically mean spectrum generalized for all the determined values. The spectral density values at frequencies of 2, 3, 4, 6, 8, 10 and 20 Hz were computed as the mean arithmetical value of 59 individual spectra. Also shown are the envelopes of the minimum and maximum spectral density values at the mentioned frequencies and the noise spectrum of the mentioned bottom seismograph amplifier. The mean spectrum has a minimum at a frequency of 10 Hz, where the spectral density is $4.5 \cdot 10^{-7}$ cm·sec^{-1}·Hz$^{-1/2}$. In the direction of the low frequencies the noise level increases sharply and at a frequency of 2 Hz its mean spectral density is $7.5 \cdot 10^{-6}$ cm·sec^{-1}·Hz$^{-1/2}$; there is also a relatively small rise in the level of bottom noise in the direction of the high frequencies. The mean curve agrees well with the spectra obtained by T. Asada and H. Shimamura [5].

Figure 1 shows that the deviations of the spectra of real noise from the statistical mean can be significant (for the limiting case by a factor of 6), taking in a range of 1-1.5 orders of magnitude. The lower curve is at the level of weakest bottom noise registered earlier and analyzed by D. D. Prentiss and J. Ewing [2]; the range of change of spectral density for it was from 10^{-6} to $5 \cdot 10^{-8}$ cm·sec^{-1}·Hz$^{-1/2}$ at frequencies of 2 and 10 Hz respectively. The upper curve passes near the spectra obtained by L. N. Rykunov and V. V. Sedov [1] and the lowest spectra in level, obtained by H. Bradner [3].

The results of observations in regions with different seismogeological conditions made it possible to analyze the dependence of the level of bottom noise on the thickness of the sedimentary cover at the registry points. Two mean spectra were computed for this purpose: one of these was obtained using data from the registry of noise in regions with a thickness of sediments less than 300 m (0-300 m), whereas the other was based on data for regions with a thickness of sediments greater than 300 m (300-4000 m). Information on the thickness of sediments in the regions of placement of bottom seismographs was obtained using materials from continuous seismic profiling and deep seismic sounding on corresponding expeditions; the sedimentary stratum includes rocks with velocities of propagation of longitudinal waves not greater than 2.5-3.0 km/sec. The limiting value for the thickness of sediments of 300 m was selected because it divided the available archives of 59 spectra approximately in half. This made it possible to compute the mean spectra with a greater accuracy than each individual spectrum, thereby making it possible to consider the difference in the resulting mean spectra to surpass the errors in measuring them. Figure 2 shows that the mean level of bottom seismic noise increases with an increase in the thickness of the sediments at the registry point; this dependence becomes clearer for the high-frequency noise components. The dependence of the level of bottom noise on the thickness of sediments agrees with the results of a study by G. V. Latham and C. H. Sutton [4], where it was noted that the presence of unconsolidated sediments on the ocean floor leads to a concentration of seismic energy in this layer and a considerable increase in the level of bottom noise.

We also analyzed the dependence of the mean level of bottom seismic noise on hydrometeorological conditions. As a point of departure we used the well-known fact of an intensification of cyclonic activity in the oceans in autumn and

spring in comparison with the summer period. A study of the experimental data indicated that in many cases more intense but briefer changes in the noise level caused by other factors (bottom currents, sea transport, etc.) are superposed on seasonal fluctuations of the mean noise level. Thus, the averaging of the 59 spectra at our disposition made it possible for each frequency to discriminate "long-period" fluctuations of bottom noise (period of about 3 months) of a low intensity against a background of its more intense and briefer variations. Figure 3 shows the mean spectra for spring and autumn (averaging for 24 spectra), and also for summer (averaging for 35 spectra). It can be seen that during periods of intensification of cyclonic activity in the oceans the mean level of the bottom seismic noise increases by a factor of approximately 1.5 in the investigated frequency range. The influence of a local cyclone on the level of bottom seismic noise directly in the region affected by a cyclone was examined in a separate study [6].

In order to refine and supplement the dependences between bottom seismic noise on seismogeological and hydrometeorological conditions which have now been clarified it is necessary to recommend the formulation of planned expeditionary investigations of this problem, preferably in a broader frequency range (from 0.1 to 100 Hz).

BIBLIOGRAPHY

1. Rykunov, L. N. and Sedov, V. V., IZV. AN SSSR: FIZIKA ZEMLI (News of the USSR Academy of Sciences: Physics of the Earth), No 7, pp 30-39, 1965.

2. Prentiss, D. D. and Ewing, J., BULL. SEISMOL. SOC. AMER., Vol 53, No 4, pp 765-781, 1963.

3. Bradner, H., Dodds, J. G. and Foulks, R. E., GEOPHYSICS, Vol 30, No 4, pp 511-526, 1965.

4. Latham, G. V. and Sutton, C. H., J. GEOPHYS. RES., Vol 71, No 10, pp 2545-2573, 1966.

5. Asada, T. and Shimamura, H., "The Geophysics of the Pacific Ocean Basin and Its Margin," AMER. GEOPHYS. UNION, GEOPHYS. MONOGRAPH, Vol 19, p 286, 1976.

6. Ostrovskiy, A. A., Manuscript deposited at the All-Union Institute of Scientific and Technical Information, No 3056-80, 1980, 14 pages.

5303
CSO: 1865/147

UDC 551.465

INFLUENCE OF TURBULENCE INTERMITTENCE ON FORMING OF OCEAN SURFACE STRUCTURE

Moscow DOKLADY AKADEMII NAUK SSSR in Russian Vol 263, No 5, Apr 82 (manuscript received 3 Aug 81) pp 1225-1229

[Article by V. S. Belyayev and R. V. Ozmidov, Institute of Oceanology imeni P. P. Shirshov, USSR Academy of Sciences, Moscow]

[Text] Ocean turbulence, together with other factors, plays an important role in forming of ocean surface characteristics. Turbulent heat conductivity of water is one of the important parameters determining ocean surface temperature. Turbulent velocity fluctuations, interacting with wave movements of fluid, exert an influence on roughness of the water surface. However, the concepts concerning the discontinuous distribution of turbulence in the ocean prevailing only recently should lead to the conclusion that there is a uniformity of these manifestations of turbulence over great expanses of the ocean. But extensive observations of ocean turbulence carried out during recent years have shown that it is characterized by a strong intermittence: zones of turbulent fluid alternate in the ocean with sectors in which the observed regime of water motion is close to laminar [1]. In this connection, manifestations of turbulence at the ocean surface should have a "spotty" structure which, in general, can be detected by both contact and remote methods.

In [2] the author proposed a model of vertical turbulent exchange in the ocean in the presence of turbulence intermittent with depth. According to this model the mean value of the coefficient of vertical exchange $\overline{K}$ is described by the expression

$$\overline{K} = cn_1 \int_0^\infty \int_0^\infty h^2 \sigma\, p(h, \sigma)\, dh\, d\sigma, \qquad (1)$$

where h is the thickness of the turbulent layer of fluid, σ is the intensity of turbulence in the layer, $p(h, \sigma)$ is the joint probability distribution function of the parameters h and σ, n_1 is the mean number of the turbulent layers in a unit interval of depths (the Poisson law parameter for the distribution of turbulent layers in the ocean), c is a dimensionless universal constant of the order of 0.1. Using the presently available experimental data on the function $p(h, \sigma)$ and the parameter n_1 in [2] the authors obtained evaluations of the $\overline{K}$ values varying for different regions of the ocean from a few to several tens of cm^2/sec. We note that expression (1) for $\overline{K}$ was obtained in [2], in essence under the condition of smallness of the lifetime of the turbulent

layers in comparison with the characteristic time of propagation of passive impurities in the upper layer of the ocean.

We will evaluate the possible statistical scatter of the K values caused by the turbulence intermittence effect. In the case of a Poisson distribution of turbulent layers with depth the dispersion of the coefficient of vertical turbulent exchange

$$D(K) = c^2 n_1 \int_0^\infty \int_0^\infty h^3 \sigma^2 p_{\sigma h}(\sigma, h)\, d\sigma\, dh \tag{2}$$

and evaluations of the mean square scatter of K values in accordance with formula (2) with the use of the experimental data enumerated in [2] in order of magnitude constitute $\overline{K}$.

We will examine how variations of the coefficient of vertical turbulent exchange are manifested in the temperature field of the ocean surface. We will consider the coefficient of turbulent thermal diffusivity K_T to be proportional to the coefficient of turbulent exchange of momentum K with the proportionality factor α (of the order of 0.1) and we will examine the nonstationary problem of the propagation of heat from the surface into the depths of the ocean, described by the equation

$$\frac{\partial T}{\partial t} = \alpha K \frac{\partial^2 T}{\partial z^2}, \tag{3}$$

where T is water temperature, z is the vertical coordinate with the origin of coordinates at the ocean surface, t is time, reckoned from some initial time $t_0 = 0$.

As the boundary conditions for equation (3) we will assume that

$$\alpha K \frac{\partial T}{\partial z}\bigg|_{z=0} = \begin{cases} 0 & \text{when } t < t_0 = 0 \\ -q/C_p\rho & \text{when } t \geqslant t_0 = 0 \end{cases}; \quad T(z,t)\Big|_{z\to\infty} = 0, \tag{4}$$

here q is the heat flow through the ocean surface, ρ is water density and C_p is its heat capacity at a constant pressure.

Since we are interested in the deviations of temperature from some equilibrium distribution, then, without reducing the universality of the problem, we will assume an initial temperature distribution in the form

$$T(z,0) = 0. \tag{5}$$

The solution of equation (3) with the boundary conditions (4) and the initial condition (5) has the form

$$T(z,t) = \frac{2q\sqrt{t}}{C_p \rho \sqrt{\alpha K}} \left\{ \frac{1}{\sqrt{\pi}} \exp(-\zeta^2) - \zeta\,[1 - \operatorname{erf}\zeta] \right\}, \tag{6}$$

where

$$\operatorname{erf}\zeta = \frac{2}{\sqrt{\pi}} \int_0^{\zeta} e^{-\xi^2}\, d\xi; \quad \zeta = \frac{z}{2\sqrt{\alpha K t}},$$

and for the ocean surface

$$T(0,t) = \frac{2q\sqrt{t}}{C_p \rho \sqrt{\pi \alpha K}}. \tag{7}$$

Figure 1 shows curves of dependence of ocean surface temperature on time with several values of the coefficient $K_T + \alpha K$. The values of the determining parameters for the computations were: $q = 10^{-3}$; 10^{-4} cal/cm^2·sec (the left and right scales along the y-axis), $\rho = 1$ g/cm^3, $C_p = 1$ cal/g·°C. With the course of time the range of temperature change of the ocean surface with different K_T values expands: for example, with t = 1 hour it is 0.02-1.81°C, and with t = 10 hours it is already 0.07-5.72°C.

The depth of penetration of disturbances of the temperature field z_0 is determined from the condition

$$\frac{T(z_0, t)}{T(0, t)} = 0{,}01. \tag{8}$$

It follows from (6) and (7) that

$$\frac{T(z_0, t)}{T(0, t)} = \exp(-\zeta_0^2) - \sqrt{\pi}\,\zeta_0\,[1 - \operatorname{erf}\zeta_0]. \tag{9}$$

From (8) and (9) we find the solution

$$z_0 = 3{,}21\sqrt{\alpha K t}. \tag{10}$$

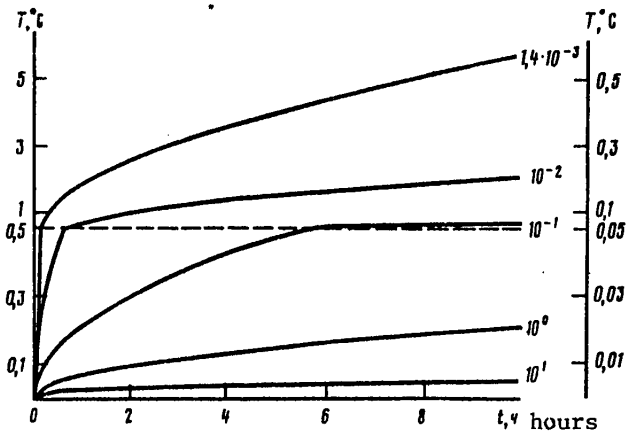

Fig. 1. Anticipated deviation of the ocean surface temperature from an equilibrium distribution for different coefficients of turbulent thermal diffusivity $K_T = \alpha K$.

In accordance with (10), with a variation of K_T and t in the ranges from $1.4 \cdot 10^{-3}$ to 10^1 cm^2/sec and from 1 minute to 10 hours the z_0 value varies in the range from 0.9 cm to 19 m, as a result of which the adopted boundary condition (4) with $z \to \infty$ must be considered justified.

Thus, the scatter of values of the coefficient of vertical turbulent exchange caused by the intermittence of turbulence can lead to substantial variations of ocean surface temperature (the model considered above, not taking the horizontal nonuniformity of the temperature field and horizontal turbulent heat exchange into account, can be used because the horizontal dimensions of individual turbulent zones in the ocean are usually much greater than their thickness). And since there will alternately be more and then less turbulent layers of fluid in different regions of the ocean near its surface, the temperature field of the ocean surface acquires a "mosaiced" structure. Accordingly, the temperature drops between adjacent spots in such a structure will be dependent on the differences in the turbulence levels in the surface layers of the ocean and on the lifetime of the turbulent layers. Evidently, 1 hour can be used as the characteristic (in order of magnitude) lifetime of the approximately constant turbulence level in individual layers. Then with molecular vertical heat exchange in one of the ocean zones and with a value $K_T = 10$ cm^2/sec in the adjacent zone the drop in surface temperature between these zones ΔT attains 1.8°C. However, if in one zone $K_T = 1$ cm^2/sec, and in the other $K_T = 10$ cm^2/sec, ΔT after the elapsing of 1 hour will be only 0.046°C. With quite typical values $K_T = 0.1$ cm^2/sec in one zone and $K_T = 1$ cm^2/sec in the other ΔT attains values 0.15°C. According to [3], the typical dimensions of spatial inhomogeneities of ocean surface temperature in the ocean in calm weather are 1-10 km, whereas the temperature between adjacent spots can differ by 1-2°C. However, according to observations made in a number of regions in the North Atlantic under different weather conditions, the typical ΔT values at distances of about 1 km were $\Delta T = 0.04$-0.20°C [4].

The different turbulence of the upper layer of the ocean must also exert an influence on the characteristics of surface waves. True, in most cases the waves themselves are the principal factor in the turbulence of this layer and therefore they must be in some dynamic equilibrium with the turbulence generated by them. However, if turbulence is generated by other factors (such as shear instability of the current) or the boundary of some turbulent layer under the influence of diffusional or advective processes advances into the zone occupied by wave motion, there will be a process of interaction between waves and such "external" turbulence. If there is a gradient grad E in the layer of wave movement, in the density distribution of the energy of potential wave movement E a flow of wave energy arises which is directed against the gradient and is equal to [5]

$$\mathbf{j} = -K_E \operatorname{grad} E, \tag{11}$$

where K_E is the coefficient of exchange of wave energy, which can be considered equal to the coefficient of turbulent exchange of momentum K.

Thus, "external" turbulence causes an outflow of wave energy in a downward direction, which should lead to an attenuation of surface wave amplitude. Such an effect of extinction of gravitational waves due to strong interaction with

"external" turbulence was noted for the first time by G. I. Barenblatt [6, 7]. The change in the E parameter with time can be described by the equation

$$\frac{\partial E}{\partial t} = K \frac{\partial^2 E}{\partial z^2}. \tag{12}$$

With the boundary conditions

$$\left.\frac{\partial E}{\partial z}\right|_{z=0} = 0; \quad \left. E \right|_{z\to\infty} = 0 \tag{13}$$

and the initial density distribution of wave energy with depth

$$E(z, 0) = E_0 \exp(-\lambda z) \tag{14}$$

the solution of equation (12) has the form

$$E(z, t) = \frac{E_0}{2\sqrt{\pi K t}} \int_0^\infty \left\{ \exp\left[-\frac{(z-\xi)}{4Kt}\right] + \exp\left[-\frac{(z+\xi)}{4Kt}\right] \right\} \exp(-\lambda\xi)\, d\xi, \tag{15}$$

and with z = 0 from (15) we obtain

$$E(0, t) = E_0 \exp(\lambda^2 K t)\, [1 - \operatorname{erf}(\lambda\sqrt{Kt})]. \tag{16}$$

Table 1

K, $cm^2 \cdot sec^{-1}$	λ, m					
	10	5	1	0.5	0.1	0.05
10^2	43.8 min	10.9 min	26.3 sec	6.57 sec	0.263 sec	0.0657 sec
10^1	7.30 hrs	1.82 hr	4.38 min	1.09 min	2.63 sec	0.657 sec
10^0	73.0 hrs	18.2 hrs	43.8 min	10.9 min	26.3 sec	6.57 sec
10^{-1}			7.30 hrs	1.82 hr	4.38 min	1.09 min
10^{-2}			73.0 hrs	18.2 hrs	7.30 hrs	10.9 min

It can be assumed approximately that a decrease in the amplitude of a wave with the length λ occurs at a depth equal to $\lambda/2$; in this case the energy decreases by a factor of e at the depth $\lambda/4$. On the basis of expression (16), Table 1 gives estimates of the time intervals τ during which the energy density of surface waves is reduced to one-quarter of the initial energy density E_0. Depending on the value of the K coefficient and the λ parameter (Table 1 gives the corresponding values $\lambda = 4/\lambda$) the time interval τ changes in a wide range; the attenuation of the short-wave part of the wind wave spectrum occurs most rapidly in this case. Such an effect should lead to the "spottiness" of the wave field at the ocean surface.

There are a number of assumptions and simplifications in the constructions cited above. In particular, in a model of vertically intermittent turbulence the assumption was made that there is a statistical uniformity of the process, although the upper layer of the ocean is usually more turbulent than the underlying water masses. The schemes for computing the influence of intermittent

turbulence on surface temperature and sea waves are also simplified.

We note in conclusion that the determined orders of magnitude graphically illustrate the important role of the turbulence intermittence factor not taken into account up to the present time in the forming of the structural features of hydrophysical fields in the surface layer of the ocean.

BIBLIOGRAPHY

1. Monin, A. S. and Ozmidov, R. V., OKEANSKAYA TURBULENTNOST' (Ocean Turbulence), Leningrad, Gidrometeoizdat, 1981, 320 pages.

2. Belyayev, V. S. and Ozmidov, R. A., DAN (Reports of the USSR Academy of Sciences), Vol 254, No 4, p 995, 1980.

3. Fedorov, K. N., Ginzburg, A. I. and Piterbarg, L. I., OKEANOLOGIYA (Oceanology), Vol 21, No 2, p 203, 1981.

4. Karabasheva, E. I. and Pozdynin, V. D., IBID., Vol 18, No 4, p 614, 1978.

5. Benilov, A. Yu., IZV. AN SSSR: FIZ. ATM. I OKEANA (News of the USSR Academy of Sciences: Physics of the Atmosphere and Ocean), Vol 9, No 3, p 293, 1973.

6. Barenblatt, G. I., IBID., Vol 13, No 6, p 845, 1977.

7. Barenblatt, G. I., PODOBIYE, AVTOMODEL'NOST', PROMEZHUTOCHNAYA ASIMPTOTIKA (Similarity, Self-Similarity, Intermediate Asymptotic Behavior), Leningrad, Gidrometeoizdat, 1978, 208 pages.

5303
CSO: 1865/147

UDC 550.38:550.37

FUNDAMENTAL PROBLEMS IN MARINE ELECTROMAGNETIC RESEARCH

Moscow FUNDAMENTAL'NYYE PROBLEMY MORSKIKH ELEKTROMAGNITNYKH ISSLEDOVANIY in Russian 1980 (signed to press 19 Nov 79) pp 2-5, 258-271

[Annotation, table of contents and abstracts from collection of articles "Fundamental Problems in Marine Electromagnetic Research", responsible editor A. N. Pushkov, doctor of physical and mathematical sciences, Institut zemnogo magnetizma, ionosfery i rasprostraneniya radiovoln, 300 copies, 272 pages]

[Text] Annotation. This collection of articles contains papers presented at the 2d All-Union Seminar on Fundamental Problems in Marine Electromagnetic Research held at the Institute of Terrestrial Magnetism, Ionosphere and Radio Wave Propagation, USSR Academy of Sciences, in 1978. The collection includes articles devoted to the development and use of marine magnetometric instrumentation, investigations of the permanent geomagnetic field related to the compilation of a catalogue of magnetic surveys, creation of a bank of magnetometric data, and also work in the field of a geohistorical analysis of the earth's anomalous field. In addition, the collection contains a number of articles on the theory and practice of marine electromagnetic sounding and profiling, including the development of methods for the numerical and physical modeling of the electromagnetic field in ocean areas. One of the sections in the collection is devoted to theoretical and experimental investigations of electromagnetic fields caused by the movement of water masses. The collection is of interest to specialists concerned with study of the geomagnetic field and also for a wide group of geophysicists working in the field of investigations of the earth's deep structure.

Contents

UDC 550.380.8

MBM SEA TOWED MAGNETOMETER

[Abstract of article by Lovotov, L. L., Nikolayev, A. A. and Semevskiy, R. B.]

[Text] This article is devoted to a description of the design and construction of the first Soviet-produced series-capable magnetometer developed and introduced into standard production at the "Geofizika" Scientific-Production Combine. It is intended for the measurement of weak magnetic fields in the seas and oceans from aboard surface ships and submersibles. Experimental use of the instrument under real navigational conditions confirmed its high technical and operational qualities. The MBM apparatus has undergone expert metrological testing by the USSR Gosstandart and has been included in the State Register of Measurement Instruments.

UDC 550.380.8

TWO-COMPONENT QUARTZ BOTTOM MAGNETIC VARIATION STATION

[Abstract of article by Bobrov, V. N., Gaydash, S. P. and Kulikov, N. D.]

[Text] Four two-component magnetic variation stations have been developed and have undergone tests in the Caspian Sea. A station is oriented on the magnetic meridian by analogy with a sea compass using a special orienting magnet. The station uses quartz antitilt z and H variometers and a special optical system of mirrors making it possible to record the variations of two components on photofilm with a sensitivity of 0.5 nT in the range ±550 nT. The duration of self-contained operation is 7 days. Figures 1.

UDC 550.380.8

DIGITAL THREE-COMPONENT BOTTOM MAGNETIC VARIATION STATION

[Abstract of article by Belov, V. A., Burtsev, Yu. A., Murashov, V. P. and Gaydash, S. P.]

[Text] A digital three-component bottom magnetic variation station has been developed. Station operation is based on the inclusion of a quartz sensor in a sweep conversion system. Two sensors are used in measuring three components. Registry is with a cassette magnetic recorder employing an intermediate memory. The registry range is ±1000 nT with a sensitivity of 0.1 nT. The duration of self-contained operation is 10 days. Figures 2, references 3.

UDC 550.380.8

BOTTOM THREE-COMPONENT VARIOMETER WITH MAGNETOSTATIC CONVERTERS

[Abstract of article by Krotevich, N. F., Panurovskiy, V. N. and Klekovkin, V. A.]

[Text] The article gives a description of a bottom three-component variometer, based on the principle of an arbitrary orientation of primary magnetostatic transducers. The authors give a functional diagram of the measurement channel of this variometer and its technical specifications. Variometers with electronic and electromechanical compensation are compared. Figures 3, references 5.

UDC 550.380.6

SEA BOTTOM THREE-COMPONENT FERROSONDE MAGNETIC VARIATION STATION -- MVS-3K

[Abstract of article by Pyatibrat, O. M., Ignatov, I. I. and Ryabushkina, T. P.]

[Text] This paper reports on a bottom sea ferrosonde 3-component magnetovariation station, the MVS-3K, developed and constructed at the Institute of Terrestrial Magnetism, Ionosphere and Radio Wave Propagation. The authors give the

principal schematic solutions and station parameters. On the basis of the results of in situ tests the conclusion is drawn that the new instrument is highly promising. Figures 1, references 2.

UDC 550.380.8

MAGNETOMETRIC COMPLEX FOR MEASURING VARIATIONS AND MAGNETIC FIELD GRADIENT IN THE FREQUENCY RANGE 0-400 Hz

[Abstract of article by Kozlov, A. N. and Abramov, Yu. M.]

[Text] This report describes the development of a measurement complex for registering variations and the gradient of the earth's magnetic field on the basis of the recording apparatus of the KMV magnetometer-gradient meter in the range 0-1 Hz with a resolution of 0.1 nT and variations of electromagnetic processes in the frequency range 1-400 Hz with a resolution of about 1 $nT \cdot Hz^{-1/2}$ under sea conditions. References 4.

UDC 551.46.083:621.317.7

METHODS AND INSTRUMENTATION FOR INVESTIGATING THE NATURAL ELECTROMAGNETIC FIELD IN THE OCEAN IN THE FREQUENCY RANGE ABOVE SEVERAL Hz

[Abstract of article by Karnaushenko, N. N. and Kukushkin, A. S.]

[Text] The authors describe measurement methods and give the makeup and principal technical specifications of specialized measurement apparatus for investigating the natural electromagnetic field in the ocean in the frequency range above several Hz developed taking into account the principal requirements and specifics of measurements of such fields. The elements for the input of data into an electronic computer are described. Figures 1, references 7.

UDC 550.370

EVALUATION OF THE EFFECTIVENESS OF VIBRATIONAL PROTECTION OF A TOWED VARIABLE MAGNETIC FIELD TRANSDUCER

[Abstract of article by Artamonov, L. V., Beresten', L. N. and Popov, M. K.]

[Text] This is an analysis of the technical possibilities of vibrational protection of the primary transducers for measuring a variable, extremely low-frequency magnetic field at sea using apparatus towed behind a ship. The results of an experimental investigation (on a vibrating stand) of a unit for measuring the horizontal field component, protected against vibration by the inertial shock-absorbing suspension method, are described. It was established that suppression by not less than 40 db in comparison with vibration of the body of the towed "fish" is technically attainable. Figures 2, references 1.

UDC 550.389

EXPERIENCE IN WORK WITH THE KMS QUANTUM DIFFERENTIAL MAGNETOMETER UNDER CONDITIONS OF A SEA MAGNETIC SURVEY

[Abstract of article by Gordin, V. M., Lyubimov, V. V. and Popov, A. G.]

[Text] The results of an experimental determination of the horizontal gradients of the geomagnetic field in the southern part of the Atlantic Ocean with the KM8 quantum differential magnetometer are given. The authors analyze the results of a number of methodological experiments related to an investigation of the influence of the cable and towing ship on the gradient meter readings. The optimum regime for registering the gradient of the earth's magnetic field was determined. Figures 5, tables 2, references 4.

UDC 550.838

COMPONENT GEOMAGNETIC SURVEY ON 21st VOYAGE OF THE SCIENTIFIC RESEARCH SHIP 'DMITRIY MENDELEYEV'

[Abstract of article by Belyayev, I. I., Perfilov, V. I., Gorodnitskiy, A. M. and Suzyumov, A. Ye.]

[Text] The concise technical specifications are given for a model of the KMZ-4 component magnetometer developed by the Special Design Bureau for Physical Instrument Making, USSR Academy of Sciences. The article describes the method for the processing of data obtained during the voyage using a "Minsk-22" electronic computer. Also given are the results of a hydromagnetic survey of individual regions of the Pacific Ocean. The error in a component survey of a polygon in the region of the central part of the Shatskiy Rise was determined. References 2.

UDC 550.380.8

BUOY DIFFERENTIAL PROTON MAGNETOMETER FOR DETERMINING TEMPORAL VARIATIONS OF GEOMAGNETIC FIELD IN SEA MAGNETIC SURVEYS

[Abstract of article by Machinin, V. A., Tsvetkov, Yu. P., Pushkov, A. N. and Kharitonov, A. L.]

[Text] Tests of a buoy proton station intended for determining the temporal variations of the geomagnetic field when carrying out sea magnetic surveys are described. The results of an "observatory" investigation of the station and its practical use in a local magnetic survey in the Caspian are given. It is shown that the mean square survey error, without allowance for time variations, is ± 6.5 nT and it can be reduced to ± 3.3 nT, introducing corrections in the buoy station magnetograms. Allowance for variations at shore stations makes it possible to reduce the error only to ± 5 nT. Figures 6, tables 1, references 5.

UDC 550.380

EXPERIENCE IN CARRYING OUT GRADIENT MAGNETIC MEASUREMENTS IN THE ARCTIC OCEAN

[Abstract of article by Abramov, Yu. M. and Abramova, L. M.]

[Text] Technical specifications are given for a quantum variometer-gradient meter developed at the Institute of Terrestrial Magnetism, Ionosphere and Radio Wave Propagation. Also described is an experiment for measuring the gradients of variations of the earth's magnetic field from a drifting floe. The possibility for using a quantum variometer-gradient meter in the high latitudes and at low temperatures is demonstrated. Figures 1, references 3.

UDC 550.370

ELECTRIC FIELD HYDROMODULATION TRANSDUCER

[Abstract of article by Klekovkin, V. A., Selyatitskiy, V. G., Sypko, A. P. and Fedyunin, S. G.]

[Text] The article describes a primary measurement transducer for the strength of the electric field for measuring weak constant and infralow-frequency signals in a sea medium. The equivalent circuit of the transducer is analyzed. A conversion factor equation is derived and a structural diagram of the instrument is given. Figures 4, references 5.

UDC 550.380.8

DYNAMIC BAROSENSITIVITY AND TRIBOPOLARIZATION EFFECTS OF MEASUREMENT ELECTRODES

[Abstract of article by Bogorodskiy, M. M.]

[Text] The errors in the measurement electrodes of the IELAN-IZMIRAN system caused in a shallow-water zone by the dynamic effect of the waves (pressure, velocity of flow around the electrodes, wave collapse effect) are experimentally evaluated. With a salinity of 13% there is a dynamic barosensitivity of about 15-30 μV/(m H_2O)$\cdot sec^{-1}$ and the tribopolarization for the pair of electrodes is about 50-500 μV/m$\cdot sec^{-1}$. In the case of collapsing crests the effective value of the dynamic barosensitivity, judging from the form of the wave, increases by a factor of 4-5. The presence of different kinds of noise, including with a "long-period" component, of the wave group envelope type, is demonstrated. The effectiveness of protective measures, including treatment of the electrodes, is demonstrated. Figures 7, tables 1, references 8.

UDC 550.380.8

STATIC BAROSENSITIVITY OF MEASUREMENT ELECTRODES AND EVALUATION OF ERRORS IN MEASUREMENT OF ELECTRIC FIELDS OF WAVES

[Abstract of article by Bogorodskiy, M. M.]

[Text] An experimental study was made of the response of silver chloride electrodes to pressure. A special electrolytic pressure chamber outfit was also created for this purpose. The author obtained the absolute values of static barosensitivity of the measurement electrodes. It is noted that barosensitivity anomalies correspond to internal defects of the electrodes. It is shown that it is possible to evaluate the error in measuring the elements of electric fields corresponding to the barosensitivity of the electrodes and channel noise. An evaluation of the errors was made applicable to the potential, vertical difference and divergent methods for observing the electric fields of well-developed wind waves on a deep sea. The optimum dimensions of the measurement probes were computed. A decrease in the error can be obtained by treating the electrodes by the cited method in combination with a decrease in the noise of the measurement channel. Figures 10, references 22.

UDC 550.383

PROBLEMS IN INVESTIGATING THE GEOMAGNETIC FIELD OF THE WORLD OCEAN ON THE BASIS OF A SPECIALIZED SYSTEM FOR THE ACCUMULATION, STORAGE AND PROCESSING OF DATA

[Abstract of article by Kolesova, V. I., Petrova, A. A. and Pushkov, A. N.]

[Text] The article sets forth the principal requirements on an automated system and its data support taking into account the tasks involved in using the system for: a) obtaining a unified bank of magnetometric data for the world ocean; b) studying the structure and formulating models of the main and anomalous parts of the geomagnetic field and its secular variations; c) solving geological-geophysical problems. References 12.

UDC 550.383

FEATURES IN CREATING A BANK OF MAGNETOTELLURIC DATA

[Abstract of article by Tsipis, Ya. L. and Gubenko, N. D.]

[Text] A study was made of the problem of forming a data base for magnetic surveys and an operational system for work with this base, making it possible to solve a broad range of problems ranging from informational to the representation of the spatial-temporal structure of the geomagnetic field. The rapid increase in the volume of experimental data dictates the necessity for the speediest possible creation of such a system.

UDC 550.383

ANALYSIS AND REPRESENTATION OF THE EARTH'S MAGNETIC FIELD BY THE OPTIMUM INTERPOLATION METHOD

[Abstract of article by Zolotov, I. G. and Roze, Ye. N.]

[Text] A method for the optimum interpolation of magnetometric data has now been developed. Algorithms are proposed for evaluating the statistical characteristics of the anomalous geomagnetic field and their errors. Figures 6, references 8.

UDC 550.382

INVESTIGATION OF METHODOLOGICAL ERRORS IN GRADIENTOMETRIC MEASUREMENT METHOD

[Abstract of article by Roze, Ye. N.]

[Text] An evaluation was made of the errors in gradientometric measurements of the earth's magnetic field over the areas of the seas and oceans. Measures are proposed for increasing the accuracy of the gradientometric method. Figures 4, tables 1, references 3.

UDC 550.382:550.383

MAGNETIC ANOMALIES IN THE OCEAN ON THE WORLD SCHEMATIC MAP OF THE ANOMALOUS MAGNETIC FIELD

[Abstract of article by Karasik, A. M., Desimon, A. I. (deceased), Pozdnyakova, R. A. and Sochevanova, N. A.]

[Text] This is a validation and discussion of the principles, procedures and results of representation of magnetic anomalies of the oceans on the world map of the anomalous magnetic field at a scale of 1:15 000 000, compiled at the SEVMORGEO Scientific-Production Combine and the Leningrad Division, Institute of Terrestrial Magnetism, Ionosphere and Radio Wave Propagation, USSR Academy of Sciences, for the higher schools. In contrast to the continental part (in $(\Delta T)_a$ or z_a isolines), the field of the ocean floor is shown in the form of numbered axes of paleomagnetic anomalies; and only in the places where the axes are not traced is the field given in the form of zero isolines $(\Delta T)_a$ or quiet field zones. The world magnetic map is the first experience in global representation of the anomalous magnetic field and in the oceanic part it differs considerably from the map of the axes of linear magnetic anomalies constructed by W. Pitman, et al. (1974) due to the use of Soviet sources and new materials. Figures 1, references 9.

UDC 550.382

INVESTIGATION OF STRUCTURE OF GEOMAGNETIC FIELD ELEMENTS ALONG A GEOTRAVERSE IN THE NORTH PACIFIC OCEAN

[Abstract of article by Kolesova, V. I., Petrova, A. A. and Efendiyeva, M. A.]

[Text] The article gives the results of a spectral-profile analysis of the geomagnetic field along a sublatitudinal profile in the North Pacific Ocean. A joint analysis of component and modular measurements made possible the most complete study of the spectral structure of the geomagnetic field, clarification of the principal classes of anomalies and determination of their spatial and dispersion properties and also made it possible to ascertain the characteristic features of the spectral structure of the field in different geomorphological provinces and to refine the position of the boundaries of individual anomalous regions. In the spectral structure of the components and the modulus of strength of the geomagnetic field there are individual spectral minima which are of interest for determining the base levels for anomalous fields of different frequency composition. The features of the spectral structure of the geomagnetic and gravity fields are compared. Figures 1, references 6.

UDC 550.382

PALEOMAGNETIC APPLICATION OF DATA FROM COMPONENT MAGNETIC INVESTIGATIONS IN OCEAN

[Abstract of article by Shreyder, A. A. and Trukhin, V. I.]

[Text] A method for determining the parameters of the vector of magnetization of a two-dimensional disturbing body on the basis of anomalies of the vertical and horizontal components of the vector of the earth's magnetic field is described. The results of an analysis of the errors of the method and the results of computations on the basis of real magnetic anomalies observed in the Indian Ocean during the 58th voyage of the scientific research ship "Vityaz'" are given. References 6.

UDC 550.382:550.838

MAGNETIC CHARACTERISTICS OF TWO MAJOR TRANSFORMAL DISLOCATIONS IN THE SOUTHEASTERN PACIFIC OCEAN

[Abstract of article by Gorodnitskiy, A. M., Litvinov, E. M. and Luk'yanov, S. V.]

[Text] The materials of a hydromagnetic survey in two polygons in the southeastern part of the Pacific Ocean, carried out on the 24th voyage of the scientific research ship "Akademik Kurchatov" in 1977, are analyzed. The southern polygon (polygon IV) was selected in the zone of development of the

Eltanin fault zone; the northern (polygon V) polygon was selected in the recently discovered Kurchatov fault. Magnetometric observations made it possible to clarify the specifics of the structural-tectonic plan of both zones of dislocations, define the principal stages in their formation and evolution and compare this with the nature of the geological development of the entire southeastern part of the Pacific Ocean. The results of the analysis emphasize the role of magnetometry in the general geological-geophysical complex of regional study of the ocean floor. Figures 3, references 2.

UDC 550.383

SOLUTION OF THE INVERSE PROBLEM OF DETERMINING THE SOURCE OF A PHYSICAL FIELD IN A DIPOLE MODEL

[Abstract of article by Semenov, V. G.]

[Text] New unambiguous and invariant express methods have been developed for determining the localization of a physical field in a dipole model. An equation for the interrelationship of gradient parameters of a physical field was derived for an arbitrary model of a source. Figures 2, references 4.

UDC 550.382

ONE ALGORITHM FOR FINITE-DIFFERENCE MODELING OF ELECTROMAGNETIC FIELDS

[Abstract of article by Varentsov, I. M. and Golubev, N. G.]

[Text] The article examines the possibilities of formulation of an effective algorithm for the modeling of two-dimensional electromagnetic anomalies (in the case of an E-transform) suitable both for the mass solution of direct problems and for the solution of inverse problems by the method of automated trial-and-error. The modeling problem is reduced to a system of linear difference equations solved by the upper relaxation iteration method. The optimum value of the relaxation parameter, ensuring rapid convergence of the upper relaxation iteration method, is determined by means of the prediction and correction procedures. Provision was made for additional means for accelerating the process of solution of the problem and checking the accuracy of modeling results. The algorithm is applied using a YeS electronic computer and makes it possible to solve a broad range of problems in geoelectrics. Figures 3, tables 5, references 31.

UDC 550.382

SOLUTION OF INVERSE PROBLEMS IN GEOELECTRICS BY ITERATIVE TRIAL-AND-ERROR METHOD

[Abstract of article by Zhdanov, M. S., Varentsov, I. M. and Golubev, N. G.]

[Text] A method for solving two-dimensional inverse problems is examined. It makes it possible to use the results of both synchronous observations of fields and point soundings. The trial-and-error principle is used in the

solution. The parameterization method is employed for increasing stability of the problem, that is, a solution is sought in a definite class of functions. The minimizing of the functional of deviation of the selected field from the observed field is accomplished by methods not using derivatives and allowing limitation of the search region. A solution of the direct problem is found by the finite differences method. Figures 2, tables 1, references 9.

UDC 550.37:550.380

USE OF MODULAR MAGNETOMETERS IN SEA MAGNETIC VARIATION RESEARCH

[Abstract of article by Berdichevskiy, M. N., Zhdanov, M. S., Trofimov, I. L. and Fonarev, G. A.]

[Text] The practical feasibility and suitability of sea electromagnetic soundings by means of modular magnetometers is emphasized. Formulas for computing impedance are given in a new form. References 3.

UDC 550.380

PROMISING METHODS FOR ELECTROMAGNETIC INVESTIGATIONS OF STRUCTURE OF THE EARTH'S CRUST IN THE OCEANS

[Abstract of article by Kalashnikov, N. I. and Korepanov, V. Ye.]

[Text] The article discusses different variants of apparatus for shelf and deep-water placement, especially a sea variant of the long cable method and a station for sea magnetotelluric sounding. The authors give the principal results of in situ tests of both types of apparatus carried out in 1974-1978. Figures 3, references 7.

UDC 550.37:550.380

ELECTROMAGNETIC SOUNDINGS WITH MEASUREMENT OF THE ELEMENTS OF THE POLARIZATION ELLIPSE IN THE AREAS OF NORTHERN SEAS

[Abstract of article by Molochnov, G. V., Radionov, M. V. and Rybakin, V. N.]

[Text] This is an analysis of the dynamics of behavior of effective resistance curves for geological sections characteristic for the areas of northern seas, on the basis of which a method is proposed for carrying out electromagnetic soundings. The results of field work are given. Figures 1.

UDC 550.37:550.380

EXPERIENCE IN MEASURING VARIATIONS OF THE MAGNETIC AND ELECTRIC FIELDS AT GREAT DEPTHS IN THE PACIFIC OCEAN

[Abstract of article by Belyayev, I. I., Polonskiy, Yu. M., Svetov, B. S. and Khalizov, A. L.]

[Text] This paper gives the results of experiments for registry of variations of the earth's electric and magnetic fields on the floor of the abyssal Pacific Ocean carried out in 1978. During the 21st voyage of the scientific research ship "Dmitriy Mendeleyev" specialists registered variations of the latitudinal component of the electric field by means of a conducting line 1 km in length and a magnetic field module using a proton magnetometer. Basic data are given on the bottom magnetometric station used, as well as information on formulation of the experiments. The recorded variations are described. References 1.

UDC 550.380

EXPERIENCE IN THE REGISTRY OF VARIATIONS IN THE MODULUS OF THE VECTOR OF THE EARTH'S MAGNETIC FIELD BY THE KM5 SEA QUANTUM MAGNETIC VARIATION STATION ON THE SEA FLOOR

[Abstract of article by Finger, D. L., Filatov, O. V. and Ignatov, I. I.]

[Text] A method is described for the placement of a quantum sea magnetic variation station (KM5) on the sea floor. Three such placements were carried out in the Caspian Sea at depths of 80-110 m. Experimental investigations indicated the suitability of the KM5 for the registry of variations on the sea floor. Figures 2, references 2.

UDC 550.37:550.380

PRELIMINARY RESULTS OF MAGNETIC VARIATION MEASUREMENTS IN THE SOUTHERN CASPIAN AREA

[Abstract of article by Shneyer, V. S., Finger, D. L., Dubrovskiy, V. G., Pyatibrat, O. M., Pukhomelin, A. F., Bobrov, V. N., Gaydash, S. P. and Ignatov, I. I.]

[Text] The authors give the results of a preliminary analysis of magnetic variations on sublatitudinal and meridional magnetic variation profiles in the Southern Caspian. On the basis of measurements with bottom stations it was possible to determine the distribution of the normalized amplitudes of variations of the z-, H- and D-components. A strong variability of z and D on the submeridional profile and a weak variability on the sublatitudinal profile were discovered. The preliminary interpretation reveals a marked nonuniformity of the sedimentary cover in the submeridional direction, in the zone of contact between the megadepression and the platform, and its slight variability in a sublatitudinal direction. No asthenospheric inhomogeneities were discovered. Figures 1, references 3.

UDC 550.380.8

SOME RESULTS OF MEASUREMENTS OF THE ELECTRIC FIELD IN THE COASTAL ZONE OF THE CASPIAN SEA

[Abstract of article by Novysh, V. V. and Bogorodskiy, M. M.]

[Text] The investigations were made near Krasnovodsk in the coastal zone by means of an electric field meter with two orthogonal measurement bases, each of 3.8 m. During a storm there are slowly changing fields -- up to 120-150 μV/m with a decrease in their values as the storm attenuates. Figures 1, references 1.

UDC 550.37:550.380

INVESTIGATION OF THE ELECTRIC FIELD OF SUBMARINE SOURCES IN THE CASPIAN SEA

[Abstract of article by Korotayev, S. M.]

[Text] The article presents the results of profiling of the natural electric field along the eastern shore of the Caspian for the purpose of seeking submarine sources and their quantitative evaluation. It was found that there is a group of submarine sources on the Krasnovodskiy Peninsula traverse. The characteristic velocity at the sources, computed on the basis of field anomalies, was about 0.01 mm/sec. Figures 2, references 6.

UDC 550.37

COMPUTATION OF DISTURBANCES OF THE EARTH'S MAGNETIC FIELD BY LONG-PERIOD VARIATIONS OF OCEAN

[Abstract of article by Belokon', V. I., Rodkin, A. F. and Smal', N. A.]

[Text] A system of equations and boundary conditions was formulated for computing variations of the earth's magnetic field induced by long-period variations of the ocean. The use of the approximation $h/\alpha << 1$, where h is ocean depth, α is the characteristic horizontal scale, made it possible to examine the problem of flow of currents into the bottom. References 3.

UDC 550.37

GEOMAGNETIC FIELD VARIATIONS FROM SEA WAVES ALONG SHORE WITH SLOPING BOTTOM

[Abstract of article by Smagin, V. P. and Savchenko, V. N.]

[Text] A method is proposed for computing geomagnetic field variations caused by potential wave motion of a fluid along a shore with a constant bottom slope. An algorithm is given for determining the horizontal and vertical

components of the induced magnetic field along the shore, whose bottom slope is considered equal to ($\alpha_n = \pi/2$, n = 1, 2, 3,... The case of a vertical precipice ($\alpha_0 = \pi/2$) is examined in detail. References 3.

UDC 551.463.7

EXPERIMENTAL INVESTIGATIONS OF VERTICAL STRUCTURE OF THE NATURAL ELECTROMAGNETIC FIELD IN THE OCEAN IN THE FREQUENCY RANGE ABOVE SEVERAL Hz

[Abstract of article by Karnaushenko, N. N. and Kukushkin, A. S.]

[Text] The authors give the results of in situ investigations of the vertical structure of the natural electromagnetic field in the tropical zone of the Atlantic Ocean and deep regions of the Black Sea in the frequency range above several Hz. The collected data make it possible to evaluate the change in the spectral makeup and dropoff in the intensity of field variations as a function of frequency in the case of a constant depth. Figures 3, references 19.

UDC 550.37:550.380

MEASUREMENT OF THE ELECTRIC FIELD OF WAVES BY TOWED ELECTRODES

[Abstract of article by Novysh, V. V., Smagin, V. P. and Fonarev, G. A.]

[Text] It is demonstrated on the basis of experimental data that a towed electrode line -- the EMIT (electromagnetic current recorder) -- at the time of waves registers the electric field of sea waves. By using records on courses perpendicular to and parallel to the wave crests it is possible to determine the elements of the waves: period, height and length of a wave. Figures 1, references 1.

UDC 550.37:550.380

INVESTIGATION OF STATISTICAL CHARACTERISTICS IN MAGNETIC FIELDS OF WIND WAVES

[Abstract of article by Kazakov, A. V., Medzhitov, R. D., Rutenko, A. N. and Shekhovtseva, Ye. L.]

[Text] The article gives the results of investigations of the magnetic fields of surface waves carried out in the summer of 1977-1978 in the coastal zone of the Sea of Japan. The measurements were made at depths of 8 and 30 m over a long period of time under different hydrometeorological conditions. A quantitative relationship was established between the parameters of the waves and the magnetic field generated by them. Figures 2, references 7.

5303
CSO: 1865/162-A

UDC 551.466.3:535.31

THEORY OF OBSERVATION OF UNDERWATER OBJECTS THROUGH WAVE-COVERED SEA SURFACE

Moscow IZVESTIYA AKADEMII NAUK SSSR: FIZIKA ATMOSFERY I OKEANA in Russian Vol 18, No 4, Apr 82 (manuscript received 9 Dec 80, after revision 6 Apr 81) pp 408-415

[Article by S. V. Dorenko, Marine Geophysical Institute, Ukrainian Academy of Sciences]

[Text]

Abstract: The article gives a theoretical analysis of the distortions introduced by the wave-covered sea surface in the image of underwater features observed from the atmosphere. It is postulated that the spatial structure of both observed features and waves has a random character. The quality of observation is evaluated using the magnitude of the error in measuring the spatial luminosity of the feature. It is shown that there is an optimum relationship between the statistical characteristics of the distribution of luminosity and waves and the parameters of the measuring instrument ensuring a minimum of this error.

The possibility of observing underwater features from the atmosphere is dependent on their contrast, degree of turbidity of the water and atmosphere, superposing of the brightness of air haze, light scattered in the sea and brightness of the water-air discontinuity on the image [1].

We will investigate the joint influence exerted on transmission of the image of underwater features by the wave-covered sea surface and the averaging effect of the measuring instrument, neglecting other interfering factors, allowance for which is possible independently.

A problem similar in its formulation was solved in [1], where the influence of the sea surface on image transmission was studied by an analysis of the scattering function, the energy distribution in the edge image and the frequency contrast of the transfer function. In source [2] a study was made of the image transfer of a point through a one-dimensional sinusoidal wave and formulas were given for computing the displacement of a point and the blurring of an object

with an increase in the exposure. An approximate model of image transfer through the wave-covered discontinuity of two media with different refractive indices was described in [3], where the author determines the multipoint statistical characteristics of the brightness image of a self-luminescent object or feature observed through the wave-covered discontinuity.

A feature of this study is that it examines the observation of random spatially elongated features using optical radiation detectors which perform spatial averaging of the image. Many natural formations on the bottom and in the water layer can be modeled by features of the mentioned structure whose investigation is possible by optical methods. The spatial averaging of the received image is a property of any real radiation detector. Accordingly, the combination of such initial premises makes it possible to obtain research results suitable for direct practical application. The quality of observation is evaluated using the mean square error between the initial and measured luminosity distributions [4]. It is shown that it is dependent on the choice of the degree of averaging and is the highest when it has a finite value. Here we will examine observations at the nadir as ensuring minimum image distortion [1].

In order to simplify the analysis we will examine a problem in which the object of measurement and waves are assumed to be one-dimensional (Fig. 1).

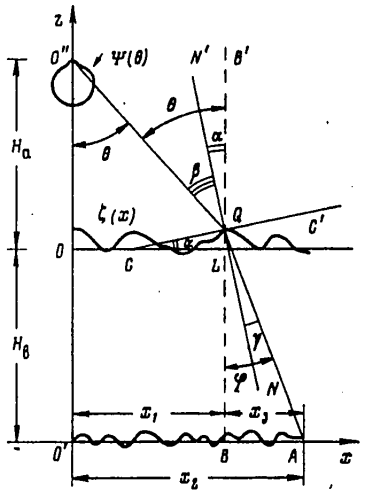

Fig. 1. Diagram explaining derivation of principal relationships.

Retaining the physical essence of the analyzed phenomena, such an approach makes it relatively simple to obtain final numerical results. The x-axis of the mean level of the wave-covered surface is stipulated in the figure by the point O.

The atmosphere is situated above it and the water below. At the depth H_w below the sea surface there is a diffuse self-luminescent object to be observed, extending in the direction of the x-axis, whose spatial distribution of luminosity is described by the random function f(x). At the height H_a above the sea surface at the point O" there is a detector of optical radiation whose optical axis is directed to the nadir. The difference in the level of the wave-covered surface from the mean is described by a centered random function of the space coordinate $\zeta(x)$.

An analysis of the process of observation of an underwater feature will be made on the basis of the premises of geometrical optics without allowance for the absorption and scattering of light in the water. The ray emerging from the point A of the observed feature and received by the detector at the point O" travels the following path. It is propagated in the water medium at the angle φ to the vertical BB' to the point Q at the water surface. The tangent CC' to the sea surface at this point is slanted to the horizontal at the angle α, whereas the normal NN' to this surface also is deflected by the angle α from the vertical BB'. At the point Q there is refraction of the ray and it emerges from the water at the angle β to the normal NN'. The detector at the point O" picks it up arriving at the angle θ to the vertical.

Since the $\zeta(x)$ surface is curvilinear and random, the picture picked up by the instrument differs from the f(x) function describing the distribution of luminosity of the observed object and this difference has a random character. We will find the error introduced by the wave-covered sea surface and instrument to the image sensed by the latter and we will evaluate the limits of applicability of such a method for observing underwater objects. For this purpose we will first obtain the correlation between the output signal Y of the measuring instrument and the investigated object f(x).

We will find the position of the point A, situated on the observed object, which is sensed by the instrument as visible at the angle θ to the vertical. The segment LQ is the $\zeta(x)$ value. Accordingly, the abscissa of the points L and B is

$$x_1 = [H_a - \zeta(x_1)] \operatorname{tg} \theta. \tag{1}$$

Since the straight line CC' is the tangent to the $\zeta(x)$ curve at the point with the abscissa x_1, then

$$\operatorname{tg} \alpha = \frac{d\zeta(x)}{dx}\Big|_{x=x_1} = \zeta'(x_1).$$

It follows from Fig. 1 that the distance of the point A from the point B is equal to $x_3 = [H_w + \zeta(x_1)] \operatorname{tg} \varphi$. Accordingly, the abscissa of the point A is

$$x_2 = x_1 + x_3 = [H_a - \zeta(x_1)] \operatorname{tg} \theta + [H_a + \zeta(x_1)] \operatorname{tg} \varphi, \tag{2}$$

where $\varphi = \alpha + \gamma$. Equation (1) can be regarded as an equation for finding the abscissa x_1. However, due to the random character of the $\zeta(x_1)$ parameter its precise solution cannot be obtained. We will take advantage of the circumstance that in actual practice the amplitude of the wave $|\zeta_{max}|$ is much less than the height H_a at which the measuring instrument is situated. From expression (1) we find that $x_1 = H_a \operatorname{tg} \theta$, and expression (2) assumes the form

$$x_2 = [H_a - \zeta(H_a \operatorname{tg} \theta)] \operatorname{tg} \theta + [H_a + \zeta(H_a \operatorname{tg} \theta)] \operatorname{tg} \varphi. \tag{3}$$

Thus, at the angle θ to the normal the measuring instrument picks up the point of an object whose abscissa is given by expression (3). The luminosity $f(x_2)$ of the object at this point has the form

$$f\{[H_a-\zeta(H_a \operatorname{tg}\theta)]\operatorname{tg}\theta+[H_a+\zeta(H_a \operatorname{tg}\theta)]\operatorname{tg}\varphi\}. \tag{4}$$

The argument of this function is random since the parameters ζ and φ are random. Accordingly, the value (4) is random even for a specific f(x) record. We will simplify its argument. For this we use the notation $\xi = \operatorname{tg}\alpha$, $\eta = \operatorname{tg}\theta$. Remote optical instruments usually have a very high angular resolution. Accordingly, it can be assumed that $|\eta|_{max} \ll 1$. The angles of inclination of the waves are usually also small, that is $|\xi|_{max} \ll 1$. In this case $\operatorname{tg}\varphi = \xi + (\eta - \xi)/n$, where n is the refractive index of water and the distribution of luminosity (4) assumes the form

$$f\left[A_0 x_1 + \frac{n-1}{n} H_a \xi(x_1)\right], \tag{5}$$

where

$$A_0 = 1 + \frac{H_a}{nH_a} \tag{6}$$

[B = w(ater)]

and it is taken into account that $\eta = x_1/H_a$. Thus, with the mentioned assumptions the random character of parameter (5) is determined by the random form of the function f(x) and the random character of wave slope $\xi(x) = d\zeta(x)/dx$.

The total signal received by the optical instrument is a superposing of the signals (5), that is

$$Y(\xi) = \int_{-\infty}^{\infty} h(x) f\left[A_0 x + \frac{n-1}{n} H_a \xi(x)\right] dx, \tag{7}$$

where h(x) is the instrument function of the sensor of this instrument, which is the projection of the directional diagram of the optical receiver $\Psi(\theta)$ onto the mean sea surface (Fig. 1), and characterizes the weight with which different parts of the image are sensed by the instrument. The $Y(\xi)$ parameter is dependent on the random function $\xi(x)$.

If the waves are absent and the resolution of the instrument is infinitely high, that is, the conditions $\xi(x) = 0$ and $h(x) = \delta(x)$ are satisfied, the instrument output signal is precisely equal to the value of the f(x) function at the nadir point, that is, $Y_0 = f(0)$. The difference between the $Y(\xi)$ and Y_0 value is determined by the presence of waves and a finite resolution of the measuring instrument. The mean square difference of the $Y(\xi)$ and Y_0 values is the dispersion of the measurement error

$$\varepsilon^2(\xi) = \overline{[Y(\xi)-Y_0]^2} = \overline{Y^2(\xi)} - 2\overline{Y_0 Y(\xi)} + \overline{Y_0^2}, \tag{8}$$

dependent on the random function of slopes $\xi(x)$. In expression (8) averaging is carried out for all possible cases of the random function f(x) with a constant record of the random function $\xi(x)$. Assuming the distribution of luminosity f(x) to be stationary and ergodic and using expression (7), we obtain

$$\overline{Y_0^2}=\overline{f^2(0)}=\sigma^2,$$

$$\overline{Y_0Y(\xi)}=\int_{-\infty}^{\infty}h(x)B\left[A_0x+\frac{n-1}{n}H_n\xi(x)\right]dx,$$

$$\overline{Y^2(\xi)}=\iint_{-\infty}^{\infty}h(x_1)h(x_2)B\left\{A_0(x_2-x_1)+\frac{n-1}{n}H_n[\xi(x_2)-\xi(x_1)]\right\}dx_1\,dx_2,$$

where σ^2 is the dispersion of the f(x) function; $B(\rho)$ is its correlation function. Expressing the latter through the S(k) spatial spectrum of the f(x) process, we find

$$\overline{Y_0Y(\xi)}=\iint_{-\infty}^{\infty}h(x)S(k)\exp\left\{j\omega\left[A_0x+\frac{n-1}{n}H_n\xi(x)\right]\right\}dx\,dk, \tag{9a}$$

$$\overline{Y^2(\xi)}=\iiint_{-\infty}^{\infty}h(x_1)h(x_2)S(k)\exp\left\{j\omega\left[A_0(x_2-x_1)+\right.\right.$$

$$\left.\left.+\frac{n-1}{n}H_n(\xi(x_2)-\xi(x_1))\right]\right\}dx_1dx_2\,dk. \tag{9b}$$

Since the $\xi(x)$ function is random, the dispersion of measurement error $\varepsilon^2(\xi)$ is also random. We will find the mean value of the dispersion of measurement error $\varepsilon^2=\langle\varepsilon^2(\xi)\rangle$ for the set of records of the wave process; here the symbol $\langle\ldots\rangle$ denotes such averaging. According to formula (8),

$$\varepsilon^2=\sigma^2-2\langle\overline{Y_0Y(\xi)}\rangle+\langle\overline{Y^2(\xi)}\rangle. \tag{10}$$

We will compute the values of the terms entering here. The distribution of the probability of rises $\zeta(x)$ of the sea surface is described by the normal law [1, 5]. Therefore, the process $\xi(x)=\zeta'(x)$ is also normal and its probability density has the form [5]

$$w_1(\xi)=\frac{1}{\sigma_\zeta k_1\sqrt{2\pi}}\exp\left(-\frac{\xi^2}{2\sigma_\zeta^2k_1^2}\right).$$

Here σ_ζ^2 is the dispersion of the $\zeta(x)$ function, the value $k_1^2=-B_\zeta''(0)/\sigma_\zeta^2=-R_\zeta''(0)$, and $B_\zeta(\rho)$ and $R_\zeta(\rho)$ are the correlation and normalized correlation functions of the $\zeta(x)$ process. In accordance with expression (9a) we obtain

$$\langle\overline{Y_0Y(\xi)}\rangle=\int_{-\infty}^{\infty}\overline{Y_0Y(\xi)}w_1(\xi)d\xi=$$

$$=\int_{-\infty}^{\infty}S(k)\tilde{h}^*(A_0k)\exp\left[-\frac{(n-1)^2}{2n^2}(H_n\sigma_\zeta k_1)^2k^2\right]dk, \tag{11}$$

where $\tilde{h}(k)$ is the instrument function spectrum.

The computation of the $\langle\overline{Y^2(\xi)}\rangle$ value, in accordance with (9b), requires a knowledge of the two-dimensional probability distribution $w_2(\xi_1, \xi_2)$ for the values $\xi_1 = \xi(x_1)$ and $\xi_2 = \xi(x_2)$. Since the $\xi(x)$ process is normal, this distribution has the form [6]

$$w_2(\xi_1, \xi_2) = \frac{1}{2\pi\sigma_\xi^2\sqrt{1-R_\xi^2(\rho)}} \exp\left\{-\frac{\xi_1^2-2R_\xi(\rho)\xi_1\xi_2+\xi_2^2}{2\sigma_\xi^2[1-R_\xi^2(\rho)]}\right\}, \tag{12}$$

where σ_ξ^2 and $R_\xi(\rho)$ are the dispersion and normalized correlation function of the $\xi(x)$ process, and $\rho = x_2 - x_1$. Taking into account that $\xi(x) = \zeta'(x)$, we express the coefficients entering into formula (12) through the statistical characteristics of the initial wave process

$$\begin{aligned} B_\xi(\rho) &= -\sigma_\zeta^2 R_\zeta''(\rho), \quad \sigma_\xi^2 = B_\xi(0), \\ R_\xi(\rho) &= -R_\zeta''(\rho)/k_1^2, \quad \sigma_\xi^2 = k_1^2\sigma_\zeta^2. \end{aligned} \tag{13}$$

Thus,

$$\langle\overline{Y^2(\xi)}\rangle = \int_{-\infty}^{\infty} \overline{Y^2(\xi)}\, w_2(\xi_1, \xi_2)\, d\xi_1\, d\xi_2.$$

Substituting here the expression (9b), we obtain

$$\begin{aligned} \langle\overline{Y^2(\xi)}\rangle = \iiint_{-\infty}^{\infty} S(k)h(x_1)h(x_2)\times \\ \times\theta_2\left(-\frac{n-1}{n}H_n k, \frac{n-1}{n}H_n k\right) e^{jkA_0(x_2-x_1)}dx_1\, dx_2\, dk, \end{aligned} \tag{14}$$

where $\theta_2(v_1, v_2) = \langle\exp[j(v_1\xi_1 + v_2\xi_2)]\rangle$ is the two-dimensional characteristic function of the random parameters ξ_1 and ξ_2. For a normal distribution we have the expression [6]

$$\theta_2(v_1, v_2) = \exp\left[-\frac{1}{2}(\sigma_1^2v_1^2+2r_{12}\sigma_1\sigma_2v_1v_2+\sigma_2^2v_2^2)\right],$$

where σ_1^2 and σ_2^2 are the dispersions of the parameters ξ_1 and ξ_2, and r_{12} is their correlation coefficient. In our case $\sigma_1 = \sigma_2 = \sigma_\xi$ and $r_{12} = R_\xi(\rho)$. Accordingly, with expressions (13) taken into account, we reduce expression (14) to the form

$$\begin{aligned} \langle\overline{Y^2(\xi)}\rangle = \iiint_{-\infty}^{\infty} S(k)h(x_1)h(x_2)\exp\{-[k_1^2+R_\zeta''(x_2-x_1)]\times \\ \times\left(\frac{n-1}{n}\sigma_\xi H_n k\right)^2 + jA_0k(x_2-x_1)\Big\}\, dx_1\, dx_2\, dk. \end{aligned} \tag{15}$$

We will assume that the instrument function for the sensor has a bell shape

$$h(x) = \frac{a}{2R_x}\exp\left(-\frac{\pi}{4}\frac{x^2}{R_x^2}\right), \tag{16}$$

where R_x is its characteristic radius, a is the amplification factor. Expression (16) is frequently used in order to approximate real instrument functions of optical instruments [7]. The spectrum of function (16) $h(k) = a\exp(-k^2R_x^2/\pi)$. Expressions (11) and (15) assume the form

$$\langle \overline{Y_0 Y(\xi)} \rangle = a\sigma^2 P_1, \quad \langle \overline{Y^2(\xi)} \rangle = a^2\sigma^2 P_2, \tag{17}$$

where

$$P_1 = \sigma^{-2} \int_{-\infty}^{\infty} S(k) \exp\left[-\left(\frac{A_0^2 R_x^2}{\pi} + \frac{1}{2} l^2 k_1^2 \right) k^2 \right] dk, \tag{18}$$

$$P_2 = \frac{1}{2\sqrt{2} R_x \sigma^2} \iint_{-\infty}^{\infty} S(k) \exp\left[-l^4 k_1^2 q(x) k^2 - \frac{\pi}{8R_x^2} x^2 + jkA_0 x \right] dx\, dk, \tag{19}$$

$$l^2 = \frac{n-1}{n} \sigma_t H_z, \tag{20}$$

$$q(x) = 1 + R_t''(x)/k_1^2, \tag{21}$$

and formula (10) can be written as $\varepsilon^2 = \sigma^2(1 - 2aP_1 + a^2P_2)$. In the latter expression the ε^2 parameter is dependent on the a coefficient. It is minimum with $a = P_1/P_2$, and this minimum has the value

$$\varepsilon_0^2 = \sigma^2(1 - P_1^2/P_2). \tag{22}$$

Further computations by the derived formulas are possible only when making specific the statistical characteristics of the observed object and the wave field.

We will assume that the distribution of luminosity f(x) subject to measurement has a bell-shaped spectrum

$$S(k) = \frac{\sigma^2 r_f}{\pi} \exp\left(-\frac{r_f^2 k^2}{\pi} \right),$$

where r_f is the characteristic spatial scale of this distribution. Formulas (18) and (19) assume the form

$$P_1 = \left(1 + A_0^2 z^2 + \frac{1}{2} c \right)^{-1/2}, \tag{23}$$

$$P_2 = \frac{1}{2\sqrt{2} R_x} \int_{-\infty}^{\infty} \exp\left\{ -\frac{\pi}{4} \left[\frac{A_0^2}{r_f^2(1 + cq(x))} + \frac{1}{2R_x^2} \right] x^2 \right\} \frac{dx}{\sqrt{1 + cq(x)}}, \tag{24}$$

where $z = R_x/r_f$ and $c = \pi L^4 k^2/r_f^2$.

We will examine a case when inhomogeneities of the sea surface constitute a sinusoidal wave with the wave number k_0:

$$\zeta(x) = b \sin(k_0 x + \alpha), \tag{25}$$

the phase α of which is uniformly distributed in the interval $[0, 2\pi]$. If the amplitude b is random, independent of the phase α and with a Rayleigh distribution, the $\zeta(x)$ function is stationary, ergodic and with a normal distribution [8]. Assuming that all these conditions are satisfied, we find that the correlation function of the $\zeta(x)$ process is $B_\zeta(\rho) = \sigma_\zeta^2 \cos(k_0 \rho)$, the value $k_1^2 = k_0^2$, and expression (21) assumes the form

$$q(x)=1-\cos(k_0 x). \tag{26}$$

We denote the wavelength (25) by λ_0, that is, $k_0 = 2\pi/\lambda_0$, and we introduce the coefficient

$$\varkappa=r_f/\lambda_0, \tag{27}$$

showing the ratio of the characteristic scale of the function f(x) to the wavelength of the surface wave. In this case

$$P_2=\frac{1}{2\sqrt{2}\pi z\varkappa}\int_0^\infty \exp\left\{-\left[\frac{A_0^2}{1+c\beta(t)}+\frac{1}{2z^2}\right]\frac{t^2}{16\pi\varkappa^2}\right\}\frac{dt}{\sqrt{1+c\beta(t)}}, \tag{28}$$

where $\beta(t) = 1 - \cos t$. We will transform the c parameter in the following way:

$$c=4\pi^2\left(\frac{n-1}{n}\varkappa W\right)^2,$$

where the dimensionless parameter

$$W=\frac{H_w}{r_f}\frac{\sigma_\zeta}{r_f}$$

[B = w(ater)]

is determined by the depth H_w at which the observed object is situated, the characteristic scale r_f and the mean square wave height σ_ζ. Taking into account that the refractive index n of water can be considered equal to 4/3 [9], we obtain $c = 1/4\pi^3(\varkappa W)^2$.

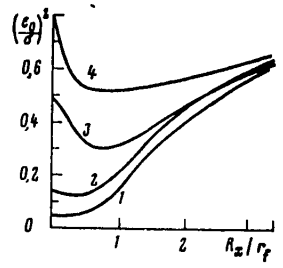

Fig. 2. Dependence of measurement error on relative averaging scale with $A_0 = 1$, W = 1: 1) $\varkappa$ = 0.1; 2) 0.2; 3) 0.5; 4) 1.0.

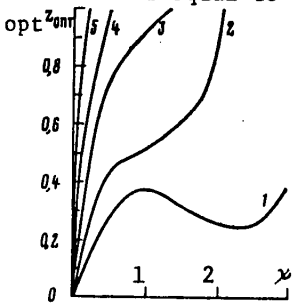

Fig. 3. Dependence of degree of optimum averaging on characteristics of observed object and waves: 1) W = 0.2; 2) 0.5; 3) 1.0; 4) 2.0; 5) 5.0.

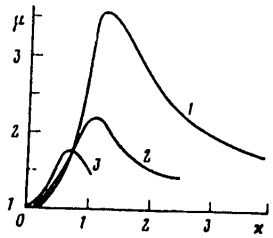

Fig. 4. Dependence of gain in measurement accuracy with optimum averaging on characteristics of observed object and waves: 1) W = 0.2; 2) 0.5; 3) 1.0.

Figure 2 shows an example of the results of computation of the error in measuring the distribution of luminosity on the basis of the determined relationships. It can be seen that the $(\varepsilon_0/\sigma)^2$ value in the case of small z with an increase in z and with the other parameters remaining constant decreases, attaining a minimum with some finite value $z = z_{opt}$. Accordingly, the measurement error is minimum not with an infinitely narrow directional diagram of the optical detector, but with some finite width. Such an increase in accuracy with an increase in $z = R_x/r_f$ is associated with the spatial filtering of the image by the detector. An increase in z leads to an averaging of both the luminosity distribution of the object f(x) and the observed wave pattern. In the case of small z an increase in z leads to an improvement of the image, but with a considerable increase in z the error increases due to the smoothing of image details with its great averaging. This circumstance is evidently one of the reasons for the well-known fact of an improvement in the image of underwater objects with an increase in observation height (to a definite level). Here the radiation detector plays the role of a filter restoring the image. In the case of very great heights the image quality again decreases. The effect of an improvement in the image by an averaging detector is particularly conspicuous in the case of large $\varkappa = r_f/\lambda_0$ (the length of the surface wave is small in comparison with the characteristic scale of the object).

It follows from Fig. 3 that the optimum averaging value is essentially dependent on the characteristics of the observed object and waves. This averaging is particularly great with large W.

It can be shown that with z = 0 (that is, for detectors with an infinitely narrow directional diagram)

$$\left(\frac{\varepsilon_0}{\sigma}\right)^2_{z=0} = \frac{c}{2+c}. \tag{29}$$

As the gain in measurement accuracy in the case of optimum averaging we have

$$\mu = \left(\frac{\varepsilon_0}{\sigma}\right)^2_{z=0} \Big/ \left(\frac{\varepsilon_0}{\sigma}\right)^2_{\text{мин}} \cdot \min \tag{30}$$

It shows by how many times the the square of the measurement error with use of a detector with an optimum width of the directional diagram is less than this same parameter with an infinitely narrow diagram. Figure 4 shows that this gain increases with a decrease in the W parameter, that is, with a decrease in the amplitude of the surface wave and the depth of the observed object and an increase in the characteristic scale of this object.

Therefore, there is not always justification for the striving to use apparatus with maximum spatial resolution for observing underwater features. The cited results of computations make it possible to determine in what cases there is assurance of a greater accuracy in measuring their luminosity distribution when there is finite spatial averaging, to find the optimum value of this averaging and to evaluate the accuracy gain occurring in this case.

BIBLIOGRAPHY

1. Mullamaa, Yu.-A. R., "Influence of the Wave-Covered Sea Surface on the Visibility of Underwater Features," IZV. AN SSSR: FAO (News of the USSR Academy of Sciences: Physics of the Atmosphere and Ocean), Vol 11, No 2, pp 199-206, 1975.

2. Levin, I. M. and Litvin, V. Kh., "Image Transfer Through a Sinusoidal Wave," IZV. AN SSSR: FAO, Vol 16, No 5, pp 490-495, 1980.

3. Veber, V. L., "Statistical Characteristics of Images Obtained During Observation Through an Uneven Interface Between Media With Different Refractive Indices," IZV. VUZov: RADIOFIZIKA (News of Institutions of Higher Education: Radiophysics), Vol 22, No 8, pp 989-1001, 1979.

4. Sondkhi, M. M., "Image Restoration: Aging of Spatially Invariant Distortions," OBRABOTKA IZOBRAZHENIY PRI POMOSHCHI TSIFROVYKH VYCHISLITEL'NYKH MASHIN (Image Processing Using Digital Computers), Moscow, Mir, pp 137-152, 1973.

5. Krylov, Yu. M., SPEKTRAL'NYYE METODY ISSLEDOVANIYA I RASCHETA VETROVYKH VOLN (Spectral Methods for Investigating and Computing Wind Waves), Leningrad, Gidrometeoizdat, 1966, 256 pages.

6. Levin, B. R., TEORETICHESKIYE OSNOVY STATISTICHESKOY RADIOTEKHNIKI (Theoretical Principles of Statistical Radio Engineering), Book I, Moscow, Sovetskoye Radio, 1969, 752 pages.

7. Levshin, V. L., PROSTRANSTVENNAYA FIL'TRATSIYA V OPTICHESKIKH SISTEMAKH PELENGATSII (Spatial Filtering in Optical Direction-Finding Systems), Moscow, Sovetskoye Radio, 1971, 200 pages.

8. Korn, G., MODELIROVANIYE SLUCHAYNYKH PROTSESSOV NA ANALOGOVYKH I ANALOGO-TSIFROVYKH MASHINAKH (Modeling of Random Processes on Analog and Analog-Digital Computers), Moscow, Mir, 1968, 315 pages.

9. Yerlov, N., OPTICHESKAYA OKEANOGRAFIYA (Optical Oceanography), Moscow, Mir, 1970, 224 pages.

5303
CSO: 1865/150

UDC 551.46.07:577.472(268)

SEMINAR ON GEOPHYSICAL HYDRODYNAMICS OF COMMISSION ON WORLD OCEAN PROBLEMS, USSR ACADEMY OF SCIENCES (CHAIRMAN: A. S. MONIN, CORRESPONDING MEMBER, USSR ACADEMY OF SCIENCES)

Moscow OKEANOLOGIYA in Russian Vol 22, No 2, Mar-Apr 82 pp 343-347

[Article by B. N. Filyushkin]

[Text] 144th session of seminar -- 9 January 1981. Report by Candidate of Physical and Mathematical Sciences G. M. Reznik (Institute of Oceanology, USSR Academy of Sciences) -- "Slightly Nonlinear Interactions of Rossby Waves."

The first part of the report gives the derivation of a kinetic equation describing the temporal evolution of the energy spectrum of slightly nonlinear waves with random amplitudes. The method of many scales ("fast" time -- the characteristic time of change in wave phases, "slow" time -- the amplitude of waves due to nonlinear interactions) was applied to an infinite series of equations for cumulants. No restrictions are imposed on random wave fields other than their spatial homogeneity. The conclusion presented here makes it possible to avoid some difficulties encountered in conclusions based on an analysis of the equations for registered series (Benin and Safman (1966), Hasselman (1962, 1967)), and it is substantially shorter than the latter.

The second part of the report discussed the results of investigation of slightly nonlinear interactions of barotropic Rossby waves. On the basis of a kinetic equation a study was made of the problem of the dependence of the rate of energy transfer in the spectrum ($\partial F/\partial t$) on the form of the spectrum $F(k, \ell, t)$, where k, ℓ are the wave numbers along the x, y axes and t is time. It was demonstrated that if the spectrum is greatly "blurred" in azimuth, energy transfer intensifies the zonal current component, which agrees with the results obtained earlier by Cannon (1966) and Rice (1975). However, with an adequately strongly expressed zonality of flow an intensive outflow of energy to the meridional component begins and thus there is no degeneration into a zonal flow. Another effect is as follows. Assume that the initial spectrum is asymmetrical. Then it can be demonstrated that energy transfer decreases the asymmetry and with time the spectrum should tend to a symmetric state. After attaining such a state the spectrum remains symmetric at all subsequent moments in time as well.

145th session of seminar -- 23 January 1981. Report by Candidate of Physical and Mathematical Sciences A. Yu. Benilov (Institute of Oceanology, USSR Academy of Sciences) -- "Formation of Thin Quasihomogeneous Layers in Stratified Ocean."

A study was made of the formation of mixed layers for two very simple models of density stratification -- a two-layer and a linearly stratified fluid. Density is determined by the change in temperature and salinity. In describing the processes of vertical turbulent transfer of momentum, heat, salt, in describing the dynamics of turbulence (kinetic energy of turbulent fluctuations) and mean square values of temperature and salinity fluctuations use is made of a system of equations for semiempirical turbulence theory. A study was made of the evolution of turbulent layers on the assumption of statistical homogeneity in the horizontal planes of all the random fields. The system of equations is integrated vertically, taking into account that the turbulent energy and all the turbulent flows outside the region of turbulent mixing equal zero. A dipole scheme is used for the mean fields of velocity, temperature and salinity. The vertical structure of the characteristics of turbulence is parameterized in such a way that the problem is reduced to a study of the temporal change in the mixing layer and the maximum values of turbulent energy in it and the mean square values of temperature and salinity fluctuations.

Then different mechanisms of formation of mixed layers were examined. In a two-layer fluid the latter arise due to instability of the initial velocity jump, the initial turbulence burst or the development of a plane turbulent jet current at an interface unperturbed at the initial moment in time. In the case of a continuous stratification their development occurs as a result of the last two of the factors mentioned above and also with a loss of stability of the background velocity shear. In the case of an unstable background stratification the enumerated mechanisms of development of turbulent mixing are sources of initial perturbations which are only intensified by unstable stratification, which in the last analysis leads to a complete mixing of the region of background instability. With different laws of stratification within the framework of a semiempirical description turbulence develops in such a way that with unstable background conditions it is intensified and the displacement zone increases; under stable conditions turbulence in the last analysis degenerates, forming a mixed layer of finite thickness. A classification of stability and instability of background conditions was made relative to turbulent perturbations. Explicit correlations were obtained between the thickness of the quasi-homogeneous layers and background conditions and initial turbulence perturbations. The laws of degeneration of turbulence are indicated for different stratification conditions. An analysis of the temporal evolution of the mean square values of temperature and salinity fluctuations indicated that with the degeneration of turbulence under the influence of buoyancy forces these parameters attain finite values, not becoming equal to zero in this case.

146th session of seminar -- 13 February 1981. Report of Candidate of Physical and Mathematical Sciences Yu. D. Chashechkin and V. S. Belyayev (All-Union Scientific Research Institute of Physicotechnical and Radiotechnical Measurements), entitled "Regimes of Free Thermoconcentration Convection Over a Point Heat Source."

A free convective current over a point heat source in a fluid with a stable gradient of the concentration of dissolved admixtures leads to the formation of a vertically periodic system of axially symmetric convective cells. Analysis of the profiles of temperature distribution with depth in the depressions of

the Red Sea rift made it possible to express the hypothesis of the existence of localized sources of thermal waters over which the fine structure of the sea medium is formed (Monin, et al., 1980). The global Rayleigh number Ra in the latter case is much greater than in laboratory experiments. In this connection laboratory experiments were carried out for a detailed study of the structure of a convective current over a point heat source with different, including large, quantities of conducted power P. The experimental method is described. The experiments did not reveal any dependence of the nature of the developing current on basin extent. A thermal heating element (THE) was also used in order to exclude the influence of electrohydrodynamic instability. This element consisted of a metallic cylinder with a height of 1 cm and a diameter of 0.8 cm, within which a Nichrome spiral was placed.

These experiments made it possible to discriminate five characteristic regimes of a convective current over a point heat source in a stratified medium. 1. Diffusion regime. With small P, when $Ra < 450$, a warm diffusion spot is formed over the heater. The profiles of temperature, salinity and density remain smooth. 2. Lateral structures. If $Ra > Ra_{cr}$ = 285-450, one (or several, depending on the height of the heater) convective cell is formed over the point heat source or along the lateral surface. 3. Laminar-cellular convection. A fine floating-up jet, surrounded by a bell-like "veil" of subsiding fluid, is formed with $1000\text{-}2250 < Ra < 20\ 000$. Axially symmetric cells with a height of 0.7-1.5 cm are formed around a salt dome. The number of cells increases with an increase in the intensity of heating. 4. Finger-cellular convection. The flow in the subsiding salt dome becomes unstable and disintegrates into salt fingers when $20\ 000 < Ra < 50\ 000$. The region of finger convection is surrounded by a system of eddy cells. 5. Intrusive regime. With $Ra > 50\ 000$ the current in the floating-up warm jet becomes unstable. Entrainment of the surrounding fluid increases sharply and a spot of partially mixed fluid is formed above the heater in which the temperature and salinity is greater than in the ambient medium. The mixed fluid flows out in individual intrusive tongues. One or more cells are formed over the mixing region.

In the regime of laminar- and finger-cellular convection the height of the structure increases with an increase in the power $P^{0.5} \sim (Ra)^{0.5}$. When $Ra > 50\ 000$ (intrusive regime) the height decreases with an increase in P. In all convection regimes the current pattern is nonstationary and the position and the number of layers change with the passage of time. The height of the cells is slightly dependent on power: $h \sim P^{0.14}$.

A study was also made of the current pattern over two heat sources situated along one vertical or along one horizontal.

147th session of seminar -- 27 February 1981. Report of Professor B. A. Kagan and V. A. Ryabchenko (Leningrad Division, Institute of Oceanology, USSR Academy of Sciences), entitled "Modeling of Distribution of Oxygen and Carbon Cycle in Ocean."

The report is devoted to a discussion of the problem of modeling the distribution and global budget of oxygen and carbon dioxide dissolved in sea water.

The basis for the proposed 2 1/2-dimensional model of the distribution of dissolved oxygen is the similarity hypothesis for the vertical structure of the oxygen field in each of the oceans. The turbulent diffusion equation, integrated vertically from the free surface to the bottom, with this hypothesis taken into account, together with the expressions for the barotropic and baroclinic components of horizontal velocity, the expressions parameterizing oxygen exchange between the ocean and atmosphere, oxygen production for photosynthesis and biochemical consumption of oxygen, boundary and initial conditions, is used in computing the mean annual distribution of the integral (vertically) concentration and the components of the natural oxygen budget in the world ocean as a whole and in individual oceans.

The results of numerical experiments show a qualitative agreement of the computed spatial distribution of integral concentration, the values of oxygen exchange between the ocean and the atmosphere and between individual oceans and observational data. At the same time there is a strong dependence of the solution on the stipulation of biochemical "inputs" and "outputs" of oxygen in the world ocean.

The carbon cycle is described within the framework of a simple and economically advantageous box model of the ocean. In contrast to the traditional approach, the thickness of the upper quasihomogeneous layer (UQL), water temperature and exchange coefficients between the UQL and the deep layer (DL) of the ocean, as well as the magnitude of the CO_2 flux at the water-air interface, are not registered, but are determined in the course of solution of the problem.

Two regions in the ocean are defined: a region of formation of cold deep waters and the entire remaining part of the ocean, within which the entry of cold deep waters from the regions of their sources is compensated by upwelling. In turn, two layers -- the UQL and the DL -- are discriminated in the upwelling region.

The equations for temperature T_i and for the total carbon concentration C_i in the three mentioned boxes, the addition of an equation for the thickness h of the UQL, expressions for the fluxes of heat and carbon at the ocean surface, at the lower boundary of the UQL and at the upper boundary of the DL, a system of algebraic equations describing the behavior of CO_2 in solution, and also the "inputs" and "outputs" of carbon of organic origin, form a closed system. The latter makes it possible to reproduce the seasonal evolution of T_i, C_i, h, CO_2 concentration, bicarbonate and carbonate ions and hydrogen ions, gas exchange with the atmosphere and exchange of heat and carbon between the UQL and the DL of the ocean. As the initial information for determining the enumerated characteristics use was made of data on the heat flow at the ocean surface, partial pressure of CO_2 in the atmosphere, dynamic wind velocity, intensity of the source of cold deep waters and on the ratio of the areas of the region of upwelling and the region of formation of cold deep waters.

The results of numerical experiments carried out for northern hemisphere ocean waters indicate that the proposed model describes the principal qualitative characteristics of the thermal regime and carbon cycle in the ocean. However, the accuracy in their reproduction is determined to a considerable degree by stipulation of the rate of upwelling, the mean annual surface heat flow, and also "inputs" and "outputs" of carbon of organic origin.

148th session of seminar -- 27th March 1981. Report of Candidate of Physical and Mathematical Sciences V. P. Krasitskiy (Institute of Oceanology, USSR Academy of Sciences) -- "Two-Dimensional Cortewega-De Vries Equation for Gravitational-Capillary Waves."

The first part of the report, using one of the modifications of asymptotic methods, gives the derivation of the two-dimensional Cortewega-De Vries equation (Kadomtsev-Petviashvili equations) for the case of gravitational-capillary waves in shallow water. This equation is similar to the corresponding equation for the case of purely gravitational waves, except that in the considered case the dispersion parameter (coefficient on the dispersion term in the equation) changes sign with a depth of the undisturbed water layer of about 0.5 cm. Then the speaker gave an analysis of the known solutions of the Kadomtsev-Petviashvili equation in application to the case of gravitational-capillary waves. Particular attention was devoted to an examination of the properties of two-dimensional rational solitons which for the considered problem are stable formations with a depth less than 0.5 cm (positive dispersion corresponding to a negative dispersion parameter) and represent "depressions" with an insignificant increase in the level of the undisturbed water at the edges of the depression. A detailed study was made of the geometry of such solitons and numerical evaluations are given showing the fundamental possibility of observing such solitons under laboratory conditions.

149th session of seminar -- 3 April 1981. Report of Academician Ya. B. Zel'dovich and Candidate of Physical and Mathematical Sciences A. A. Rumzaykin (Institute of Applied Mathematics, USSR Academy of Sciences), and Candidate of Physical and Mathematical Sciences D. D. Sokolov (Moscow State University) -- "Generation of Magnetic Fields in a Well-Conducting Medium."

The magnetic field in a moving conducting medium, on the one hand, changes under the influence of deformation of velocity, and on the other hand, is subject to ohmic diffusion. The relative force of these effects is determined by the magnetic Reynolds number Rm. With large Rm there can be an unlimited exponential growth or maintenence of the field (dynamo process). The Reynolds magnetic number is quite great in the liquid cores of the planets ($3 \cdot 10^2$ for the earth, $2 \cdot 10^4$ for Jupiter), convective envelopes of stars (for the sun $Rm \approx 10^8$), accretion disks in binary star systems ($\sim 10^{10}$), galactic and other cosmic bodies. Accordingly, the dynamo theory problem is a clarification of the conditions for generation of a magnetic field in an asymptotic regime $Rm \gg 1$. The authors only touched on some results of the theory in a so-called kinematic approximation, that is, when the velocity field is considered stipulated.

A decisive role is played by current topology. If the fluid moves along a plane or a spherical surface a dynamo is impossible (exclusion theorem). Only a temporary increase in the field is possible; it is then replaced by asymptotic attenuation. With movement of a conducting fluid along stationary surfaces of a more general type (such as a torus or a cylinder) there can be an exponential increase in the magnetic field. However, it will be slow and the rate of field increase in the long run becomes equal to zero when $Rm \to \infty$.

A rapid dynamo, for which the rate of field increase does not become equal to zero when $Rm \to \infty$, is possible for some three-dimensional currents. The simple mechanism of such a dynamo is the simple folding of the field loop into a figure eight with subsequent doubling. A realistic example of a rapid dynamo is a dynamo in turbulence having average spiraling. Such turbulence naturally arises in the cores of planets and the convective envelopes of stars due to rotation and density stratification of the fluid. A rapid dynamo, operating due to spiraling of turbulence and nonuniform rotation, is the principal mechanism of the solar (stellar) activity cycle.

Another example of a rapid dynamo is the generation of microscale magnetic fields in turbulence, on the average mirror-symmetric. Field excitation is already possible with relatively small Rm ($\gtrsim 60$) and with a Prandtl magnetic number less than unity. The latter condition is not satisfied in the cores of planets.

Recently many new results have been obtained in nonlinear dynamo theory, with allowance for the inverse influence of the magnetic field on motion. The nonlinear dynamo makes it possible to explain complex global stochastic regimes in the behavior of the magnetic field. One of these phenomena is random reversals of the earth's magnetic field and another is global minima of solar activity of the well-known Maunder minimum type.

150th session of seminar -- 15 May 1981. Report of Corresponding Member USSR Academy of Sciences G. S. Golitsyn (Institute of Atmospheric Physics, USSR Academy of Sciences) -- "Investigation of Convection of a Rapidly Rotating Fluid."

The first part of the report gave the derivation of a formula for the mean velocities of convective movements of a quite rapidly rotating fluid with application of the concepts of similarity and dimensionality, using some self-similarity hypotheses, on the assumption of nonessentiality of the precise values of the molecular coefficients of transfer and depth of the fluid. Simple experiments with convection in carbonated mineral water and in water cooling from the surface indicated a satisfactory coincidence between the measured and predicted velocities and made it possible to estimate the numerical value of the coefficients in theoretical formulas. However, observations of the propagation of a tracer in a rotating fluid show that this propagation occurs in thin layers or tongues where the effects of viscosity must be substantial.

The assumption that these layers are internal boundary layers of the Ekman type and an analysis of the balance of dissipation of the kinetic energy of movements solve the paradox which arises, aggravated further by the exclusion of vertical movements in an ideal fluid by the Proudman-Taylor theorem. A detailed analysis of the balance of dissipation in the entire volume of the rotating fluid shows that movements with the estimated velocities occupy only a small fraction of the total volume. Rough estimates show that this fraction can fall in the range 0.1-0.01.

This was followed by a discussion of the laws of heat or mass transfer during convection of a rotating fluid on the basis of laboratory measurements by H. T. Rossby. A qualitative explanation is given for the lag in development of convection, the decrease in the Nusselt number (rate of heat transfer) with an increase in the velocity of rotation. Use was made of the known analogies between currents of rotating and stratified fluid (in the latter there is also a stratification of movements).

In conclusion there was a discussion of the application of the results to an estimate of the rates of convection in the giant planets, having internal heat sources, and to the earth's liquid core. The rates of movements in the core are estimated at several kilometers annually, which in order of magnitude coincides with the velocities of drift of nondipole geomagnetic field components. The resulting observed structure of currents can explain the geomagnetic dynamo. For the ocean, as in the case of the sun, the role played by rotation in formation of the structure of convection is small in the sense that the effects studied here should usually still not be manifested.

151st session of seminar -- 12 June 1981. Report of Professor V. Ye. Zakharov (Institute of Theoretical Physics imeni Landau, USSR Academy of Sciences) and Candidate of Physical and Mathematical Sciences M. M. Zaslavskiy (Institute of Oceanology, USSR Academy of Sciences) -- "Theory of Wind Waves in the Approximation of Weak Turbulence."

On the basis of experimental data on the closeness of the energy-carrying components of sufficiently well-developed waves to linear free waves, for their description use is made of the kinetic equation of the "weak turbulence" approximation, taking into account nonlinear interactions, pumping from the wind and dissipation. It is shown that with the natural assumption of localization of pumping and dissipation in a microscale region there is a significant physical simplification of the general kinetic equation for wind waves related to the circumstance that the $S(\omega)$ spectrum of adequately developed waves in the energy-carrying region is determined only by the integral characteristics of interaction of waves with the wind and drift currents. In this case $S(\omega)$ is determined by a dimensional analysis of the kinetic equation: $S(\omega) = 2ap^{1/3} \cdot g^{4/3}\omega^{-11/3} \cdot \theta_S(\omega/\omega_m)$, where a is a dimensionless coefficient dependent on the angular distribution of energy; p is the integral flux of the wave effect into the long-wave region; θ_S is the "blurred" Heaviside function, forming the spectrum at the frequency of the spectral maximum ω_m. The derived expression for $S(\omega)$ is in satisfactory agreement with the experimental data.

On the basis of the initial equation in a general horizontally inhomogeneous and nonstationary case an equation is then derived for the correlation of the parameters ω_m and p of the derived expression for $S(\omega)$, which is reduced to an equation in partial derivatives for ω_m in the approximation of a constant flux of the effect, taking into account all the processes of interaction between waves and the wind and drift currents by the introduction of the single parameterization constant p = const. All the corollaries from this equation available for comparison with experimental data satisfactorily describe the results of in situ measurements of the parameters of adequately developed

wind waves. This gives basis for counting on the suitability of this theory in predicting wind waves; the derived equation for ω_m has only one empirical constant p.

152d session of seminar -- 19 June 1981. Report of Candidate of Physical and Mathematical Sciences V. D. Larichev (Institute of Oceanology, USSR Academy of Sciences) -- "Nonlinear Dynamics on the β-Plane and Solitary Waves.

The general tendencies in the nonlinear evolution of disturbance on the β-plane (barotropic problem) localized in space were examined. It was demonstrated that in the nonlinear problem, due to the conservation of potential vorticity, there will be a restriction on the wave radiation at infinity and therefore situations are possible when in an unlimited region the amplitude of the localized disturbance does not decrease to zero with time (in contrast to the linear problem). The author gave an analysis of several such situations differing with respect to the geometry of the boundaries and the structure of the current. Applications to Gulf Stream rings are given. On the basis of these considerations the paper gives a comparison of two-dimensional antisymmetric Rossby solitary waves which indicates a greater stability of the waves moving to the west than to the east.

The concept of a closed potential vorticity isoline is introduced; this determines the behavior of the amplitude of the disturbance over greater times. The presence of closed isolines means a conservation of a nonlinear regime at all times, which gives a cessation of the spectral energy flux. The conservability of closed potential vorticity isolines leads to the appearance of a "memory" in the system and as a result, the absence of universal spectra. Two "anti-soliton theorems" are formulated: the first gives the necessary condition for the initial vorticity field in which two-dimensional solitary Rossby waves do not appear with the passage of time; the second shows that antisymmetric solitary waves do not survive collisions. The role of two-dimensional Rossby solitary waves in the dynamics of the ocean is discussed.

5303

CSO: 1865/149

UDC 656:551.46(268)

POLAR NORTHEASTERN EXPEDITION OF INSTITUTE OF OCEANOLOGY IMENI P. P. SHIRSHOV, USSR ACADEMY OF SCIENCES (1978-1981)

Moscow OKEANOLOGIYA in Russian Vol 22, No 2, Mar-Apr 82 pp 349-350

[Article by Yu. I. Vozovik, A. S. Ionin and Yu. M. Babayev]

[Text] In 1978 the Institute organized the First Polar Northeastern Expedition (FPNEE) for the purpose of studying relief, geological structures and sediments on the shelf of the Chukchi and Bering Seas (expedition chief Yu. A. Pavlidis). This expedition planned the implementation of its work in collaboration with the Geography Faculty of Moscow State University and the Provideniya hydrological base. The institute regards work on the Arctic shelf to be highly important, especially when carrying out leading geological-geomorphological investigations.

In 1978 the FPNEE, aboard the ship "Dmitriy Laptev" of the Provideniya hydrological base, carried out a complex of studies, including geophysical investigations on the shelf, by the continuous seismic profiling method, drilling of the stratum of sediments with a vibrating piston corer, echo sounding measurements and on-shore geological-geomorphological investigations [1].

In 1980 expeditionary work was carried out in this same region, first on the ship "Vega," and later on the ship "Dmitriy Laptev" (expedition chief Yu. I. Vozovik). The work program provided for the carrying out of further geological-geomorphological investigations, including forming of a denser grid of sea runs and stations with the taking of bottom samples and also underwater photographing of the surfaces of characteristic bottom relief elements. Particular attention was devoted to the study of relief and bottom sediments of the fiord bays of southeastern Chukotka in connection with the problem of their origin, and also for solving the problem of the nature of Late Pleistocene glaciation, leaving its traces in the form of relict glacial relief in the coastal-shelf zone.

The ship "Dmitriy Laptev" was used in running the following extended geological profiles with the taking of bottom samples: along the entire Bering Sea shelf from its southern edge in the neighborhood of Cape Navarin to Bering Strait and then to Cape Golovnin (Hope) in Alaska, in the Chukchi Sea -- a submeridional profile to Kolyuchinskaya Bay with studies in the latter and the profile

Wrangel Island - Bering Strait. During the expeditionary period a total of 1800 miles of geological profiles were run, 700 miles of echo soundings were run, 122 geological stations were occupied with the taking of cores with an impact corer and with taking of dredged samples, and samples of the surface layer of bottom sediments were fixed. Underwater photography of the bottom was taken at 57 stations.

In 1981 expeditionary investigations on the shelf of seas in the Northeastern USSR, on the one hand, were finalized (in the Chukchi Sea and in the northern part of the Bering Sea), and on the other hand represented the first attempt of institute specialists to carry out reconnaissance geological-geomorphological and lithological work in the East Siberian and Laptev Seas. In the Chukchi and Bering Seas the plan called for carrying out additional geological exploration along lines of long-planned sea runs not executed in preceding years in connection with ice conditions or stormy weather. A new type of investigation was lithodynamic studies, specifically the use of bathometers to take water samples from different horizons for determining the quantity of suspended matter and its mineralogical composition in the water layer of these seas. This is necessary for clarifying the problem of the nature of transport of suspended matter from the Bering Sea to the Chukchi Sea and the role of solid runoff of the Yukon River and other rivers in the processes of morpholithogenesis in the southeastern part of the Chukchi Sea.

In order to carry out research work for PNEE-81 (expedition chief A. S. Ionin) the Provideniya hydrological base was given the ship "Dmitriy Laptev" and the icebreaker "Georgiy Sedov." The ship "Dmitriy Laptev" (detachment heads V. S. Medvedev and Yu. A. Pavlidis) was used in carrying out geological runs with the taking of cores, dredged samples and suspended matter in the following directions: Lavrentiya Gulf-Cape Douglas (Alaska), Bering Strait - Cape Golovnin (Alaska), Cape Golovnin - Cape Serdtse Kamen' (Chukotka), Vankar' village - Wrangel Island, Wrangel Island - Herald Bank, Cape Chukotskiy - mouth of the Yukon River. Geological sections were accompanied by echo sounding measurements. The icebreaker "Georgiy Sedov" (detachment heads Yu. I. Vozovik and V. V. Kalinenko) carried out the following sections: Long Strait - Chaunskaya Bay, Ayon Island - Bear Islands, Bear Islands - Strait Dmitriy Laptev - Tiksi Bay. The detachments carried out much geological-geomorphological work in polygons in the neighborhood of the Bear Islands.

In all, during the expeditionary period, somewhat shortened as a result of the severe ice conditions, the detachments carried out: 17 geological runs with a total extent of about 1600 miles, echo sounding runs of 1800 miles and 102 geological stations. During the time of work 135 dredged bottom samples were taken, as well as 181 samples of water from different horizons and 63 bottom cores.

In the course of the work material was collected on geological structures, the characteristics of relief structure and the lithology of the sedimentary strata of the northeastern shelf of the USSR. Investigations were made of the distribution and composition of the suspended matter, making possible a deeper comprehension of the mechanism of polar morpholithogenesis and a determination of the rate of sedimentation processes.

In general it should be noted that as a result of the three Polar Northeastern Expeditions of the Institute it was possible to determine the principal characteristics of the structure of the upper stratum of bedrocks on the shelf, primarily the Chukchi Sea, ascertain its principal morphostructural elements and prepare a general map of the latest vertical movements of these structures. Lithological investigations made it possible to characterize sedimentation conditions in the Chukchi Sea, determine the balance of sedimentary material and ascertain the facies-lithological zones on the shelf. Micropaleontological investigations of bottom cores made possible a stratigraphic breakdown of Holocene shelf deposits. The collected materials to a considerable degree broadened existing concepts concerning the Late Pleistocene history of development of the shelf zone of the Chukchi-Bering region. The collected materials served as a basis for developing a theory of morpholithogenesis on the shelves of the world ocean and in particular, made it possible to ascertain the characteristics of polar morpholithogenesis on the shelf of the Northeastern USSR.

BIBLIOGRAPHY

1. Pavlidis, Yu. A., Babayev, Yu. M., Ionin, A. S., Vozovik, Yu. I. and Dunayev, N. N., "Characteristics of Polar Morpholithogenesis on the shelf of the Northeastern USSR," KONTINENTAL'NYYE I OSTROVNYYE SHEL'FY. REL'YEF I OSADKI (Continental and Island Shelves. Relief and Sediments), Moscow, Nauka, pp 33-96, 1981.

5303
CSO: 1865/149

UDC 551.46.085

OSCILLATIONS OF CURRENT RECORDERS AT SELF-CONTAINED BUOY STATIONS AND THEIR EFFECT ON MEASUREMENTS OF CURRENT PARAMETERS

Moscow OKEANOLOGIYA in Russian Vol 22, No 2, Mar-Apr 82 (manuscript received 12 Nov 80, after revision 2 Apr 81) pp 329-336

[Article by V. M. Kushnir and V. I. Remchukov, Marine Hydrophysical Institute, USSR Academy of Sciences, Sevastopol']

[Text]

Abstract: A recorder of fluctuations of relative current velocity and angular deviations relative to the longitudinal, transverse and vertical axes of a current meter is described. Methods for the statistical processing of data for the purpose of determining the contribution of different components to the total dispersion of the error in measuring current velocity are analyzed. Also discussed are the results of measurements made in the Caribbean Sea at different depths.

Among the principal factors determining the errors in measuring the parameters of oceanic currents at self-contained buoy stations are the characteristic motions of current meters. These motions consist of the angular movements of the body of the automatic recorder relative to the suspension point, horizontal and vertical oscillations of the suspension point, slow movements of the line relative to the anchor. The main disturbances responsible for these movements are surface waves, periodic and aperiodic currents at different depths, elasticity forces in the line and its changing geometry and torsional oscillations of the supporting line under the influence of changing tension.

The motion of the supporting buoy at a buoy station and the slow oscillations of the line associated with it were investigated by Rebaynis [7] using navigational methods. These investigations revealed the most characteristic periods of oscillations: 1.5, 3.2, 6 and 12 hours with velocities from 2 to 30 $cm \cdot sec^{-1}$.

At the present time extremely little study has been made of the more high-frequency oscillations, primarily by means of a motion picture survey of the behavior of the instruments at shallow-water buoy stations [1] and by means of

modeling of the effect of currents and waves on the body of the instrument in a hydrodynamic basin [2]. The results of these investigations indicated that oscillations of the current meters have a substantial effect on the observation results.

Oscillations of current recorders at buoy stations are considerably more complex than can be modeled in a basin or registered by a motion picture survey in the case of shallow water near a pile base. In order to evaluate the real errors in measuring currents under different conditions there must be investigations of characteristic movements under in situ conditions.

In order to solve this problem, on the proposal of V. G. Kort, corresponding member, Ukrainian Academy of Sciences, specialists at the Marine Hydrophysical Institute, Ukrainian Academy of Sciences, created a special apparatus and method for the processing of data and carried out the first measurements during the 38th voyage of the scientific research ship "Mikhail Lomonosov" in the Caribbean Sea. This article gives the results of these investigations.

The DISK-M self-contained recording instrument was incorporated in the body of the DISK current recorder [6, 9]. The placement of individual units in the instrument is shown in Fig. 1. The programming unit 6 of the DISK-M cuts the measurement system and the recorder into the power circuit at a stipulated time ($\sim$10 hours) after triggering of the clock mechanism. The measurements are made with a discreteness of 0.8 sec over the course of 1.5 hour. Fluctuations of the relative flow velocity are measured by an impeller 3 mounted on the upper cover of the instrument. The position of the axis of the impeller relative to the plane of the magnetic meridian is measured by a magnetic compass 9 held in a Cardan joint. The measuring transducer of this compass ensures continuous readings with an absolute error of 3°. The instrument also registers oscillations of two pendulums 4 whose axes are registered relative to the body parallel and perpendicular to the axis of the impeller.

The registry of all four parameters in the form of a binary code is accomplished using a standard miniaturized magnetic recorder cassette 7. The reproduction of the recorded information is by use of a cassette magnetic recorder through a special reproduction unit directly in the electronic computer operational memory.

The impeller of the DISK-M measurement apparatus has four blades with a radially variable pitch, at the bottom resting on supports. The diameter of the screw is 133 mm, the geometric pitch of the impeller is 255 mm, the start-up threshold is 0.5-1 $cm \cdot sec^{-1}$, reading is contactless, by means of 12 small magnets embedded in a rim. Specially formulated investigations revealed that the impeller synchronization path is 16-18 cm. The equivalent time constant is equal to the ratio of the synchronization path to the current velocity and for typical measurement conditions in the ocean does not exceed 1-1.5 sec.

The pendulums are 500-gram weights attached eccentrically on the axes of precision wire potentiometers and placed in oil. The nominal period of the attenuating oscillations of the pendulums is 0.4 sec, the attenuation time of the oscillations is $\sim$2 sec. The mean square error in measuring deflections of the pendulums is 0.36 degree.

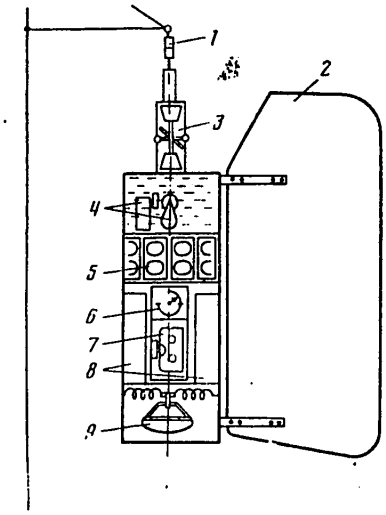

Fig. 1.

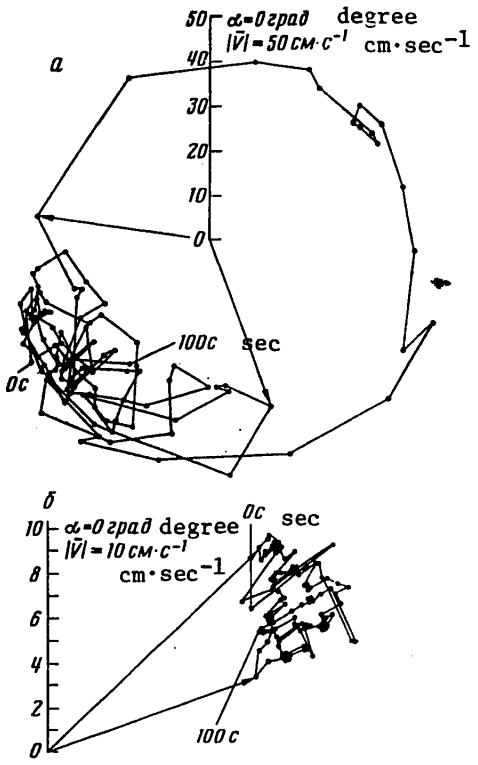

Fig. 2.

Fig. 1. Makeup of DISK-M instrument. 1) pivot; 2) stabilizer; 3) impeller; 4) pendulums; 5) power unit; 6) programming mechanism; 7) magnetic recorder ; 8) measurement system; 9) magnetic compass.

Fig. 2. Hodographs of vector of relative velocity according to readings of DISK-M instrument at buoy station 1 (a) and buoy station (2) in 100 sec.

For an analysis of the interrelationship between the readings of the pendulums and the horizontal rate of movements of the instrument, which is registered by the impeller, we will use the known equations of motion of the pendulum in the presence of a forcing force [4, 8]. In a linear approximation and on the assumption that the vertical accelerations are considerably less than the acceleration of gravity, the equation for fluctuations of the β angle of pendulum deflection relative to the body of the instrument and the horizontal velocity V of instrument movement can be written in the following form:

$$K_M V = \dot{\beta} + 2\delta\omega_0\beta + \omega_0^2 \int_0^\tau \beta(\tau_1)\, d\tau_1, \qquad (1)$$

where δ is the relative attenuation coefficient; ω_0 is the frequency of the natural nonattenuating pendulum oscillations; $k_M = m\ell/I$ is a constant coefficient in which m is pendulum mass; ℓ is the distance between the pendulum center of gravity and the axis of rotation; I is the moment of inertia.

The resultant fluctuations of velocity V are represented in the form of the sum of the three components V_1, V_2, V_3, corresponding to the contribution to the total movements of the three terms on the right-hand side of equation (1), and we will compute their dispersions σ_1^2, σ_2^2 and σ_3^2.

Since the stationary random processes and their derivatives at coinciding moments in time are uncorrelated [5], we find

$$M(V^2) = M[(V_1 + V_2 + V_3)^2] = \frac{1}{k_M^2} M(\dot{\beta}^2) + \\ + \frac{4\delta^2\omega_0^2}{k_M^2} M(\beta^2) + \frac{\omega_0^4}{k_M^2} M\left[\left(\int_0^\tau \beta(\tau_1)\, d\tau_1\right)^2\right] = \sigma_1^2 + \sigma_2^2 + \sigma_3^2, \quad (2)$$

where M is the symbol for averaging of the random value in the set.

In order to determine the dispersions σ_1^2- σ_3^2 we will use the characteristics of cross-statistical processing of fluctuations of the β angle and velocity V. In general form

$$M[V_1(\tau) V_1(\tau+\tau_1)] = \frac{1}{k_M} M[\dot{\beta}(\tau) V_1(\tau+\tau_1)] = \frac{1}{k_M^2} M[\dot{\beta}(\tau)\dot{\beta}(\tau+\tau_1)]; \quad (3)$$

$$M[V_2(\tau) V_2(\tau+\tau_1)] = \frac{2\delta\omega_0}{k_M} M[\beta(\tau) V_2(\tau+\tau_1)] = \frac{4\delta^2\omega_0^2}{k_M^2} M[\beta(\tau)\beta(\tau+\tau_1)]; \quad (4)$$

$$M[V_3(\tau) V_3(\tau+\tau_1)] = \frac{\omega_0^2}{k_M} M[\beta^{(-1)}(\tau) V_3(\tau+\tau_1)] = \\ = \frac{\omega_0^4}{k_M^2} M[\beta^{(-1)}(\tau)\beta^{(-1)}(\tau+\tau_1)], \quad (5)$$

where $\beta^{(-1)}(\tau) = \int_0^\tau \beta(\tau_1)\, d\tau_1$.

Using expressions (3)-(5), the dispersions σ_1^2- σ_3^2 and the proportionality factors between the components of the velocity fluctuations and the corresponding derivatives of the angle of pendulum deflection are determined through the cross-correlation functions with zero drift. Taking into account that the fluctuations of the angle of pendulum deflection β are in quadrature with the velocity components V_1 and V_3, and the velocity component V_2 is in phase with the fluctuations of the β angle, and omitting intermediate transforms, we find

$$\sigma_1^2 = \frac{\frac{1}{2\pi}\left[\int_{\omega_1}^{\omega_2} \omega S_{-}(\omega)\, d\omega\right]^2}{\int_{\omega_1}^{\omega_2} \omega^2 S_\beta(\omega)\, d\omega}; \quad (6)$$

$$\sigma_2^2 = \frac{\frac{1}{2\pi}\left[\int_{\omega_1}^{\omega_2} S_+(\omega)\,d\omega\right]^2}{\int_{\omega_1}^{\omega_2} S_\beta(\omega)\,d\omega}; \tag{7}$$

$$\sigma_3^2 = \frac{\frac{1}{2\pi}\left[\int_{\omega_1}^{\omega_2} \frac{1}{\omega} S_-(\omega)\,d\omega\right]^2}{\int_{\omega_1}^{\omega_2} \frac{1}{\omega^2} S_\beta(\omega)\,d\omega}, \tag{8}$$

where $$S_-(\omega) = \frac{1}{2}\int_{-\infty}^{\infty} [R_{V\beta}(\nu) - R_{V\beta}(-\tau)] \sin \omega\tau\, d\tau$$

is the quadrature spectrum of fluctuations of velocity and angle;

$$S_+(\omega) = \frac{1}{2}\int_{-\infty}^{\infty} [R_{V\beta}(\tau) + R_{V\beta}(-\tau)] \cos \omega\tau\, d\tau$$

is the cospectrum and $R_V\beta\,(\tau)$ is the cross-correlation function of these values, $S\beta\,(\omega)$ is the autospectrum of angle fluctuations; $\omega_1 - \omega_2$ is the frequency range of the fluctuations.

In processing real records of current velocity fluctuations and fluctuations of the angle of deflections of the pendulums we use the cospectra of these values for computing σ_2^2 (the components V_1 and V_3 make no contribution to the cospectrum values), whereas for computing σ_1^2 and σ_3^2 we use the quadrature spectra and the phase characteristic. The latter makes it possible to evaluate the contribution of V_1 and V_3 to the values of the total quadrature spectrum since the component of the V_1 fluctuations outpaces the β fluctuations by 90°, whereas the V_3 component lags behind them by the same value.

Thus, having synchronous measurements of fluctuations of current velocity and the angles of deflection for the pendulums, as well as the results of their cross-statistical processing, it is possible to compute the dispersions of the natural oscillations of the current velocity measurement transducer in different ranges of periods of fluctuations and to evaluate their contribution to the total dispersion of the registered fluctuations of ocean current velocity.

Investigations of natural oscillations of the self-contained current recorders were made in the Caribbean Sea at two buoy stations with a surface buoy of the GM-51 type. At buoy station 1 the depth of placement of the DISK-M instrument was 30 m, wind velocity was 10.5 $m \cdot sec^{-1}$, sea waves were class 4, and the wave period was 6-8 sec where the ocean depth was 2230 m. At buoy station 2 the measurements were made at a depth of 175 m with a wind velocity of 6 $m \cdot sec^{-1}$ and waves of class 2; the wave period was 2-4 sec and the ocean depth was 2220 m.

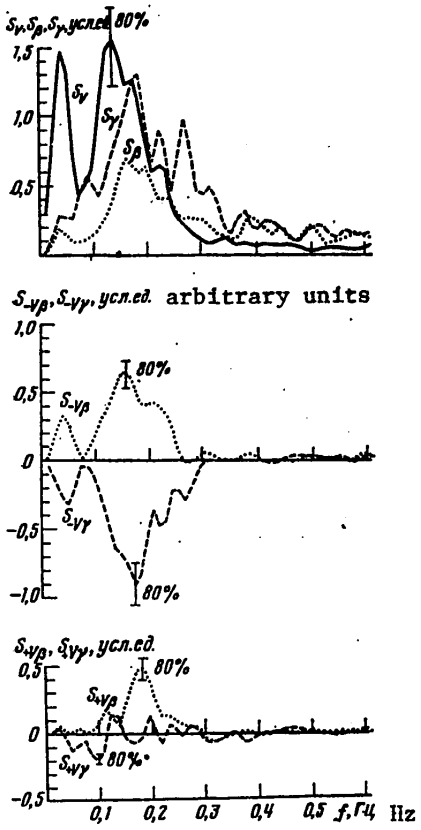

Fig. 3.

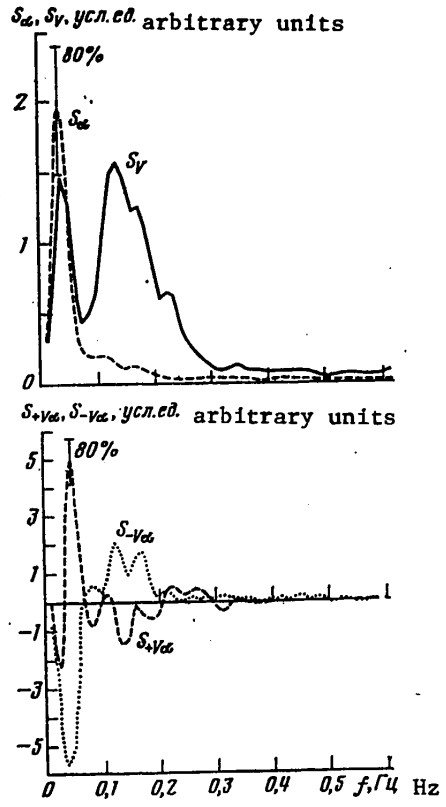

Fig. 4.

Fig. 3. Spectra of fluctuations of relative velocity and angles of deflection of pendulums (buoy station 1).

Fig. 4. Spectra of fluctuations of relative velocity and yawing angle (buoy station 1).

Figure 2 shows hodographs of the vector of relative velocity constructed on the basis of readings with the DISK-M instrument installed at buoy station 1 (Fig. 2,a) and buoy station 2 (Fig. 2,b) during a time interval of 100 sec. The scatter of readings for the instrument installed at buoy station 1 falls in the 120°-sector with a width of 30 cm·sec^{-1} in absolute value. In the considered interval there was a complete rotation of the hodograph of the vector of relative velocity. The scatter of readings for the instrument installed at buoy station 2 falls in a 25° sector with a width of 6 cm·sec^{-1} in absolute value.

Figure 3 shows the spectra of fluctuations of current velocity S_V and the angles of deflection of the pendulums S_β and S_γ (the β angle was measured in the plane of the longitudinal section of the instrument and the γ angle was measured in

the plane of the transverse section), obtained using records for buoy station 1. The number of degrees of freedom of evaluations of the spectra was 26; the range of their selective variability with a probability 0.8 is shown in Fig. 3. This same figure shows the quadrature spectra S_{-V} and S_{-V} and also the cospectra $S_{+V\beta}$ and $S_{+V\gamma}$ of these same fluctuations and shows the regions of selective variability of these evaluations with the probability 0.8 [3].

In the spectrum of velocity fluctuations there are two distinct maxima: the first in the range of fluctuation periods 20-30 sec, the second in the range of periods 6-8 sec. The quadrature spectra $S_{-V\beta}$ and $S_{-V\gamma}$ each have two maxima at these same frequencies; the $S_{-V\beta}$ values are positive and the $S_{-V\gamma}$ values are negative. The $S_{+V\beta}$ cospectrum has a small positive maximum in the region of 6-second fluctuation periods.

Figure 4 shows the spectra of fluctuations of current velocity S_V and the angle of instrument yawing S_α on the basis of data from measurements with a magnetic compass at buoy station 1. This same figure shows the quadrature spectrum of fluctuations of velocity and the yawing angle and cospectrum of these values. The S_α spectrum has one clearly expressed maximum in the range of periods of fluctuations 20-30 sec; the cospectrum $S_{+V\alpha}$ and the quadrature spectrum $S_{-V\alpha}$ have maxima for these same periods of fluctuations.

The noted maxima S_V and S_α for periods 20-30 sec correspond to amplitudes for yawing 12-14° and a relative current velocity of 1.5 $cm \cdot sec^{-1}$. An analysis of the variability of the vector of relative velocity for such fluctuations is evidence that their possible cause may be vibrational motions of the supports relative to the line and the drift movements of the line itself with an amplitude of oscillations 40-50 cm and a drift velocity of the line 1-2 $cm \cdot sec^{-1}$.

Oscillations with periods of 6-8 sec, where the principal characteristics of the spectra are manifested, coincide in frequency with the wind waves. Insignificant $S_{+V\alpha}$ and $S_{-V\alpha}$ values in this frequency range, instability of the phase shift and the insignificant coherence indicate that at the frequency of the wind waves the fluctuations of relative velocity and the yawing angle are statistically independent.

The period of natural oscillations of the DISK-M instrument container is 2-3 sec. In the velocity spectrum in this frequency range there are no maxima and the spectra of fluctuations of the β and γ angles contain small maxima.

For an analysis of the contribution of the registered oscillations to the total dispersion of errors in current velocity, in accordance with the analytical method presented above, the investigated frequency range was broken down into three parts corresponding to the mentioned features of the spectral characteristics. The first frequency range takes in the periods of oscillations 80-14 sec, corresponding to oscillations of the supports with instruments relative to the line; the second frequency range corresponds to periods of 14-3 sec of wind waves and swell waves; the third frequency range corresponds to periods of 3-1.9 sec of characteristic oscillations of the instrument container relative to the suspension point.

Table 1

Dispersions of Fluctuations of Current Velocity Associated With Fluctuations of the Angles of Deflection of Pendulums in Longitudinal (β) and Transverse (γ) Planes of Instrument Section, $cm \cdot sec^{-2}$

Range of periods of oscillations, sec	Angle β			Angle γ			Computed	Actual
	σ_1^2	σ_2^2	σ_3^2	σ_1^2	σ_2^2	σ_3^2		
80-14	1	0.023	---	---	0.0417	0.93	2.00	5.04
14-3	2.91	1.33	---	---	0.0017	3.5	7.74	14.42
3-1.9	0.0032	0.00004	---	---	0.0008	0.005	0.009	0.196
80-1.9	3.91	1.353	---	---	0.043	4.435	9.75	19.656

The computed dispersion of velocity fluctuations σ_1^2, σ_2^2 and σ_3^2 for the β and γ angles, computed using expressions (6)-(8), are given in a table.

The actual dispersion of the velocity fluctuations was determined by integration of the S_V spectrum in a stipulated frequency range and for the entire investigated frequency range it is approximately 2 times greater than the value computed using expressions (6)-(8). This shows that the possible contribution of oscillations of current recorders to the registered oscillations in the investigated frequency range is approximately half the total energy of the fluctuations of current velocity.

The results of the computations in the table also indicate that the greatest contribution to the total dispersion is from oscillations with the frequencies of wind waves and swell waves (79%), then oscillations with a period of tens of seconds (20%) and an insignificant contribution ($<1\%$) is from oscillations with periods characteristic for the frequency of the natural oscillations of the instrument housing. Oscillations in the longitudinal plane of the current meter (β angle) introduce a 15-20% greater contribution to the total dispersion of oscillations of instrument velocity in comparison with oscillations in the transverse plane (γ angle). The mean square value of velocity fluctuations caused by instrument oscillations in the investigated frequency range is 3.12 $cm \cdot sec^{-1}$, which for the measurement conditions is somewhat greater than 7% of the mean hourly current velocity.

The spectra of velocity fluctuations S_V, the angles of deflection of the pendulums S_β, S_γ, yawing S_α, and also the quadrature spectra and cospectra of these parameters obtained at buoy station 2 at a depth of 175 m in general are similar to the curves shown in Fig. 3 and differ for the most part with respect to lesser values along the y-axis. The spectra of velocity and the angle β of pendulum deflection in the longitudinal plane of the current meter and the quadrature spectrum of these parameters have clearly expressed maxima in the region of periods of oscillations 10-30 sec and relatively small maxima in the region of periods of oscillations 3.5-5 sec. The corresponding cospectrum $S_{+V\beta}$ has a maximum peak in the region of periods 4-5 sec and a lesser maximum for periods of 10 sec. The spectrum of angles of deflections in

the transverse S_γ plane is close to "white noise." Values of the mean square fluctuations of velocity and angles of deflections of the pendulums registered at a depth of 175 m were equal to $\sigma_V = 0.83$ cm·sec^{-1}, $\sigma_\beta = 0.72°$ and $\sigma_\gamma = 0.35°$. These values are close to the instrumental measurement errors, which makes a more detailed analysis for this case infeasible.

We note in conclusion that the method for investigating oscillations of the current meters and their influence on the errors in measuring current parameters, based on direct measurements of fluctuations of the relative velocity of currents and angles of deflection relative to the longitudinal, transverse and vertical axes of the current meter makes it possible to study the parameters of such fluctuations for the entire diversity of conditions for the measurement of currents under real conditions (depth of placement of instrument and depth of ocean, state of sea surface, type of buoy installation and its parameters, design of current recorder, method for its suspension, etc.).

Already the first measurements described in this article indicated that the parameters of oscillations of the current recorders can differ significantly from one another depending on the depth of measurement and the state of the sea surface. For example, the standard deviation of the velocity fluctuations caused by instrument oscillations at a depth of 30 m was approximately four times greater than the similar value at a depth of 175 m.

Direct measurements of fluctuations of velocity and the angles of deflection made it possible to detect a number of new characteristics of the behavior of instruments and to evaluate their contribution to the general dispersion of error. These characteristics include the angular oscillations of the instruments in the horizontal plane relative to the line with characteristic amplitudes of 40-50 cm and periods of 20-30 sec, a predominant contribution of oscillations with the periods of wind waves in the upper horizons, and an insignificant contribution of instrument oscillations relative to the suspension point to the total energy of the oscillations.

Further investigations of oscillations of current meters will make it possible, first of all, to obtain statistical data on the measurement errors under different conditions, and second, to find the most rational designs of measuring instruments, buoy apparatus and suspension of the current meters, to evaluate the influence of different types of sensing elements and measurement converters on measurement accuracy.

BIBLIOGRAPHY

1. Burnashev, V. Kh. and Kunets, T. A., "Influence of Waves and Currents on Motion of the BPV-2 in a Buoy Installation in Shallow Water," MORSKIYE PODVODNYYE ISSLEDOVANIYA (Marine Underwater Research), Moscow, Nauka, pp 184-189, 1969.

2. Gorodenskiy, N. B., Kudryavtsev, N. F. and Labeysh, V. G., "Investigation Using a Model of Effect of a Current and Waves at an Autonomous Station for Current Observations," TRUDY AANII (Transactions of the Arctic and Antarctic Scientific Research Institute), No 210, pp 13-22, 1961.

3. Jenkins, G. and Watts, D., SPEKTRAL'NYY ANALIZ I YEGO PRILOZHENIYA (Spectral Analysis and Its Applications), No 2, Moscow, Mir, 1972.

4. Krylov, A. N. and Krutkov, Yu. A., "Shipboard Pendulum Inclinometer," OBSHCHAYA TEORIYA GIROSKOPOV I NEKOTORYKH TEKHNICHESKIKH IKH PRIMENENIY (General Theory of Gyroscopes and Some Technical Applications), Leningrad, Izd-vo AN SSSR, pp 192-203, 1932.

5. Levin, B. R., TEORIYA SLUCHAYNYKH PROTSESSOV I YEYE PRIMENENIYE V RADIOTEKHNIKE (Theory of Random Processes and Its Application in Radio Engineering), Moscow, Sovetskoye Radio, 1957.

6. Kushnir, V. M., Zaikin, V. M., Kolomoytsev, M. M., Koltakov, Yu. N., Vlasova, L. N. and Shevchenko, E. A., "DISK Instrument Complex and the Results of its in situ Tests," EKSPERIMENTAL'NYYE ISSLEDOVANIYA PO MEZHDUNARODNOY PROGRAMME POLIMODE (Experimental Investigations Under the International POLYMODE Program), Sevastopol', Izd. MGI AN UkSSR, pp 171-175, 1978.

7. Rebayns, E. A., "Characteristic Motions of Anchored Buoy Stations and Their Influence on the Registry of Currents," TROPEKS-74 (TROPEX-74), Vol II, Leningrad, Gidrometeoizdat, pp 196-204, 1976.

8. Rivkin, S. S., TEORIYA GIROSKOPICHESKIKH USTROYSTV (Theory of Gyroscopic Apparatus), Vol 1, Leningrad, Gos. Soyuzn. Izd-vo Sudostr. Prom-sti, 1962.

9. Paramonov, A. N., Kushnir, V. M. and Zaburdayev, V. I., SOVREMENNYYE METODY I SREDSTVA IZMERENIYA GIDROLOGICHESKIKH PARAMETROV V OKEANE (Modern Means and Methods for Measuring Hydrological Parameters in the Ocean), Kiev, Naukova Dumka, 1979.

5303
CSO: 1865/149

UDC 551.462:681.208

WIDE-ANGLE SEISMIC PROFILING IN OCEAN USING TOWED RADIO BUOY

Moscow OKEANOLOGIYA in Russian Vol 22, No 2, Mar-Apr 82 (manuscript received 30 Sep 81) pp 325-328

[Article by Yu. P. Neprochnov, Institute of Oceanology imeni P. P. Shirshov, USSR Academy of Sciences, Moscow]

[Text]

Abstract: The author proposes a new method for seismic profiling in the ocean with the use of a towed radio buoy and a pneumatic sound source. The distance between the sound source and the radio buoy is selected in such a way as to ensure the optimum conditions for the tracing of reflecting boundaries (registry of waves reflected in the region of critical angles). In individual reference segments of the profile it is possible to obtain long travel-time curves of reflected waves necessary for determining the velocity parameters of the medium. The article gives the results of testing of the method in the Atlantic Ocean on the 24th voyage of the scientific research ship "Akademik Kurchatov."

One of the promising directions in seismic investigations in the ocean is the introduction of long multichannel receiving systems making possible use of the common deep point (CDP) method. The CDP method in work on the land and in shallow sea regions makes possible a more reliable discrimination and tracing of deep seismic boundaries and a determination of the velocity characteristic of the section. However, its use in abyssal regions of the ocean, although it has unquestionable advantages over the standard continuous seismic profiling (CSP) method, nevertheless is inadequately effective due to the small ratio of the measurement base to the depth of the reflecting boundaries. If the problem is a study of the entire earth's crust in the ocean, for the reliable discrimination of deep discontinuities and correct determinations of mean and stratum velocities it is necessary to ensure at least an equality of the total thickness of the water and crust to the measurement base, that is, 10-12 km.

The length of the multichannel receiving systems in seismic reconnaissance by the CDP method in the sea and in work similar to this by the deep seismic sounding-reflected waves method in the ocean [2] is usually 1.5-3.0 km, which does not meet the indicated requirements. This difficulty can be overcome when working from two ships, which makes it possible to eliminate the source of seismic oscillations at the necessary distance from the receiving system. Such experiments were carried out in 1962 in the Black Sea, where travel-time curves of reflected waves with a length up to 10 km were obtained [1]. In 1976 the seismic profiling method from two ships was used with a 20-km distance between a source and receiving system in successful tests on an American expedition in the Pacific Ocean [5]. However, the organization of synchronous investigations from two ships is not always possible and is technically complex.

On the basis of the work experience of the Institute of Oceanology, USSR Academy of Sciences with a seismic buoy of the Lunarskiy design [3] and lowering of bottom seismographs on a Kapron line on the 24th voyage of the scientific research vessel "Akademik Kurchatov" (1977) it was possible to test a new seismic profiling method along long bases with the transmission of seismic signals through a radio channel. Such seismic profiling, using the terminology of American scientists, can be called wide-angle reflection.

Physical basis of method. The idea of the method is as follows. The ship moves along the profile with a constant velocity and tows a pneumatic sound source (PSS) which is activated at equal time intervals, such as each minute. A radio buoy which is adapted for towing is lowered from the ship's stern on a Kapron line (or still better, propylene) line. The radio buoy signals, after demodulation and filtering, are registered with a RDD-RUM-type apparatus (from the "Gorizont" seismoprofilograph outfit), which is triggered by the same quartz clock.

In the first stage of the work the Kapron line is let out at a rate equal to the ship's speed, which ensures obtaining a travel-time curve of seismic waves with a fixed reception point and the source at an increasing distance from it. Using this travel-time curve it is possible to determine the mean and stratum velocities and the depth of the reflecting boundaries by the use of known methods. The maximum distance between the PSS and the radio buoy is selected with allowance for the objectives of the experiment and seismogeological conditions and can attain 5-10 km or more. The best conditions for the registry of reflected waves from a studied discontinuity, as is well known, will be at "critical" distances (R_{cr}), that is, with reflection of waves from a discontinuity in the region of critical angles.

In the second work stage the letting-out of the Kapron line stops and the radio buoy is towed behind the ship at a stipulated distance $\triangle R$, which is the best for obtaining reflected waves from one or more of the most important discontinuities. This ensures continuous tracing of the reflecting boundaries along the profile, with use of quasicritical reflected waves most favorable for the study of deep discontinuities.

In the third stage of the work the Kapron line is drawn in by the winch at a rate equal to the ship's speed and the radio buoy gradually approaches the PSS. This ensures obtaining a travel-time curve of seismic waves as in the first stage of the work, but already at a different point on the profile.

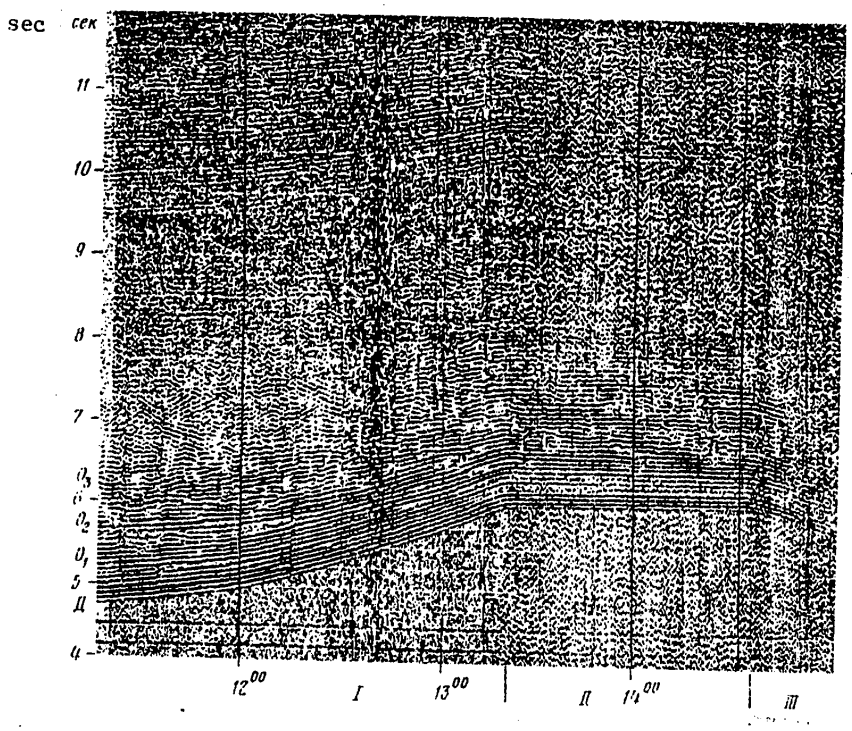

Fig. 1. Record of reflected waves obtained during testing of wide-angle seismic profiling method using radio buoy in Canaries Basin of Atlantic Ocean on 24th voyage of the scientific research ship "Akademik Kurchatov." D -- reflection from bottom surface; O_1, O_2 and O_3 -- reflections from bottom horizons; I, II and III -- segments of record corresponding to first, second and third stages of work.

Then the sequence of work can be repeated -- continuous profiling is alternated with the registry of long travel-time curves necessary for control determination of the velocity characteristics of the medium.

Description of experiment. Experimental work for testing of the proposed method was carried out in the Canaries Basin of the Atlantic Ocean in a sector with an even bottom. Due to the nonadaptability of the existing radio buoy to towing while the ship was proceeding on course the work was done while the ship was at drift (the rate of drift under the influence of the wind was about 1.5 knot), which simulated towing at a slow rate. The ship was oriented with the starboard to the wind. The radio buoy was let out on a Kapron line by means of an LK winch. The depth of the radio buoy hydrophone was 40 m.

The pneumatic sound source with a volume 2 x 3 liters operated at a depth of 200 m with an interval of 1 minute. The PSS was triggered by a shipboard quartz clock.

The radio buoy signals were received with a whip antenna mounted on the ship's mast, were fed to an R105D radio station and then to a reconversion unit where they were demodulated and filtered. The signals were fed from the filter output (frequency band 10-40 Hz) to an RDD-RUM apparatus where they were registered on electrochemical paper and on a magnetic recorder. At the same time seismograms were registered on an N-327/5.

The figure shows an example of the record obtained with the RDD. On the record it is possible to discriminate three segments corresponding to the three stages of the work described in the preceding section. In the first stage a Kapron line was let out until the radio buoy was 5 km from the ship. A travel-time curve of waves reflected from the bottom surface and from the underlying reflecting discontinuities (to depths of 1.5-2 km below the bottom) was obtained. It can be seen that with an increase in the distance from the source the correlation of some bottom reflections ceases, but the most stable deep waves are retained. The interpretation of this travel-time curve made it possible to refine the velocity model of the sedimentary layer of the Canaries Basin [4].

In the second stage the letting-out of the Kapron line ended and the radio buoy drifted (was towed) behind the ship at a constant distance. In the corresponding segment of the record, despite the increasing noise background, horizontal discontinuities are easily traced in the upper part of the section, as well as the boundaries of the lower structural stage, having a complex relief.

In the third stage of the work the Kapron line was drawn onto the LK winch, drawing the radio buoy to the ship. The noise background in this case increased greatly and the discrimination of the reflected waves deteriorated.

In order to reduce the noise background during the towing of the radio buoy its standard hydrophone was replaced by a 50-m section of a hose oil-filled line of seismic detectors from the continuous seismic profiling system. Thereafter, the entire work cycle with the radio buoy was repeated, but the duration of each cycle had to be reduced due to an inadequacy of time. The use of a section of the string of seismic detectors was extremely effective in the second stage of the work -- during the towing of the radio buoy behind the ship at drift at a speed of about 1.5 knot. However, with pulling-in of the radio buoy with the winch in the third stage there was a marked deterioration of audibility of radio buoy radio signals. This evidently occurred due to the radio buoy losing its vertical position and the antenna touching the water surface (the ocean waves during the time of the experiment attained 5-6 units). In general, the use of a section of a string of seismic detectors gave encouraging results.

The experiments carried out on the 24th voyage of the scientific research ship "Akademik Kurchatov" with wide-angle seismic profiling in the ocean with a radio buoy and a pneumatic sound source confirmed the effectiveness and practical possibility of such studies. In the further use of the method on expeditions it is

necessary to change the design of the radio buoy, adapting it for towing at a speed up to 5-6 knots. As indicated by experiments, in order to decrease noise during the towing of the radio buoy instead of a single hydrophone it is desirable to use a group detector -- a section of a line of seismic detectors.

Taking part in the sea tests of the proposed wide-angle seismic profiling method were V. V. Sedov, G. A. Semenov, P. S. Strelkov, L. R. Merklin and I. N. Yel'nikov, to whom the author expresses deep appreciation.

BIBLIOGRAPHY

1. Yel'nikov, I. N., Neprochnov, Yu. P. and Neprochnova, A. F., "Study of the Velocity Characteristic of the Sedimentary Layer of the Black Sea Depression Using Travel-Time Curves of Reflected Waves," TRUDY IO AN SSSR (Transactions of the Institute of Oceanology, USSR Academy of Sciences), Vol 87, pp 42-57, 1970.

2. Kogan, L. I., Malovitskiy, Ya. P. and Udintsev, G. B., "Deep Seismic Profiling by the Reflected Waves Method in an Investigation of the Ocean Floor," PRIKLADNAYA GEOFIZIKA (Applied Geophysics), No 83, pp 12-17, 1977.

3. Lunarskiy, G. N. and Saidov, A. Yu., SISTEMA RADIOBUYA DLYA SEYSMICHESKIKH ISSLEDOVANIY (Radio Buoy System for Seismic Investigations), VINITI, No 6000-73 DEP, 1973, pp 1-22.

4. Semenov, G. N. and Levchenko, O. V., UTOCHNENIYE SEYSMICHESKOGO RAZREZA OSADOCHNOY TOLSHCHI V KANARSKOY KOTLOVINE (Refinement of the Seismic Section of the Sedimentary Stratum in the Canaries Depression), VINITI, No 4000-79 DEP., pp 1-20, 1979.

5. Stoffa, P. and Talwani, M., EXPLORING THE CRUST BENEATH THE OCEANS, Lamont-Doherty Geological Observatory of Columbia University, Yearbook, Vol 5, pp 23-29, 1978.

5303
CSO: 1865/149

UDC 551.46.01:551.463.2

MEASUREMENTS OF VOLUME SOUND SCATTERING IN OCEAN USING ABYSSAL ACOUSTIC SYSTEM

Moscow OKEANOLOGIYA in Russian Vol 22, No 2, Mar-Apr 82 (manuscript received 20 Feb 81) pp 211-213

[Article by Yu. Yu. Zhitkovskiy, V. A. Mozgovoy and V. V. Savel'yev, Institute of Oceanology imeni P. P. Shirshov, USSR Academy of Sciences, Moscow]

[Text]

Abstract: A study of volume sound scattering in the central Atlantic by means of an abyssal acoustic system indicated that the sound-scattering layer, observed at depths of 500-600 m, was formed by individual "targets," evidently constituting shoals of fish. The volume sound scattering coefficient within a "target" can exceed by two orders of magnitude the volume scattering coefficient for the particular layer.

During the 31st voyage of the scientific research ship "Akademik Kurchatov" specialists carried out measurements of volume sound scattering in the ocean using an abyssal acoustic system (AAS), constituting a deep-water sealed container lowered over the ship's side. This container contains emitting and receiving channels. An emitter (piezoceramic ring) and a receiver (piezoceramic sphere) are attached to the container. An oscillograph and a digital magnetic recorder are used as recorders. The duty cycle of the tonal-pulsed signal was 5 KHz; pulse duration was 2, 4 and 8 msec; pulse repetition rate was 1 sec.

Figures 1 and 2 show the results of measurements of the intensity of volume sound scattering 10 lg m_V obtained in the central part of the Atlantic Ocean during the daytime on 16 July 1980. The volume scattering coefficient m_V was determined (see [1]) as the ratio of the power w scattered by the volume V in a unit solid angle in a backward direction to the intensity I of an acoustic wave incident on the scattering volume: $m_V = w/IV$.

It can be seen from Fig. 1, which shows the vertical profile of the intensity of volume scattering, that the sound-scattering layer (SSL) was at a depth of 500-600 m; the averaged values of the intensity of volume scattering in this

layer (about -70 db relative to 1 m^{-1}) are typical for the similar layer in the Atlantic at a frequency of 5 KHz. At other horizons there was only ambient noise whose level corresponded to the intensity of scattering -81.6 db. The measurements were made each 50 m vertically to the bottom, situated at a depth of 2600 m; the horizons below 1500 m are not indicated in Fig. 1. As an illustration, the right-hand side of Fig. 1 gives a fragment of an echo sounder record obtained using a shipboard echo sounder operating at a frequency of 10 KHz in a region close to the point where the measurements were made. There is a good correspondence between sounding data from the abyssal acoustic system and echo sounder measurements.

The frequency of the $m_v(z)$ curve must be considered high. The cited profile was measured twice: during the lowering of the measurement system and during its raising. At all depths there were no appreciable deviations of the m_v values obtained during lowering from the values obtained during raising.

The employed method makes it possible to determine the nature and position of both the upper and lower boundary of the sound-scattering layer, something which cannot be done with widely used remote acoustic methods. This fact affords the possibility, in the case of repeated successive measured $m_v(z)$ profiles, to determine small-scale spatial-temporal variability of both horizontal boundaries and the structure of the sound-scattering layer.

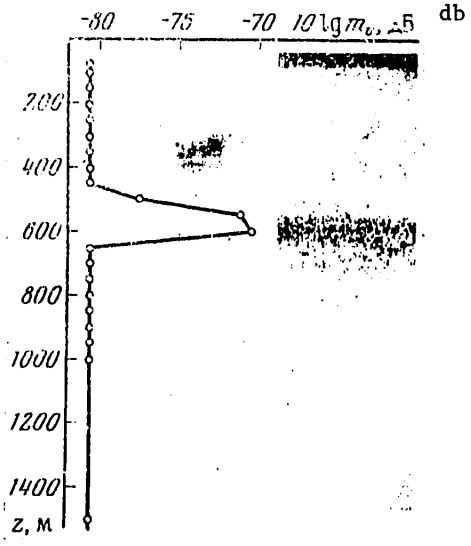

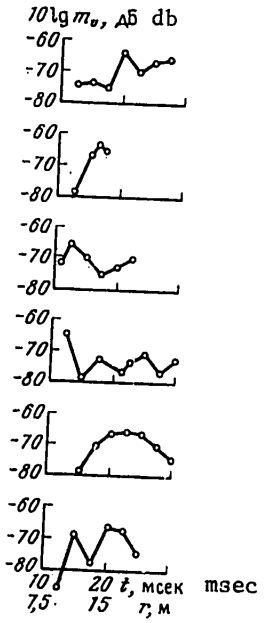

Fig. 1. Vertical profile of the intensity of volume scattering. The values 10 lg m_v in db relative to 1 m^{-1} are plotted along the x-axis.

Fig. 2. Dependence of the intensity of volume scattering on distance (time) between the emission-reception point and scattering volume.

Since the measurement of sound scattering with this system was carried out in a small volume, it was possible to observe interesting local patterns of scattering at the horizon where the sound-scattering layer is situated. Figure 2 shows the dependence of the intensity of volume scattering 10 lg m_v on time t (or distance r from the emission-reception point) at successive (each 10 seconds) moments in time. Each curve in Fig. 2 represents the dependence 10 lg $m_v(t)$ (or 10 lg $m_v(r)$) averaged for five pulses. From pulse to pulse there were considerably greater fluctuations in the intensity of volume scattering than indicated on the averaged curves in Fig. 2, caused by the change in the phase relationships of echo signals from individual scatterers.

It was found that this sound-scattering layer was not formed by uniformly distributed scatterers but by individual "targets," evidently constituting schools of small fish. One of these "targets," moving near the acoustic system, is also seen in the form of a maximum of the intensity of volume scattering in Fig. 2. We note that the volume scattering coefficient was computed for the entire volume occupied by the spherically scattering signal [1]. It is improbable that the fishes occupied the entire spherical scattering layer situated at this distance r from the emission-reception point and synchronously approaching the acoustic system or withdrawing from it. Evidently the observed shoal occupied a solid angle considerably smaller than 4π and the values of the volume scattering coefficient m_v within the "target" must be substantially greater. An approximate evaluation of m_v within the "target" on the assumption that the mean distance to the shoal was 10-15 m, and the shoal itself had a spherical form with a radius 5 m, gave an m_v value exceeding the value computed for the entire volume by two orders of magnitude, which substantially exceeds the m_v values known in the literature for a frequency 5 KHz.

Unfortunately, the limitation of experimental material at the present time does not make it possible to give the numerical characteristics of the spatial-temporal variations of the volume scattering coefficient in the sound-scattering layer. Henceforth such measurements will be continued.

BIBLIOGRAPHY

1. Andreyeva, I. B., "Sound Scattering in Oceanic Sound-Scattering Layers," AKUSTIKA OKEANA (Ocean Acoustics), edited by L. M. Brekhovskikh, Moscow, Nauka, pp 491-558, 1974.

5303
CSO: 1865/149

UDC 551.465

LABORATORY INVESTIGATION OF INFLUENCE OF INTERNAL WAVE ON REGULAR SURFACE WAVES

Moscow OKEANOLOGIYA in Russian Vol 22, No 2, Mar-Apr 82 (manuscript received 28 Jan 81, after revision 20 Apr 81) pp 204-210

[Article by S. A. Yermakov, S. I. Kozlov, K. V. Pokazeyev and A. D. Rozenberg, Institute of Applied Physics, USSR Academy of Sciences, Gor'kiy; Moscow State University imeni M. V. Lomonosov; Institute of Oceanology imeni P. P. Shirshov, USSR Academy of Sciences, Moscow]

[Text]

Abstract: The authors made a laboratory study of the development of amplitude and frequency modulation of a regular surface wave under the influence of an internal wave up to the formation of slicks. It was found that in the spectrum of a surface wave there are satellites displaced by a frequency which is a multiple of the frequency of the internal wave. The number of satellites increases with the length of the interaction.

1. As is well known, great attention is being devoted to the problem of investigating internal waves (IW) on the basis of their manifestations on the wave-covered sea surface, which have the form of slicks. A considerable number of studies (for example, see [1, 3, 5, 6] and the bibliography cited there) are devoted to the in situ study of slicks, and also a theoretical analysis of the interaction of internal and surface waves. With respect to laboratory investigations, it is possible to mention only a single study [7] in which an investigation was made of the influence of a monochromatic internal wave on a regular surface wave (SW). As was demonstrated in [7], an internal wave leads to the modulation of a SW both in amplitude and wavelength; the strongest effect is observed with satisfaction of resonance conditions: coincidence of the phase velocity c of an internal wave with the group velocity c_g of surface waves. However, in [7] a study was made of an extremely weak interaction in which it was possible to examine only the initial stage in the development of modulation. In this article a study is made of a stronger interaction of SW and IW, characterized by a considerable broadening of the spectrum of an initially monochromatic SW and the transformation of SW, up to the stage of slick formation.

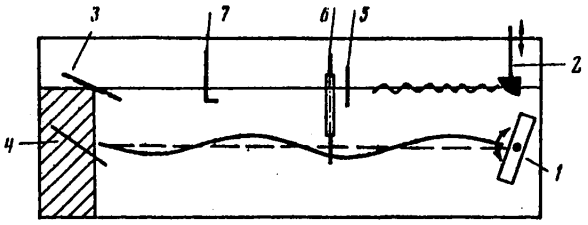

Fig. 1. Generalized diagram of experiments. 1, 2) wave producers of internal and surface waves; 3, 4) wave dampers; 5) wave recorder for measuring surface waves; 6) wave recorder for measuring surface waves; 7) anemometer.

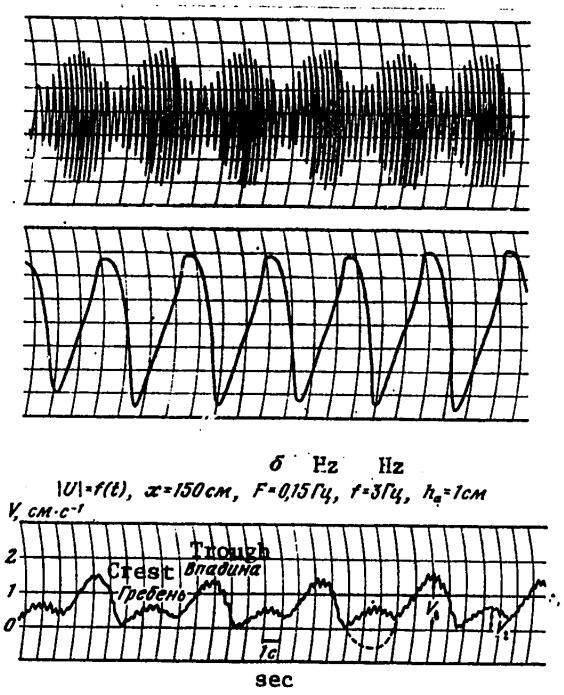

Fig. 2. Records of surface and internal waves. a) synchronous record (f = 4 Hz, F = 0.21 Hz, x = 60 cm, c/c_g = 1); b) record of modulus of horizontal current velocity; the dashed line indicates how to convert from the velocity modulus to velocity itself.

2. Instrumentation and measurement method. The experiments were carried out independently using two laboratory apparatuses: experiment I -- in a flume at the Institute of Applied Physics, USSR Academy of Sciences (measuring 4.5 x 0.4 x 0.3 m), experiment II -- in a flume at Moscow State University (measuring

8.25 x 0.6 x 0.6 m). A two-layer stratification model was used in the experiments; the upper layer was fresh water and the lower layer was a solution of sodium chloride with densities varying in the range from 1.06 to 1.13 $g \cdot cm^{-3}$ in experiment I and from 1.013 to 1.06 $g \cdot cm^{-3}$ in experiment II. A dye was introduced into one of the layers for the visualization of IW. In both apparatuses IW were excited by using plates oscillating with an adjustable frequency and amplitude about a horizontal axis situated at the interface of the fluids (Fig. 1). The frequencies F of the IW generated by the wave producer varied in the range from 0.05 to 0.3 Hz and their heights varied from 0.5 to 3 cm. SW were created using wave producers of the vibrational type generating waves with frequencies f from 2 to 10 Hz and with amplitudes 0.1-1 mm. Sufficiently effective wave dampers for IW and SW were placed at the end of the flumes (the fraction of reflected wave energy in no case exceeded 10%).

Waves were measured with electrode wave recorders supplied a d-c current. The working part of the wave recorder is an electrode across which the voltage is dependent on the spreading resistance of the submergible part, which makes it possible to register a wave on the basis of change in submergence depth.

Experiment I was made using two wave recorders: one for measuring the SW and the other for IW (the working part of the second wave recorder was placed in the interface between fresh and salt water and was isolated from the surface). The wave recorders were calibrated using a device for inducing vertical oscillations of electrodes with stipulated amplitudes and frequencies. It was established that the sensors have a good linearity (no worse than 1%) and their readings are not dependent on the frequency of oscillations at least to frequencies of 15 Hz. Signals from both wave recorders were registered on an automatic recorder and also with a measuring magnetic recorder with subsequent analysis of the SW spectrum on an analog computer. An example of a simultaneous record of SW and IW is shown in Fig. 2,a. The corresponding spectra of SW at different distances x from the wave producer of SW are represented in Fig. 3.

In experiment II we used one wave recorder registering the total displacements for IW and SW. In the registry we used a five-channel automatic recorder, registry with which was accomplished both directly from the wave recorder and after the signal passed through a selective amplifier. The presence of an amplifier with a frequency characteristic having a sharp dropoff in the low-frequency region made it possible to have separate registry of the SW and IW profiles. A photographic survey through the side wall of the flume was used in determining the heights and lengths of IW. The amplitude of the horizontal velocity U of the orbital motion of particles in an internal wave near the surface was usually computed in experiments on the basis of the measured amplitude A of interface displacement. For a two-layer stratification model it is easy to obtain $U = A\Omega(\mathrm{sh}Kh)^{-1}$, where $\Omega = 2\pi F$ is the angular frequency of the IW; K is the wave number of the IW; h is the depth of the upper homogeneous layer. In addition, in experiment II a film anemometer was used in making individual direct measurements of the modulus of the horizontal component of orbital velocity at different depths h_a and different distances from the wave producer. Figure 2,b is an example of registry of the horizontal velocity modulus. The figure clearly shows velocity fluctuations associated with both SW and IW. In the interpretation of the record it must be taken into account that the sensor measures only

the velocity modulus. As a result of these measurements, in addition to the fluctuation component of the velocity of particles in the internal wave it was possible to detect the presence of a constant wake whose intensity was 0.5 cm·sec^{-1}.

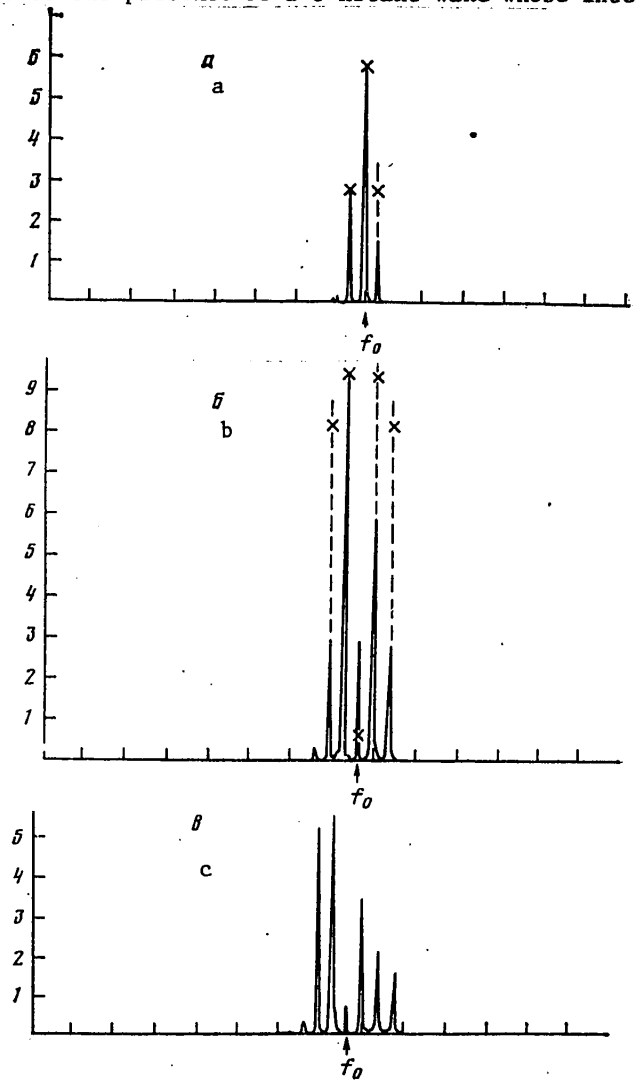

Fig. 3. Energy spectra of surface wave modulated by internal wave. The spectral density is plotted along the y-axis; the frequency in arbitrary units is plotted along the x-axis: a) x = 0.5 m; b) x = 1 m; c) x = 1.5 m (f = 4.6 Hz, F = 0.21 Hz).

As follows from the records of SW series, an IW leads to a considerable amplitude and frequency modulation of the surface wave. The experimentally obtained data were used in computing the amplitude modulation coefficient $m = (a_{max} - a_{min})/(a_{max} + a_{min})$, the frequency modulation coefficient $\nu = (f_{max} - f_{min})/(f_{max} + f_{min})$ (the value of the latter was also determined from the SW spectra)

and a study was made of the nature of the dependence of these parameters on the amplitude of the internal wave, the ratio of velocities U/c and the x distance.

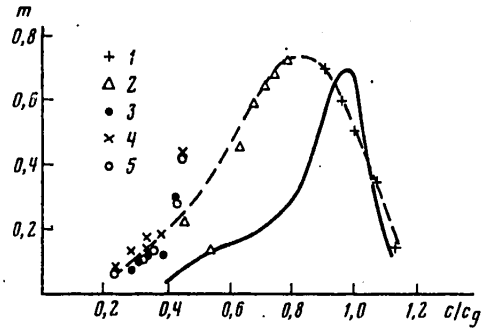

Fig. 4. Resonance interaction curves. The solid curve was computed in accordance with [7]; the dashed curve was obtained using experimental data: 1) T = 6 sec, Kx = 7.6, V/c = 0.045; 2) T = 6 sec, Kx = 7.4, V/c = 0.034; 3, 4, 5) T = 8.5 sec, Kx = 7.8, V/c = 0.037.

3. Results of experiments. With the excitation of a harmonic SW in the presence of an IW in the experiments there was a relatively rapid (at distances of about 0.5-1 m) appearance of amplitude and frequency modulation of SW (Fig. 2,a). Accordingly in the energy spectrum of SW, initially having a peak at the frequency f_0, satellites were formed at the frequencies $f_0 + nF$. With an increase in distance both amplitude and frequency modulation increased and accordingly there was an increase in the number of satellites, attaining 6-7. The SW spectrum became increasingly asymmetric: the amplitudes of the high-frequency ($n>0$) satellites exceeded the amplitudes of the low-frequency satellites ($n<0$) (Fig. 3). Finally, at lengths of about 1-2 m the amplitude modulation attained 100%, after which the SW were broken down into individual trains separated by sectors of almost smooth water -- slicks. It should be noted that the slicks were also observed visually. After the breakdown of SW into trains the frequency modulation decreased and accordingly the high-frequency part was suppressed in the SW spectra. This is evidently associated with the strong damping effect of the surface-active film, which, despite the cleaning of the surface, to some degree was present on the water surface.

First we will discuss the resonance characteristics. Figure 4 shows the dependence of the amplitude modulation coefficient m determined in experiment II on the value of the velocity ratio c/c_g with fixed Kx. It can be seen that with approach of the c/c_g value to unity the m value increases and attains a maximum with $c \simeq c_g$. This indicates a resonance character of the interaction, for the first time experimentally confirmed by measurements [7]. It should only be noted that the resonance observed in this case is broadened in comparison with [7], which is associated with greater U values and accordingly with a greater interval of lengths of the trapped SW [1].

The results presented below from measurement of the m and ν parameters relate to resonance interaction when $c \simeq c_g$. Figure 5 gives the experimental values of the amplitude modulation coefficient m, normalized to the parameter β = U/c, as

a function of the dimensionless distance Kx. The points on the graph in the region $Kx \lesssim 8$ were obtained with $\beta = 0.045$ and 0.057 on the basis of data from experiment II, in the region $Kx > 8$ -- with $\beta = 0.029$ and 0.04 on the basis of the data in experiment I. It can be seen that the modulation is directly proportional to the amplitude (orbital velocity) of the IW and increases with distance. The values $m/\beta \sim 33$ (with $\beta \simeq 0.03$) corresponds to 100% modulation, which is attained with $Kx \sim 16$-18.

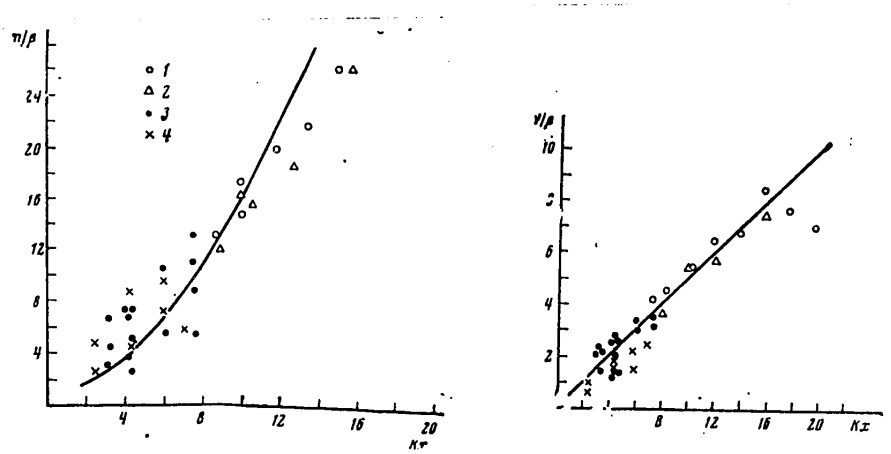

Fig. 5. Dependence of amplitude modulation coefficient on distance ($c/c_g = 1$). 1) $\beta = 0.029$; 2) $\beta = 0.04$ (experiment I); 3) $\beta = 0.045$; 4) $\beta = 0.057$ (experiment II); the curve was computed using data in [7].

Fig. 6. Dependence of frequency modulation coefficient on distance ($c/c_g = 1$). Notations are the same as in Fig. 5.

The dependence of the frequency modulation coefficient normalized to β on Kx is represented in Fig. 6; the same as in Fig. 5, the ν values with $Kx < 8$ were obtained in experiment II, and in the region $Kx > 8$ the data from experiment I are given. It can be seen that ν increases with x linearly, up to lengths $Kx \sim 16$, and, as in the preceding case, is proportional to β. With sufficiently great Kx ($Kx \gtrsim 16$) the ν parameter, as already noted above, begins to decrease.

4. Discussion of results. The authors of [7], in an investigation of the influence of IW on the characteristics of SW, made use of the equations of geometrical optics for slowly changing amplitude and wave number of a quasimonochromatic SW in the field of a variable current created by an IW. On the assumption of smallness of change in SW parameters computations were made of the dependence of the coefficients of modulation of the amplitude a and the wave number k on the parameters β, Kx, c/c_g. For example, the m/β (Kx) curve for a resonance case is shown in Fig. 5. On the basis of an analysis of the corresponding formula for m it is possible to find the characteristic length x_a of development of amplitude modulation:

$$x_a \simeq 2/K\sqrt{\beta}. \qquad (1)$$

which agrees with the evaluation of the SW "blocking length" [1]. It should be noted that there is a good agreement between experiment and computations [7] up to lengths not exceeding x_a (in the experiments $Kx_a \sim 10\text{-}12$). This is understandable since the formulas in [7], in general, describe weak modulation and are incorrect in the stage of slick formation, that is, with $x \geqslant x_a$.

In a study of the spectra of SW it is more convenient to proceed from the spectral form of writing of equations for the interaction of IW and SW. The equations describing the evolution of the complex spectral amplitude a_0 at the carrier frequency $\omega = 2\pi f$ and the spectral amplitudes of the satellites a_n at the frequencies $\omega + n\Omega$, appearing with the presence of IW with the spectral amplitude A, can be written in the following form (compare [4]):

$$da_n/dx = iV_{n,\,n+1}a_{n+1}A^*e^{i\Delta_n x} + iV_{n,\,n-1}a_{n-1}Ae^{-i\Delta_n x}, \quad n = 0, \pm 1, \pm 2, \ldots, \tag{2}$$

here V is a matrix coefficient of nonlinear interaction between IW and SW; Δ_n is wave frequency difference, which under the condition $\Omega \ll \omega$, $K \ll k$ is equal to $\Delta_n = K[(1 - c/c_g) + c_g^{-1}dc_g/dkKn]$. Computations of the interaction coefficient, carried out, in particular, in [2], neglecting the dependence on n for the case of short SW, give the following result

$$VA = \frac{1}{2}k\beta. \tag{3}$$

Neglecting the frequency difference, and also not taking into account the dependence of V on n, it is possible to write a precise solution of system (2). Under the condition $a_n(x = 0) = a_0\delta_{n0}$ we have [4]

$$a_n(x) = i^n a_0(0) J_n(\beta k x). \tag{4}$$

In this case the surface wave $a(x, t) = \sum_n a_n(x) e^{i[\omega(k+nK)t - (k+nK)x]}$

has (with fixed x) a constant amplitude and is modulated in frequency with a modulation coefficient

$$\nu = \frac{1}{2}\beta K x. \tag{5}$$

Allowance for $\Delta(n)$ and V(n) leads to the appearance of amplitude modulation, but if the characteristic length of development of frequency modulation

$$x_* = 1/k\beta \tag{6}$$

is less than x_0, at lengths $x \sim x_\omega \leqslant x_a$ it is possible to expect a good agreement of the ν parameter with expression (5). We note that under the conditions of these experiments the amplitude of the IW is quite great and x_ω on the average is three times less than x_a.* As indicated by Fig. 6, the experimentally measured ν values fall well on the theoretical dependence (5) to $Kx \sim 15$, that is, to lengths of the order x_a.

* On the other hand, in experiment [7], the inverse relationship ($x_a < x_\omega$) is observed; therefore the frequency modulation there was extremely weak and the principal effect was SW modulation in amplitude.

With respect to the spectra of SW, since with $x \sim x_\omega$ the amplitude modulation is small, the appearance of satellites at these distances is associated primarily with frequency modulation. In Fig. 3 the crosses indicate the amplitudes of the satellites, computed in accordance with (4). It can be seen that at distances $x \sim x_\omega$ the spectra of SW in actuality are described well by expression (4); at greater distances, however, there is an increasing deviation from (4) associated with considerable amplitude modulation and also attenuation of SW.

BIBLIOGRAPHY

1. Basovich, A. Ya., "Transformation of Spectrum of Surface Waves Under the Influence of an Internal Wave," IZV. AN SSSR: FIZIKA ATMOSFERY I OKEANA (News of the USSR Academy of Sciences: Physics of the Atmosphere and Ocean), Vol 15, No 6, pp 655-661, 1979.

2. Yermakov, S. A. and Pelinovskiy, Ye. N., "Intensification of Internal Waves by Wind Waves," TEORIYA DIFRAKTSII I RASPROSTRANENIYA VOLN (Theory of Diffraction and Wave Propagation), Vol 2, Moscow, Nauka, pp 257-260, 1977.

3. Yermakov, S. A., Pelinovskaya, Ye. N. and Talipova, T. G., "Influence of Films of Surface-Active Substances on Change of Wind Wave Spectra Under Influence of Internal Waves," IZV. AN SSSR: FIZIKA ATMOSFERY I OKEANA, Vol 16, No 10, pp 1068-1076, 1980.

4. Kadomtsev, B. B. and Karpman, V. I., "Nonlinear Waves," USPEKHI FIZICHESKIKH NAUK (Advances in the Physical Sciences), Vol 103, No 2, pp 103-232, 1971.

5. Phillips, O. M., DINAMIKA VERKHNEGO SLOYA OKEANA (Dynamics of the Upper Layer in the Ocean), Leningrad, Gidrometeoizdat, 1980.

6. Hughes, B. A. and Grant, H. L., "The Effect of Internal Waves on Surface Wind Waves," Pt. 1, GEOPHYS. RES., Vol 83, N C1, pp 449-465, 1978.

7. Lewis, J. E., Lake, B. M. and Ko, D. R. S., "On the Interaction of Internal Waves and Surface Gravity Waves," J. FLUID MECH., Vol 63, No 4, pp 773-800, 1974.

5303
CSO: 1865/149

UDC 551.465.8:7.021.2

MODEL OF CLIMATIC SPECTRUM OF INTERNAL WAVES IN OCEAN

Moscow OKEANOLOGIYA in Russian Vol 22, No 2, Mar-Apr 82 (manuscript received 27 Feb 81) pp 182-185

[Article by A. S. Samodurov, Marine Hydrophysical Institute, Ukrainian Academy of Sciences, Sevastopol']

[Text]

Abstract: On the basis of an analysis of the spectral wave equation in a ray approximation the author has derived expressions for the spatial-temporal energy spectra for internal waves in the ocean.

In connection with the increasing volume of information on internal waves in the ocean and the development of theory it is possible to predict some mean state of the wave field for the open part of the ocean. The principal attainments in this field were made by Garret and Munk, who for the first time proposed a background spectral model in 1972 [3]. A discussion of the further development of the model is given in [4-6]. The essence of the employed semiempirical method is that on the basis of linearized equations describing the phenomenon in the main thermocline and some physical assumptions it is possible to develop an analytical power-law form of spectrum and then with the use of extensive factual material select the values of the free parameters, including the exponents.

Our model is based on an equation for linear internal waves in spectral form and the unique (following from observations) important assumption that the spectral level is poorly dependent on geographic latitude.

The following equation was derived in [1, 2] for describing the evolution of the spectral density of waves in a ray approximation

$$\frac{\partial E}{\partial t} + \frac{\partial \omega}{\partial k_\alpha}\frac{\partial E}{\partial x_\alpha} - \frac{\partial \omega}{\partial x_\alpha}\frac{\partial E}{\partial k_\alpha} = S, \qquad (1)$$

which is a spectral analogue of the equation for energy conservation for a dispersing wave packet. Here $E(k_\alpha, x_\alpha, t)$ is wave energy per unit phase volume; $\omega(k_\alpha, x_\alpha, t)$ is angular frequency; $k_\alpha = (k_1, k_2, k_3)$ is the wave

vector; x_α = (x, y, z) is the radius-vector of a point in a Cartesian rectangular coordinate system; s is the rate of change of energy of a unit phase volume.

We will examine equation (1) for internal waves in an ideal, incompressible, uniformly rotating, stably stratified fluid in the absence of mean flows. In the Boussinesq approximation the dispersion expression has the form

$$\omega^2 = \frac{N^2(z)\,k^2 + f^2 k_3^2}{\varkappa^2}, \quad \varkappa^2 = k^2 + k_3^2, \quad k^2 = k_1^2 + k_2^2. \tag{2}$$

Here N(z) is the Väisälä-Brunt frequency, and f = const is the Coriolis parameter. It is assumed that N(z) changes slightly at distances of the order of the wavelength. We will seek a stationary solution of (1) in the absence of a right-hand side. Taking into account the fact that the dependence of ω and E on coordinates operates through the N(z) function, and using (2), we transform equation (1) to the form

$$\frac{N^2 - f^2}{N}\frac{\partial E}{\partial N} + \frac{\varkappa^2}{k_3}\frac{\partial E}{\partial k_3} = 0. \tag{3}$$

We make a substitution of independent variables

$$N_p = \sqrt{N^2 - f^2}, \quad \varkappa = \sqrt{k^2 + k_3^2}. \tag{4}$$

As a result (3) is transformed to the form

$$N_p\frac{\partial E}{\partial N_p} + \varkappa\frac{\partial E}{\partial \varkappa} = 0. \tag{5}$$

We will assume that the wave field is horizontally isotropic. Then the function E is determined by the following set of parameters:

$$N_p,\ \varkappa,\ k,\ \rho_0, \tag{6}$$

where ρ_0 is the local fluid density. In general, the parameter f should be among the determining parameters. However, in [7], where a study was made of the frequency spectra in the main thermocline, it was established on the basis of data from field measurements that the form of the spectrum in the immediate neighborhood of the equator and far from it is invariable, whereas the level changes insignificantly. This gives basis for excluding f from among the parameters to be determined. It is possible that the entire dependence of the E spectrum on f is contained in N_p. Taking advantage of the fact that the dependence of the sought-for function in (5) on the independent variables has the self-similar form

$$E = E(N_p/\varkappa), \tag{7}$$

from dimensionality considerations it is immediately possible to write the solution of (5)

$$E = Q\frac{N_p^2}{k^3(k^2 + k_3^2)^{1/2}}, \quad Q = c\rho_0, \tag{8}$$

where c is a dimensionless constant.

We will examine the solution of (8) in the region

$$\infty > k \geqslant k_{\min}$$
$$\infty > |k_3| \geqslant n_{\min}. \tag{9}$$

Under oceanic conditions the $2\pi k_{\min}^{-1}$ and $2\pi n_{\min}^{-1}$ values, giving the minimum admissible scales of waves horizontally and vertically, satisfy the condition

$$k_{\min}/n_{\min} \ll 1. \tag{10}$$

Using (8), we determine the form of all the one-dimensional energy spectra.

The spectrum for the vertical wave number E_{k3} is obtained by integration

$$E_{k_3} = 2\pi \int_{k_{\min}}^{\infty} Ek\, dk \tag{11}$$

and has the form

$$E_{k_3} = \frac{2\pi Q N_p^2}{k_3^2}\left(k_{\min}^{-1} - k_3^{-1}\operatorname{arctg}\frac{k_3}{k_{\min}}\right). \tag{12}$$

Taking condition (10) into account, we will neglect the contribution of the second term in parentheses. As a result we obtain

$$E_{k_3} = \frac{2\pi Q}{k_{\min}} N_p^2 k_3^{-2}. \tag{13}$$

The expression for the one-dimensional spectrum for the horizontal wave number, for example, for k_1, has the form

$$E_{k_1} = \int_{-\infty}^{\infty}\int_{n_{\min}}^{\infty} E\, dk_3\, dk_2 \tag{14}$$

or

$$E_{k_1} = 2Q N_p^2 \int_0^{\infty} \frac{\operatorname{arctg}\left(\sqrt{k_1^2 + k_2^2}/n_{\min}\right)}{\left(k_1^2 + k_2^2\right)^2}\, dk_2. \tag{15}$$

For k_1 values greater than $n_{\min}$, E_{k1} is approximated by the expression

$$\frac{\pi^2}{4} Q N_p^2 = k_1^{-3}.$$

In the neighborhood of the point $k_1 = k_{\min}$ the following evaluation is correct

$$\frac{\pi}{2} k_1^{-3} > \frac{2E_{k_1}}{\pi Q N_p^2} > \frac{k_1^{-2}}{n_{\min}}. \tag{16}$$

In order to determine the form of the frequency spectrum in (8) it is necessary to convert from the variables k, k_3 to the variables ω, k_3 or ω, k. Selecting the first, we write

$$2\pi \iint E(k, k_3)\, k\, dk\, dk_3 = 2\pi \iint \frac{E[k(\omega, k_3), k_3]\, k(\omega, k_3)}{|\partial\omega/\partial k|}\, d\omega\, dk_3. \tag{17}$$

The spectral density function $\Phi(\omega, k_3)$ has the form

$$\Phi(\omega, k_3) = 2\pi \frac{E(k, k_3)\, k}{|\partial\omega/\partial k|}. \tag{18}$$

Hence, by integration for k_3 we obtain an expression for the energy frequency spectrum Φ_ω:

$$\Phi_\omega = \pi Q N_p^2 \omega \begin{cases} [k_{\min}^2 \sqrt{(\omega^2 - f^2)(N^2 - \omega^2)}]^{-1}, & \omega_m \geqslant \omega \geqslant f, \\ [n_{\min}^2 (\omega^2 - f^2)^{3/2}]^{-1} \sqrt{N^2 - \omega^2}, & N \geqslant \omega \geqslant \omega_m, \end{cases} \tag{19}$$

where $\omega_m = \omega(k_{min}, n_{min})$. It follows from condition (10) and expression (2) that the frequency ω_m in order of magnitude coincides with f, so that the expression for the low-frequency part of the spectrum (19) is correct only in the immediate neighborhood of the inertial frequency, and with (10) taken into account has the form

$$\frac{\pi Q}{k_{\min}^2} \frac{N\omega}{\sqrt{\omega^2 - f^2}} (1 - f^2/N^2).$$

In the frequency interval $N \gg \omega \gg f$ the spectrum (19) is approximated by the expression

$$\frac{\pi Q}{n_{\min}^2} N^3 \omega^{-2} \left(1 - \frac{f^2}{N^2}\right).$$

If the wave field is vertically symmetrical, the right-hand sides of (14), (19) and the expressions associated with them must be multiplied by 2.

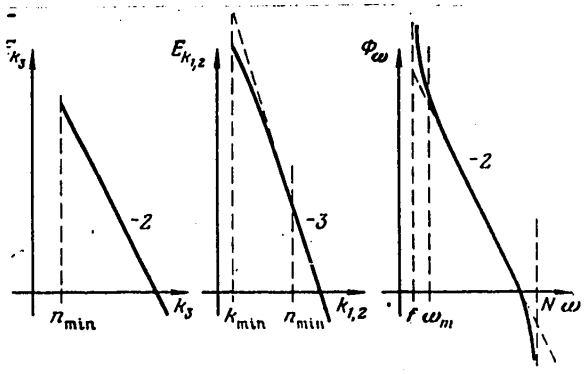

Fig. 1. Theoretical spatial-temporal energy spectra of internal waves. See text for annotations.

The curves of functions of all one-dimensional spectra are schematically represented in the figure at a bilogarithmic scale. In general, the forms of the spectra correspond to the experimental results cited in the summary in [3]. A clarification of the details of similarity and differences requires a more careful comparison with actual data.

The author expresses appreciation to G. I. Barenblatt, Ye. N. Pelinovskiy and G. K. Korotayev for useful discussions.

BIBLIOGRAPHY

1. Korotayev, G. K., "Spectral Density of Energy of Wave Packets," MORSKIYE GIDROFIZICHESKIYE ISSLEDOVANIYA (Marine Hydrophysical Investigations), No 2(77), pp 42-47, 1977.

2. Krasitskiy, V. P., "Theory of Spectral Transformation During Refraction of Wind Waves," IZV. AN SSSR: FIZIKA ATMOSFERY I OKEANA (News of the USSR Academy of Sciences: Physics of the Atmosphere and Ocean), Vol 10, No 1, pp 72-82, 1974.

3. Garret, C. and Munk, W., "Space-Time Scales of Internal Waves," GEOPHYS. FL. DYN., Vol 2, No 4, pp 225-264, 1972.

4. Garret, C. and Munk, W., "Space-Time Scales of Internal Waves: A Progress Report," J. GEOPHYS. RES., Vol 80, No 3, pp 291-297, 1975.

5. Garret, C. and Munk, W., "Internal Waves in the Ocean," ANN. REV. FLUID MECH., Vol 11, pp 339-369, 1979.

6. Gregg, M. C. and Briscoe, M. G., "Internal Waves, Fine Structure, Microstructure and Mixing in the Ocean," REV. GEOPH. SPACE PHYS., Vol 17, No 7, pp 1524-1548, 1979.

7. Wunsch, C. and Webb, S. "The Climatology of Deep Ocean Internal Waves," J. PHYS. OCEANOGR., Vol 9, No 2, pp 235-243, 1979.

5303
CSO: 1865/149

UDC 551.466.31

GRAVITATIONAL-CAPILLARY SOLITONS AT SURFACE OF FLUID

Moscow IZVESTIYA AKADEMII NAUK SSSR: FIZIKA ATMOSFERY I OKEANA in Russian
Vol 18, No 2, Feb 82 (manuscript received 25 Mar 80) pp 202-206

[Article by V. P. Krasitskiy, Institute of Oceanology, USSR Academy of Sciences]

[Text] The one-dimensional Cortewega-De Vries equation (C-DV), for the first time derived for one-dimensional purely gravitational waves at the surface of a fluid, is encountered in many applications [1]. It has a number of precise solutions, one of which is a solitary wave or soliton. Equally common is the two-dimensional C-DV equation [2, 3], taking into account a weak dependence of the wave profile on the coordinate transverse to the direction of its propagation. This equation, known as the Kadomtsev-Petviashvili equation, also allows solutions in the form of solitons [4-6]. Experimental observation of gravitational solitons is difficult, especially under laboratory conditions, since these waves must be sufficiently long in comparison with depth of the fluid. Examples of observation of gravitational two-dimensional solitons at the surface of a fluid under laboratory conditions are evidently lacking. Accordingly, the hope arises of creating two-dimensional gravitational-capillary solitons under laboratory conditions, since their length can be substantially less than the length of purely gravitational solitons. Moreover, as indicated by the text which follows, in the case of an adequately small depth of the fluid (less than 0.5 cm for water) it makes sense to examine specifically only two-dimensional gravitational-capillary solitons because the corresponding one-dimensional solitons are unstable. Although from the general point of view the existence of gravitational-capillary solitons is quite obvious (from an examination of the dispersion expression for linear gravitational-capillary waves), there is no accurate derivation of the corresponding C-DV equation from the initial equations of hydrodynamics. In this communication we give such a derivation for a two-dimensional case, based on the direct use of an asymptotic procedure proposed by Leonov [3] for the case of the general equations of hydrodynamics for a stratified fluid in a gravity field.

We note that the literature describes laboratory observations of two-dimensional solitons forming on the free surface of a thin layer of fluid flowing down along an inclined plane [7]. The formation of these solitons is associated with instability of the flow of the fluid layer onto an inclined plane caused by a predominance of gravity over viscosity, not the joint effect of

gravity and surface tension, leading to gravitational-capillary waves in a fluid layer with a horizontal bottom. Although the equation in [7] for two-dimensional solitons also takes surface tension into account, it does not belong to the type of the two-dimensional C-DV equation [2] and does not undergo transition into the equation derived in this study, with a tendency of the angle of the inclined plane to zero (transition to the case of a horizontal bottom).

We will examine a horizontal unbounded fluid layer of the depth h. If as the length scale we use layer depth h and as the time scale -- the value $T = (h^3/\gamma)^{1/2}$ (γ is the ratio of the surface tension coefficient to fluid density), the dimensionless equations of motion and the boundary conditions can be written in the following form:

$$\varphi_{xx}+\varphi_{yy}+\varphi_{zz}=0, \quad z\leqslant\zeta, \tag{1}$$

$$\zeta_t+\varphi_x\zeta_x+\varphi_y\zeta_y-\varphi_z=0, \quad z=\zeta, \tag{2}$$

$$\varphi_t+\frac{1}{2}\varphi_x^2+\frac{1}{2}\varphi_y^2+\frac{1}{2}\varphi_z^2+\alpha^2\zeta-F(\zeta)=0, \quad z=\zeta, \tag{3}$$

$$\varphi_z=0, \quad z=-1, \tag{4}$$

where

$$F(\zeta)=\frac{\zeta_{xx}+\zeta_{yy}+\zeta_{xx}\zeta_y^2-2\zeta_x\zeta_y\zeta_{xy}+\zeta_{yy}\zeta_x^2}{(1+\zeta_x^2+\zeta_y^2)^{3/2}}. \tag{5}$$

These equations were written in a rectangular coordinate system with the horizontal coordinates x and y and with the vertical coordinate z; the origin of coordinates is situated at the undisturbed fluid surface and the z-axis is directed vertically upward; φ is velocity potential; and $\zeta = \zeta(x, y, t)$ is displacement of the free surface; $\alpha^2 = gh^2/\gamma$ is a dimensionless constant. With $\alpha = 1$, $F = 0$ these equations undergo transition into equations for purely gravitational waves if in such a case $T = (h/g)^{1/2}$ is used as the time scale.

We will examine long waves propagating in the direction of the x-axis with the velocity c and slowly changing in the transverse direction y. Adhering to [3], we introduce the new variables

$$\xi=\varepsilon(x-ct), \quad \eta=\varepsilon^2 y, \quad z=z, \quad \tau=\varepsilon^3 t \tag{6}$$

and we will seek a solution of problem (1)-(5) in the form of asymptotic expansions into the small parameter ε:

$$\varphi=\varepsilon\varphi_1+\varepsilon^3\varphi_2+\varepsilon^5\varphi_3+O(\varepsilon^7),$$
$$\zeta=\varepsilon^2\zeta_1+\varepsilon^4\zeta_2+O(\varepsilon^6), \quad c=c_0+\varepsilon^2 c_1+O(\varepsilon^4). \tag{7}$$

We note that in this case the wave slope in the direction of the x-axis (that is, $\partial\zeta/\partial x$) is proportional to ε^3, whereas the wave slope in the direction of the y-axis (that is, $\partial\zeta/\partial y$) is proportional to ε^4, which corresponds to

a weaker dependence of displacement of the surface from the transverse coordinate y than from the longitudinal coordinate x. The ε parameter must be regarded as an index of the order of magnitude of the corresponding parameters; in the final expressions it is absent.

The equations for the approximations are obtained by substituting (6), (7) into (1)-(5) and equating the terms of an identical order of magnitude. The Laplace equation (1), with the boundary condition at the bottom taken into account (4), gives:

$$\varphi_1=\varphi_1(\xi,\eta,\tau),\quad \varphi_2=-\left(\frac{z^2}{2}+z\right)\varphi_{1\xi\xi}+f_1(\xi,\eta,\tau),$$
$$\varphi_3=\left(\frac{z^4}{24}+\frac{z^3}{6}-\frac{z}{3}\right)\varphi_{1\xi\xi\xi\xi}-\left(\frac{z^2}{2}+z\right)(f_{1\xi\xi}+\varphi_{1\eta\eta})+f_2(\xi,\eta,\tau), \tag{8}$$

where f_1 and f_2 are arbitrary functions. Then from the kinematic and dynamic boundary conditions (2) and (3) we obtain

$$\begin{gathered}c_0\zeta_{1\xi}-\varphi_{1\xi\xi\xi}=0,\\ \zeta_{1\tau}-c_0\zeta_{2\xi}-c_1\zeta_{1\xi}+\zeta_{1\xi}\varphi_{1\xi}+\varphi_{1\xi\xi}\zeta_1+\frac{1}{3}\varphi_{1\xi\xi\xi\xi\xi}+\varphi_{1\eta\eta}+f_{1\xi\xi}=0,\\ c_0\varphi_{1\xi}-\alpha^2\zeta_1=0,\\ \varphi_{1\tau}-c_0f_{1\xi}-c_1\varphi_{1\xi}+\frac{1}{2}\varphi_{1\xi}^2+\alpha^2\zeta_2-\zeta_{1\xi\xi\xi}=0.\end{gathered} \tag{9}$$

It follows from the first and third equations of system (9) that $c_0=\alpha$ (in dimensional variables $c_0=(gh)^{1/2}$ is the phase velocity of linear long waves without allowance for surface tension). Excluding from (9) all the functions other than ζ_1, we obtain

$$\frac{\partial\zeta_1}{\partial\tau}-c_1\frac{\partial\zeta_1}{\partial\xi}+\frac{3}{2}c_0\zeta_1\frac{\partial\zeta_1}{\partial\xi}+\beta\frac{\partial^3\zeta_1}{\partial\xi^3}+\frac{c_0}{2}\frac{\partial^2}{\partial\eta^2}\int\zeta_1\,d\xi=0, \tag{10}$$

where $\beta=(c_0^2/3-1)/(2c_0)$ is the dispersion parameter. In the variables x, y, t for the rise $\zeta=\varepsilon^2\zeta_1$ from equation (10), differentiated for ξ, we have

$$\frac{\partial}{\partial x}\left(\frac{\partial\zeta}{\partial t}+c_0\frac{\partial\zeta}{\partial x}+\frac{3}{2}c_0\zeta\frac{\partial\zeta}{\partial x}+\beta\frac{\partial^3\zeta}{\partial x^3}\right)=-\frac{c_0}{2}\frac{\partial^2\zeta}{\partial y^2}. \tag{11}$$

After replacing the variables

$$\begin{gathered}\zeta\to\operatorname{sign}(\beta)4c_0^{-1}|\beta|^{1/2}\zeta,\\ x\to\operatorname{sign}(\beta)|\beta|^{1/2}x+c_0t,\qquad y\to 6^{-1/2}c_0^{1/2}|\beta|^{1/4}y\end{gathered} \tag{12}$$

equation (11) can be reduced to some "standard" equation which is determined only by the sign on the dispersion parameter β:

$$\frac{\partial}{\partial x}\left(\frac{\partial \zeta}{\partial t}+6\zeta\frac{\partial \zeta}{\partial x}+\frac{\partial^3\zeta}{\partial x^3}\right)=-3\,\mathrm{sign}\,(\beta)\frac{\partial^2\zeta}{\partial y^2}. \tag{13}$$

Equation (11) is also the two-dimensional C-DV equation for the considered case. With an accuracy to the insignificant numerical coefficients equation (13) was for the first time derived in [2] for waves of an arbitrary nature allowing the one-dimensional C-DV equation. We note that the one-dimensional variant of linearized equation (11) corresponds to the following approximation to the precise linear dispersion expression

$$\omega=[k(c_0^2+k^2)\,\mathrm{th}\,(k)]^{1/2}\approx c_0k-\beta k^3 \tag{14}$$

(ω is frequency, k is wave number), from which is obvious the very fact of existence of the C-DV equation for the gravitational-capillary waves. For water the dispersion parameter is positive with $h>h_0=(3\gamma/g)^{1/2}\approx 0.5$ cm; in this case the phase velocity of the linear waves ω/k accordingly decreases with an increase in the wave number (negative dispersion). With $h<h_0$ the dispersion parameter β is negative and in this case the phase velocity increases with an increase in the wave number (positive dispersion). We also note that the C-DV equation for purely gravitational waves can be derived from (11), assuming formally that $c_0=1$, $\beta=1/6$; with this same time scale it is necessary to assume that $T=(h/g)^{1/2}$. The case $\beta=0$ requires allowance for higher-order dispersion.

Kadomtsev and Petviashvili [2] demonstrated that with disruption of rigorous one-dimensionality, described within the framework of equation (13), one-dimensional solitons for the C-DV equation are stable with $\beta>0$ and unstable with $\beta<0$ (also see [5], which gives a precise solution of the stability problem). Thus, with $h<h_0$ the one-dimensional gravitational-capillary solitons are unstable. However, in this case ($\beta<0$) there can be a fundamentally new class of solutions -- stable two-dimensional rational (or algebraic) solitons, the analytical expressions for which can be written explicitly in rational functions.

The series of precise solutions for the two-dimensional C-DV equation in the case $\beta>0$ was obtained in [4, 5]. For this case we will cite a solution of equation (11) of the sloping soliton type

$$\zeta=\zeta_m\,\mathrm{ch}^{-2}\left[\frac{1}{2}\left(\frac{\zeta_m c_0}{2\beta}\right)^{1/2}(x-\varkappa y-Vt)\right], \tag{15}$$

where ζ_m is the maximum of the ζ function; $V=c_0(1+\varkappa^2/2+\zeta_m/2)$ is the velocity of the soliton and $\varkappa$ is an arbitrary real number. It can therefore be seen that the velocity V of the soliton in the case of a fixed amplitude ζ_m is the greater the greater its "slope" $\varkappa$. On the other hand, with a fixed velocity V the amplitude ζ_m decreases with an increase in the slope $\varkappa$.

A precise solution of the two-dimensional C-DV solution describing the instability in the case $\beta<0$ was obtained in [5] and a precise solution in the form of stable two-dimensional rational solitons was derived in [6]. For the

considered case this solution in the form of a rational soliton in dimensional form can be written in the following way:

$$\zeta(x, y, t) = -\zeta_m \frac{(h^2/a^2)\,[h^2/a^2 - (x' + by')^2 + (ay')^2]}{[h^2/a^2 + (x' + by')^2 + (ay')^2]^2}, \tag{16}$$

where

$$\zeta_m = 16(\gamma/g)^{1/4}|\beta|^{1/4}a^2,$$
$$x' = -|\beta|^{-1/4}(x - x_0 - v_x t), \quad v_x = c - 3|\beta|^{1/4}(\gamma/h)^{1/4}(a^2 + b^2),$$
$$y' = 6^{1/4}c_0^{-1/4}|\beta|^{-1/4}(y - y_0 - v_y t), \quad v_y = -6^{1/4}(g\gamma)^{1/4}|\beta|^{1/4}b,$$

a, b, x_0, y_0 are arbitrary real constants (a and b are dimensionless and x_0 and y_0 have the dimensionality of length), v_x and v_y are the velocities of propagation of a soliton along the x- and y-axes, $c = (gh)^{1/2}$ is the phase velocity of long waves without allowance for surface tension, whereas $c_0 = \alpha$ and β are the dimensionless parameters determined above.

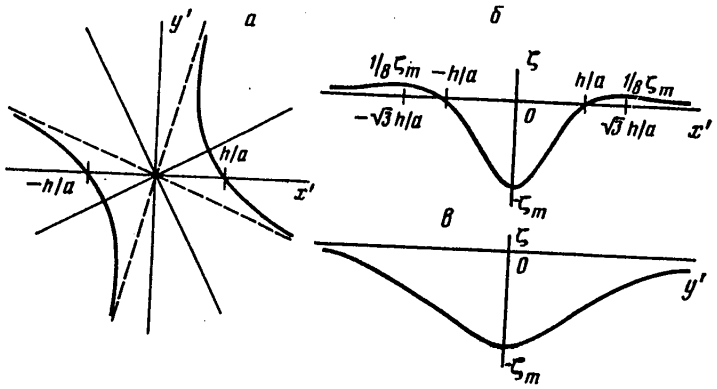

Fig. 1. Some elements of the geometry of a two-dimensional rational soliton (16): a) hyperbola corresponding to the line of a stable fluid level; b) section of soliton along x'-axis; c) section of soliton along y'-axis for position of hyperbola in Fig. a.

In contrast to solution (15), describing "wall-like humps" with infinitely long crests along the straight lines $x - \chi y - Vt = 0$ (and this means, not attenuating along these straight lines), solution (16) corresponds to troughs attenuating with x, $y \to \infty$ as $1/(x^2 + y^2)$. The maximum depth of the trough ζ_m (amplitude of the soliton) also is attained with $x' = y' = 0$. However, beyond the limits of the trough there is some positive rise of the water whose height is almost an order of magnitude less than the depth of the depression ζ_m (see Fig. 1). The zero-level lines for the fluid are hyperbolas (figure, a). The ζ-section along the x'-axis always has positive "humps" of the height $\zeta_m/8$ (figure, b) and the ζ-section along the y'-axis has positive "humps" only in a case when the branches of the hyperbola intersect the y'-axis. Otherwise the section along the y'-axis has no "humps" (figure, c). Thus, the trough is situated between the branches of the hyperbola. The positioning of

the hyperbola on the (x', y') plane is dependent on the relationship of the a and b constants. Using the formulas cited above, the velocity v_s can be represented in the form

$$v_x = c\left(1 - \frac{3}{16}\frac{\zeta_m}{h} - \frac{1}{2}\frac{v_y^2}{c^2}\right),$$

from which it can be seen that the velocity of propagation of such a soliton is less than the velocity of the long waves c, but in actual practice this difference is extremely insignificant. During collision such solitons do not interact with one another [6].

In conclusion we will cite an example of computations by the formulas given above. We will examine the case b = 0. In this case $v_y = 0$ and the axis of the hyperbola is directed along the x'-axis. For water $\gamma = 72.5$ cm^3/c^2; then $h_0 = 0.47$ cm. Assume that h = 0.4 cm and $\zeta_m = 0.2$ cm. Then c = 19.8 cm/c, $v_x = 18$ cm/c, a = 0.316, and the dimension of the trough in the direction of the x'-axis is 2h/a = 2.53 cm. If, all other conditions being equal, $\zeta_m = 0.1$ cm, then $v_x = 18.86$ cm/c, 0.224, 2h/a = 3.6 cm.

BIBLIOGRAPHY

1. Kadomtsev, B. B. and Karpman, V. I., "Nonlinear Waves," UFN (Advances in the Physical Sciences), Vol 103, No 2, pp 193-231, 1971.

2. Kadomtsev, B. B. and Petviashvili, V. I., "Stability of Solitary Waves in Slightly Dispersive Media," DOKLADY AN SSSR (Reports of the USSR Academy of Sciences), Vol 192, No 4, pp 753-756, 1970.

3. Leonov, A. I., "Two-Dimensional Cortewega-De Vries Equations in the Nonlinear Theory of Surface and Internal Waves," DOKLADY AN SSSR, Vol 229, No 4, pp 820-823, 1976.

4. Zakharov, V. Ye. and Shabat, A. B., "Scheme for the Integration of Nonlinear Equations in Mathematical Physics by the Inverse Scattering Problem Method. I," FUNKTSIONAL'NYY ANALIZ I YEGO PRILOZHENIYA (Functional Analysis and Its Applications), Vol 8, No 3, pp 43-53, 1974.

5. Zakharov, V. Ye., "Instability and Nonlinear Oscillations of Solitons," PIS'MA V ZhETF (Letters to the Journal of Experimental and Technical Physics), Vol 22, No 7, pp 364-367, 1975.

6. Manakov, S. V., Zakharov, V. E., Bordag, L. A., Its, A. R. and Matveev, V. B., "Two-Dimensional Solutions of the Kadomtsev-Petviashvili Equation and Their Interactions," PHYS. LETTERS, Vol 63A, No 3, pp 205-206, 1977.

7. Petviashvili, V. I. and Tsvelodub, O. Yu., "Horseshoe-Shaped Solitons on a Downflowing Viscous Fluid Film," DOKLADY AN SSSR, Vol 238, No 6, pp 1321-1323, 1978.

5303
CSO: 1865/160

UDC 551.463.5:536.3:551.466

MEAN COMPONENT OF INFRARED SEA RADIANCE

Moscow IZVESTIYA AKADEMII NAUK SSSR: FIZIKA ATMOSFERY I OKEANA in Russian Vol 18, No 2, Feb 82 (manuscript received 7 Dec 80) pp 206-211

[Article by Yu. I. Belousov and Ye. F. Demidov]

[Text] The mean component of energy brightness of the wave-covered sea surface can be described using a stochastic "facet" model [1-3]. In this case allowance must be made for the concealment from observation of facets whose slopes are steeper than the slope of the sighting line and the circumstance that among the remaining facets only some of them directly reflect in the direction of the observer the radiation from the sky, since in the radiation of the facets shaded relative to the sky or reflecting the radiation of the part of the space below the horizon line the descending sky radiation participates only due to multiple reflection effects. The influence of these factors is evaluated by introducing the so-called shading function [1-4] $S(\varphi, \psi)$, which within the framework of the assumption of a predominant value of single-reflection processes in the formation of sea radiance is independent of the rises and slopes of the facets. The general expression for the mean component of energy brightness of the wave-covered surface $\overline{L}(\varphi, \psi)$ in this case has the form [1]

$$\overline{L}(\varphi, \psi) = S(\varphi, \psi) \iint \left\{ L_{sea}^{0} - [L_{sea}^{0} - L_{sky}(\varphi_{sky}, \psi_{sky})] \rho(\omega) \right\} M \, dz_x dz_y, \qquad (1)$$

where L_{sea}^{0} is the energy brightness of an ideally black body (IBB) at the temperature of the radiating layer of the sea surface T_{sea}; $L_{sky}(\varphi_{sky}, \psi_{sky})$ is the energy brightness of descending sky radiation rereflected by the facet in the direction of the observer, φ, ψ; ρ is the coefficient of reflection of sea water; ω is the reflection angle; $M = \cos \omega \cos \beta \sec \varphi w(z_x, z_y)$ [1,2]. The limits of integration along the slopes of the facets z_x, z_y in (1) are found from the condition $\omega = \pi/2$ [2], expression (3), in particular $-\infty \leqslant z_y \leqslant -z_x \operatorname{tg} \psi - \operatorname{ctg} \varphi \operatorname{cosec} \psi$. The procedure of making (1) more specific involves the introduction of an analytical description of the descending sky radiation $L_{sky}(\varphi_{sky}, \psi_{sky})$.

In a general case the radiation field of the sky is a multidimensional nonstationary random process [5]. However, as indicated by experimental data, in the case of dense low continuous cloud cover (c.c.) the descending radiation can be assumed equal to the radiation of an IBB at air temperature T_{air}:

$L^{c.c.}_{sky}(\varphi_{sky}, \psi_{sky}) = \text{const} \approx L_{air}{}^0$. Then expression (1) can be reduced to the form:

$$L^{c.c.}(\varphi, \psi) = L_{sea}{}^0 K - \Delta L_{sea\text{-}sky} A, \tag{2}$$

where

$$\Delta L_{sea\text{-}sky} = L_{sea}{}^0 - L^{c.c.}_{sky} = L_{sea}{}^0 - L_{air}{}^0 = \Delta L_{sea\text{-}air}{}^0,$$

$$K = S(\varphi, \psi) \quad M\, dz_x dz_y, \quad A = S(\varphi, \psi) \iint \rho(\omega)\, M\, dz_x\, dz_y. \tag{3}$$

The values of the introduced coefficients K and A can be determined by solving (2) for the boundary conditions with $L_{sea}{}^{(0)} = L^{c.c.}_{sky} = L_{air}{}^0$, coinciding with the physically real conditions of equilibrium isothermic radiation of the ocean-atmosphere system with a continuous uniform low cloud cover and $T_{sea} = T_{air}$. In this case $\Delta L^{c.c.}_{sea\text{-}sky} = 0$, $\tilde{L}^{c.c.}(\varphi, \psi) = L_{sea}{}^0$ and from (2), (3) we obtain:

$$K = 1, \quad S(\varphi, \psi) = \left(\iint M\, dz_x\, dz_y \right)^{-1}. \tag{4}$$

Expression (4) for $S(\varphi, \psi)$ coincides with the expressions for unidirectional shading derived in [1-4] on the basis of other assumptions. The final expression for the mean component of energy radiance of the wave-covered sea surface under conditions related to c.c.: $L^{c.c.}_{sky} = \text{const}$, has the form

$$\tilde{L}^{c.c.}(\varphi, \psi) = L_{sea}{}^0 - \Delta L_{sea\text{-}sky} A, \tag{5}$$

where

$$A = \iint \rho(\omega) M\, dz_x dz_y \Big/ \iint M\, dz_x dz_y. \tag{6}$$

Under conditions when there is a smooth decrease in sky radiance from the horizon to the zenith, for example, in the case of a thin cloud cover or in a limiting case of a cloudless clear sky (c.s.), we have

$$L^{c.s.}_{sky}(\varphi_{sky}, \psi_{sky}) = L^{c.s.}_{sky}(\varphi_{sky} = \pi/2) - [L^{c.s.}_{sky}(\varphi_{sky} = \pi/2) - L^{c.s.}_{sky}(\varphi_{sky} = 0)] f(\varphi_{sky}, \psi_{sky}) = L_{air}{}^0 - [L_{air}{}^0 - L_{zen}] f(\varphi_{sky}, \psi_{sky}) = L_{air}{}^0 - \Delta L_{air\text{-}zen} f(\varphi_{sky}, \psi_{sky}), \tag{7}$$

$L_{sky}(\varphi_{sky} = \pi/2)$, $L_{sky}(\varphi_{sky} = 0)$ are the energy radiances of the sky at the horizon and at the zenith respectively; $f(\varphi_{sky}, \psi_{sky})$ is a function describing the angular distribution of descending sky radiation. According to [1, 3, 6], it is assumed that $L_{sky}(\varphi_{sky} = \pi/2) = L_{air}{}^0$, whereas for a cloudless sky $f(\varphi_{sky}, \psi_{sky})$ can be approximated, for example, by formulas from [3, 6]. For c.s. conditions we obtain

$$L^{c.s.}(\varphi, \psi) = L_{sea}{}^0 - \Delta L_{sea\text{-}air}{}^0 A - \Delta L_{air\text{-}zen} Z, \tag{8}$$

where, from the term-by-term integration of (1), with (2), (3) taken into account

$$Z = \iint f(\varphi_{sky}, \psi_{sky})\rho(\omega)M\, dz_x dz_y \Big/ \iint M\, dz\, dz'. \tag{9}$$

In the simplest case of variable cloud cover (v.c.), when sectors of clear sky alternate with sectors of continuous cloud cover, the probability of incidence of radiation of a sector of the clear sky with the coordinates φ_{sky}, ψ_{sky} on a facet equals the "probability of a free sighting line" with (φ_{sky}, k, n) [5] and is dependent on the tenths of cloud cover n and the parameter k related to the size and configuration of the clouds. Under these conditions the mean component of the energy radiance of the wave-covered sea $\bar{L}^{v.c.}(\varphi, \psi)$ will be related to the probability that the facets with the slopes z_x, z_y reflect in the direction of observation either the radiation of the ocean $L^{c.c.}$ or a sector of the clear sky $L^{c.s.}_{sky}$. In (7) representing $L_{sky}(\varphi_{sky}, \psi_{sky})^{obs}$ in the form

$$L^{v.c.}_{sky}(\varphi_{sky}, \psi_{sky}) = L^{c.c.}_{sky}(\varphi_{sky}, \psi_{sky})[1 - c(\varphi_{sky}, k, n)] + L^{c.s.}_{sky}(\varphi_{sky}, \psi_{sky})\, c(\varphi_{sky}, k, n), \tag{10}$$

For the conditions related to v.c. we obtain

$$\bar{L}^{v.c.}(\varphi, \psi) = L^{0}_{sea} - \Delta L_{sea\text{-}air}{}^{0}A - \Delta L^{c.c.}_{air\text{-}zen}\, C_1 - \Delta L^{c.s.}_{air\text{-}zen}\, C_2. \tag{11}$$

where

$$C_1 = \iint [1 - c(\varphi_{sky}, k, n)] f_1(\varphi_{sky}, \psi_{sky})\rho(\omega)\, M\, dz_x\, dz_y \Big/ \iint M\, dz_x\, dz_y, \tag{12}$$

$$C_2 = \iint c(\varphi_{sky}, k, n) f(\varphi_{sky}, \psi_{sky})\rho(\omega)\, M\, dz_x\, dz_y \Big/ \iint M\, dz_x\, dz_y, \tag{13}$$

$f_1(\varphi_{sky}, \psi_{sky})$ is a function describing the angular distribution of radiance in the presence of a cloud cover. In a special simplified case when cloud radiance can be considered uniform and equal to the radiation of an IBB at air temperature (for example, at nighttime when there is low cumulus clouds), the mean component of radiation of the sea surface has the form

$$\bar{L}^{v.c.}(\varphi, \psi) = L^{0}_{sea} - \Delta L_{sea\text{-}air}{}^{0}A - \Delta L^{c.s.}_{air\text{-}zen}\, C_2. \tag{14}$$

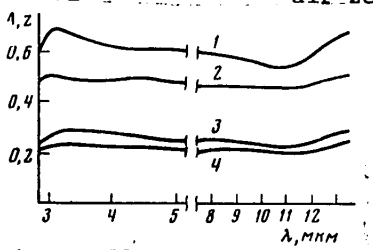

Fig. 1. Spectral dependence of A and Z coefficients with V = 5 m/sec, Φ = 2°, e = 9.5 mbar: 1) A_s; 2) A_p; 3) Z_s; 4) Z_p.

Expression (11) is more general relative to (5) and (8), which follow from it as special cases when n = 1 ($C_1 = C_2 = Z = 0$; c.c.) and when n = 0 ($C_1 = 0$; $C_2 = Z$; c.s.).

Evaluations of the possible contribution to sea radiation from the effects of multiple reflection were made by a comparison of the values of the coefficients A and Z, computed for the conditions of total reflection and total absorption of sky radiation accompanying multiple reflection. Computations show that the change of the A values for most real hydrometeorological situations does not exceed 15%, and, for example, with V = 10 m/sec -- from 6 to 12%.

The slight spectral dependence of the coefficients A, Z, C_1, C_2 is attributable to the averaging in (1) of the coefficients of reflection from the facets in a wide range of slopes (Fig. 1). The general relationship $0 \leqslant C_2 \leqslant Z \leqslant A \leqslant \rho(\omega)$ is retained with all observation conditions, whereas the dependence of the coefficients A, Z, C_1 and C_2 on the angle of elevation of the sighting line $\Phi = \pi/2 - Z$ is characterized by their smooth decrease from maximum values in the case of grazing angles of observation to minimum values in the case of nadir observations for all states of the wave-covered surface. For isotropic nondirectional waves the angle-of-elevation profiles for A, Z, C_1 and C_2 are identical, but for well-developed waves with an increase in the angle between the direction of predominant wave propagation and the direction of observation the change in the characteristics of sea radiation is similar to the decrease in the degree of waves.

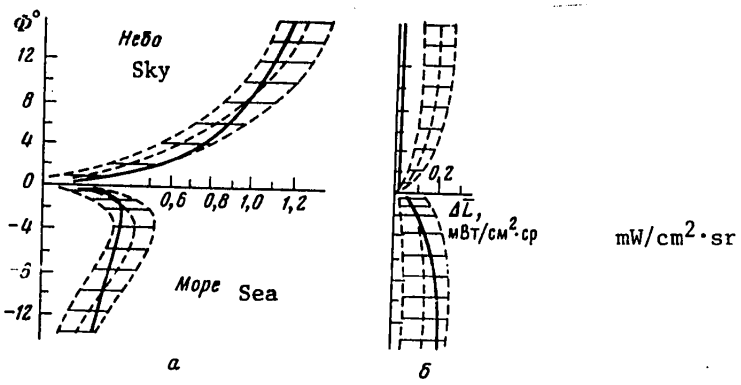

Fig. 2. Comparison of experimental data with results of theoretical computation (dashed curve -- experimental data and 90% confidence interval, solid curves -- theoretical computations): a) c.s., T_{sea} = 290.3 K, T_{air} = 290.8 K, 5 m/sec; b) c.c., T_{sea} = 290.2 K, T_{air} = 290.6 K, 2 m/sec.

A comparison of the characteristics of radiation of the sea surface with the radiation of an IBB at water temperature (L_{sea}^0) shows that the energy radiance of the sea can be less than, equal to or greater than L_{sea}^0, depending on the relationship of the air and water temperatures and the state of the sky. The introduced coefficient A has the physical sense of the equivalent reflection coefficient for the wave-covered surface, taking into account the reflection coefficient of water and the characteristics of the waves. The coefficients Z, C_1 and C_2, similar in physical sense, take into account, additionally, the determined and stochastic nonuniformity of descending sky radiation.

In the forming of sea radiation the role of reflected sky radiation increases with approach of the sighting line to the horizon and a decrease in the wind speed, as is expressed in a decrease in the coefficients A, Z with an increase

In the wind and the regularity of waves. Computations show that with c.c. the relationship of T_{sea} and T_{air} has a greater relative influence on radiation of the wave-covered surface than the change in the wave-forming factors; the difference $T_{sea}-T_{air}$ unambiguously determines the decrease or increase in radiation of the wave-covered sea relative to the radiation of an IBB at water temperature.

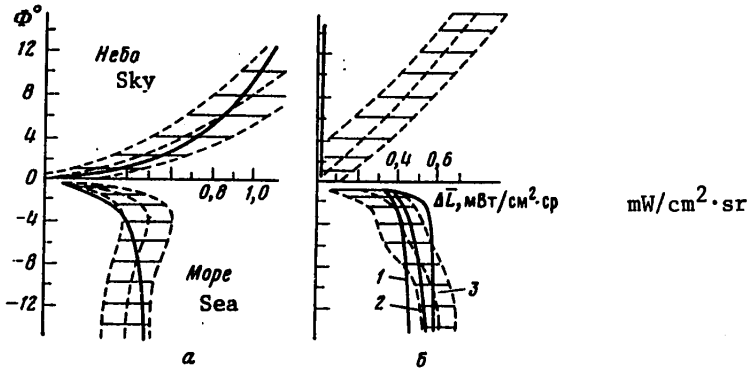

Fig. 3. Same as in Fig. 2: a) c.s., T_{sea} = 291 K, T_{air} = 295 K, 8 m/sec; b) 1) c. c., 2) n = 0.5, 3) c.s., T_{sea} = 284.6 K, T_{air} = 295 K, 8 m/sec.

For the case of a clear sky, when a nonuniform distribution of sky brightness can be described by determined expressions, the sea radiation decreases in comparison with $\overline{L}^{c.c.}$ by the additional value $\Delta L_{air-zen}Z$ as a result of the reflection of radiation closer to the zenith, that is, "colder" parts of the sky.

For meteorological situations with variable cloud cover, when sky radiation can be described by the superpositioning of radiation of sectors of c.c. and c.s., the dependence of $L^{v.c.}$ on hydrological factors is similar to the c.s. situation and the physical sense of the term $\Delta L_{air-zen}C_2$ in (11) can be interpreted as the magnitude of decrease in the energy radiance of the sea as a result of the difference between sky radiation and IBB radiation for an IBB at air temperature.

Computations on the basis of (5), (8), (11) show that with a cloud cover of 5/10 (n = 0.5) the C_2 value is an order of magnitude less than Z and with $n \geqslant 0.3L^{v.c.}$ differs from $L^{c.c.}$ by not more than 15%. In the case of c.c. the degree of polarization of radiation of the wave-covered sea $P^{c.c.}$ is complexly dependent on the relationship of T_{sea} and T_{air}, does not attain unity ($P^{c.c.}_{\lambda} < 1$) and decreases with a decrease in the air-water temperature difference ($P^{c.c.} = 0$ with $T_{sea} = T_{air}$)

$$\overline{P}^{c.c.} = \left| \overline{L}_p^{c.c.} - \overline{L}^{c.c.} \right| / (\overline{L}_p^{c.c.} + \overline{L}_s^{c.c.}) = \left| \Delta L_{sea-air}{}^{0} (A_s - A_p) \right| / \overline{L}^{c.c.}. \quad (15)$$

For a c.s. the degree of polarization of sea radiation increases

$$\overline{P}^{c.s.} = \left| \overline{L}_p^{c.s.} - \overline{L}_s^{c.s.} \right| / (\overline{L}_p^{c.s.} + \overline{L}_s^{c.s.}) = \left| \Delta L_{sea-air}^{0} (A_s - A_p) - \Delta L_{air-zen} (Z_s - Z_p) \right| / \overline{L}^{c.s.}, \quad (16)$$

where the subscripts p and s denote the polarization components for sea surface radiation.

Comparison of the experimental data obtained using a radiometer in the range 7.5-13.5 μ m and the results of computations made using (5), (8) is illustrated in Figures 2-4. Experimental measurements were made of Δ L -- the difference between the mean components of sky energy radiance directly over the sea horizon (used as natural standard radiation of an IBB at air temperature) and the energy radiance of the sea background, including sea radiance $L(\varphi, \psi)$, attenuation along the atmospheric path to the observer $\tau(l)$ and the natural radiation along this path

$$\Delta \overline{L} = [L_{air}^{0} - \overline{L}(\varphi, \psi)] \tau(l). \quad (17)$$

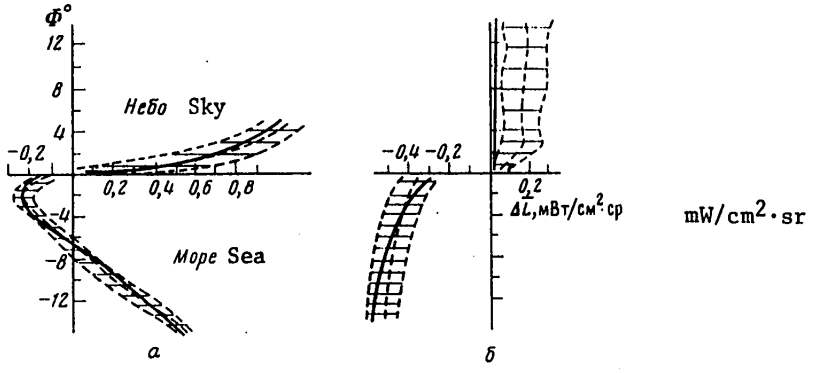

Fig. 4. Same as in Fig. 2: a) c.s., T_{sea} = 284.5 K, T_{air} = 273.9 K, 4 m/sec; b) c.c., T_{sea} = 284.7 K, T_{air} = 279 K, 7 m/sec.

The most precise agreement of the results is observed under c.s. conditions, determined with a high reliability. Under conditions related to c.c., using data from the meteorological services (for example, Fig. 3,b), the agreement is poorer, which can be attributed to the inexact determination of temperature and cloud cover density at nighttime, since the correction to cloud cover (n = 0.5 instead of n = 1 in Fig. 3,b) gives a closer agreement between the experimental and theoretical results.

The errors in the theoretical computations, in addition to failure to take multiple reflection into account, are related to the adopted assumptions and approximations of the law of distribution of the slopes of the facets $w(z_x z_y)$

and $f(\varphi_{sky}, \psi_{sky})$ [1], as well as the assumption of absence of the diffuse component in the indicatrix of sea water reflection, estimates of the characteristic radiation of the atmosphere and its transparency.

From (5), (8) the values of the A and Z coefficients, averaged for the spectral range, have the form

$$A = 1 + \Delta\bar{L}/\Delta L_{sea\text{-}air}{}^{0}\tau(\ell), \quad Z = [\Delta\bar{L} - \Delta L_{sea\text{-}air}{}^{0}(1-A)\tau(\ell)] / \Delta L_{air\text{-}zen}\tau(\ell). \tag{18}$$

The results of comparative computations for curve 4,b give the value A = 0.420, determined from (6), and $A = 0.436^{+0.045}_{-0.030}$ from (18) with $\Phi = 5°$.

In the range of angles 1-4° below the horizon it is common to observe a minimum of sea background radiation [1, 3, 6]. Computations which took into account the attenuation of sea radiation along the atmospheric path and the characteristic radiation along this path indicated that the main influence exerted on the angular position of the brightness minimum $\Delta\bar{L}$ is from variations of parameters in one way or another related to propagation along the atmospheric path: range of meteorological visibility, air humidity, height of the observer above sea level, etc. A change in the wave-forming factors exerts an influence on the angular position of the minimum $\Delta\bar{L}$ to a substantially lesser degree.

BIBLIOGRAPHY

1. Demidov, Ye. F., Bakusov, O. V. and Belousov, Yu. I., "Radiation Brightness With Passage Across the Sea Horizon in the Range 8-13μm," IZV. AN SSSR: FAO (News of the USSR Academy of Sciences: Physics of the Atmosphere and Ocean), Vol 13, No 1, pp 18-24, 1977.

2. Belousov, Yu. I. and Demidov, Ye. F., "Direct Solar Radiation Reflected From the Wave-Covered Sea Surface in the IR Range," IZV. AN SSSR: FAO, Vol 15, No 2, pp 202-214, 1979.

3. Saunders, P. M., "Radiance of Sea and Sky in the Infrared Window 800-1200 cm^{-1}," J. OPT. SOC. AMERICA, Vol 58, No 5, pp 645-652, 1968.

4. Bass, F. G. and Fuks, I. M., RASSEYANIYE VOLN NA STATISTICHESKI NEROVNOY POVERKHNOSTI (Wave Scattering on a Statistically Uneven Surface), Moscow, Nauka, 1977, 424 pages.

5. Niylisk, Kh. Yu., "Cloud Cover Characteristics in Problems of Radiation Energetics in the Earth's Atmosphere," IZV. AN SSSR: FAO, Vol 8, No 3, pp 270-283, 1972.

6. Kasatkina, O. A., "Angular Distribution of Radiation of a Cloudless Sky in the Sector 8-12μm," TRUDY GGO (Transactions of the Main Geophysical Observatory), No 275, pp 92-97, 1972.

5303
CSO: 1865/160

TERRESTRIAL GEOPHYSICS

UDC 550.34

PROSPECTS FOR DEVELOPING NEW METHODS IN SEISMIC PROSPECTING

Moscow VESTNIK AKADEMII NAUK SSSR in Russian No 1, Jan 82 pp 57-64

[Article by M. A. Sadovskiy, academician, and A. V. Nikolayev, doctor of physical and mathematical sciences]

[Text] Seismic prospecting can be said to have been formalized into an independent scientific discipline in the 1930's with the creation of the physical and theoretical principles of methods for investigating stratified media by refracted and reflected waves. These methods were developed considerably in the 1940's-1950's: their exploratory capabilities had increased and their detail, effective depth and reliability were greatly enhanced. The last decade has been notable for new major advances in seismic prospecting. The introduction of nonexplosive pulsed and vibrational sources is affording the possibility for shaping seismic sounding signals with stipulated properties with directional radiation of longitudinal and transverse waves. New methods for the processing of information, developed in the Soviet Union and abroad, are making it possible to construct the three-dimensional (and not plane, as was the case before) velocity fields of seismic waves within the framework of relatively simple determined models.

At the same time, seismic prospecting is faced with new tasks: study of complexly dislocated media, detection of nonstructural deposits of petroleum and gas, direct search for deposits, that is, the prediction of petroleum and gas deposits, ore bodies, etc. on the basis of a combination of parameters of the seismic wave field, and also tasks associated with the problems of seismic regionalization, investigations of the focal zones of strong earthquakes, burial of radioactive matter, etc. Even now it has become clear that the possibilities of traditional methods in many cases are limited and their limits can be clearly seen. Are there further possibilities for the development of seismic prospecting and experimental seismology? As indicated by the history of science, in order to take a considerable step forward in the development of any branch of science there must be a challenge to the main hypotheses of phenomenology; it is necessary to shake a little the foundation on which the structure of a scientific law has been built.

Existing seismic prospecting and seismology methods are based on the concept that rocks are a continuous linear-elastic medium in which seismic waves are identically propagated, regardless of their amplitude, and do not interact

with one another; the medium is passive, it absorbs but does not radiate seismic energy; it is unchanged with time. In addition, it is assumed that the exploratory capabilities of the seismic method have a fundamental limitation associated with the lengths of waves: small inhomogeneities cannot be detected by waves whose length exceeds their size by several times.

This is a strong schematization of the properties of a real medium which in actuality is not continuous, but instead is discrete, lumpy and contains an entire hierarchy of scales of inhomogeneities. It would be natural to regard the real medium as a system of entities which are in different stressed states. In accordance with the probabilistic distribution of stresses by entities, some small number of them already from the very beginning of the imparting of an external force must be in a state close to instability. Therefore, even a slight force from the outside will cause a change in the properties and energy state of the system with time, as is in actuality observed.

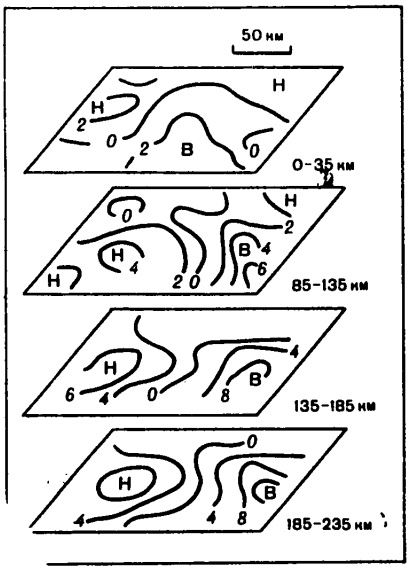

Fig. 1. Velocity section of lithosphere under NORSAR group. The figures represent the velocities of wave propagation in percent, N, B represent regions of reduced and increased velocities.

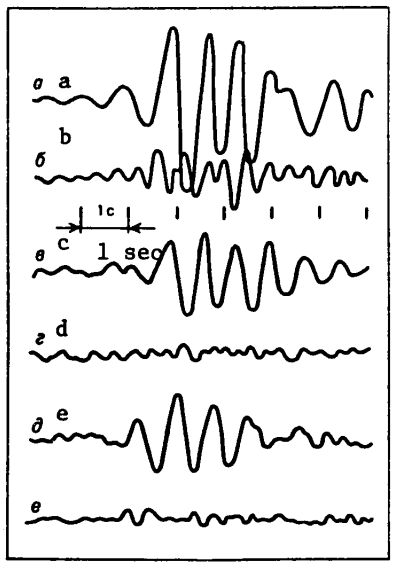

Fig. 2. Records of longitudinal wave from earthquake in one of regions of Japan. a, b) outside petroleum deposit; c, d, e, f -- over deposit; a, c, e -- in frequency band 0.7-2 Hz, b, d, f -- in frequency band 2-5 Hz.

Real rocks have well-expressed nonlinear elastic properties, constantly radiate microseismic oscillations (seismic emission) and experience temporal changes in connection with changes in stressed state caused by geodynamic and geochemical processes. A theoretical investigation of such systems lies beyond

the possibilities of the mechanics of continuous linear-elastic, elastico-plastic and other models of the medium. In order to take into account the probabilistic character of the processes transpiring in the real medium it is necessary to have a new research approach based on the methods of statistical physics and opening the way to study of the temporal development of the processes in the system. The formulation of such a theory is a matter of the future. However, many useful results can also be obtained by ordinary methods, by determining the deviations of the results of experimental observations from those prescribed by linear theory.

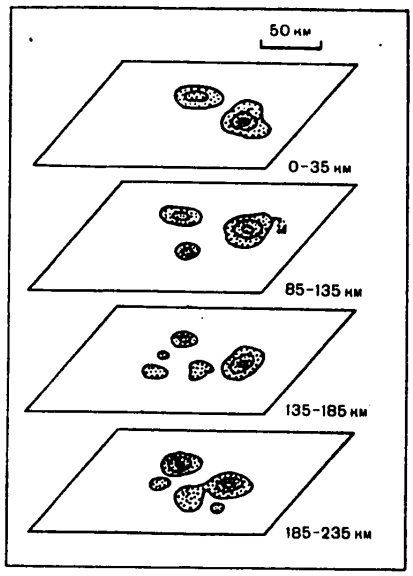

Fig. 3. Section of lithosphere beneath NORSAR group. The contours outline regions of clustering of scatterers; scattered waves from an earthquake in one of regions in Japan were used; frequency 1.8 Hz.

The possibilities of detailed investigations of the medium do not have fundamental limitations with respect to the lengths of the waves and the dimensions of the inhomogeneities. There are methods for extracting information on the fine structure of the medium from the low-frequency wave field. This requires special planning and processing of observations.

Studies in the field of seismology which are being carried out at the Institute of Physics of the Earth imeni O. Yu. Shmidt, USSR Academy of Sciences, are directed to study of the still little-known properties of real media, the possibilities and means for their use for the purposes of seismic prospecting, a comprehension of the structure of deep layers in the earth, development of processes in the focal zones of shots and earthquakes and prediction of these processes. The principal directions in the research include the development of new methods for study of the upper part of the section by remote seismic sources in the variant of probing and seismic holography, detection of spatial anomalies in the statistical structure of microseisms and coda waves (the "tail" parts of the record of seismic signals from pulsed sources), associated with petroleum or gas deposits, study of the nonlinear elastic properties of real media, seismic emission and fluorescence and temporal changes in the velocities of propagation of elastic waves.

In this method the medium under a group of recording instruments is probed by waves transmitted downward from remote sources which reveal at the surface of the anomaly their travel time, their amplitude and shape, making it possible

to ascertain the structure of the medium. The idea of use of remote sources was proposed by Academician G. A. Gamburtsev in the 1940's but was developed no further in exploratory geophysics. Methods for interpreting such observations were developed in seismology with the appearance of areal seismic arrays.

Figure 1 shows a three-dimensional seismic section under the NORSAR group* in southern Norway according to data published by K. Aki (United States), E. Husebi and C. Christofferson (Norway). The section was constructed on the basis of the travel times of waves from earthquakes whose foci were in the entire range of azimuths with epicentral distances of 3000-8000 km.

An analysis of the possibilities of the method for probing by use of remote sources for studying depths up to 10 km indicated that its use requires dense areal registry networks, "shooting" of the investigated volume from different azimuths, and a high signal-to-noise ratio. A special feature of the method is its capability for differentiating primarily horizontal inhomogeneities; it is not sensitive to plane layering. In seismic probing of this type the rays only once pass through the investigated volume, greatly distorting the wave field.

The experimental studies of the Institute of Physics of the Earth in the Pripyatskiy downwarp demonstrated the fundamental possibility of using both shots at a distance of 200-300 km and earthquakes whose foci are at a distance of several thousand km**. Figure 2 gives examples of the record of a remote earthquake registered in the neighborhood of the Vostochno-Pervomayskoye petroleum deposit in Belorussia. The first longitudinal waves transmitted through the deposit were impoverished in the high frequencies. This characteristic, together with others, can be used as an indicator in the direct search for petroleum and gas.

In the future the investigation of large areas by seismic probing can be ensured by a network of stationary vibrational sources which are situated at distances of about 500 km from one another.

Another method for studying the upper part of the medium under a group of seismic stations at which remote sources are employed applies the holographic principle of construction of inhomogeneities scattering seismic waves. Classical holography uses harmonic sources. Pulsed sources can also be used, but this requires the special transformation of the registered signals, their equivalent reduction to a harmonic source. In the image reconstruction method each

---

* The group is a network of 132 vertical short-period seismometers covering an area of 100 x 100 km.

** The first probings of the petroleum deposit by remote earthquakes were carried out in 1959 at the Mayli Su petroleum deposit in the Fergana valley by I. L. Nersesov and A. S. Alekseyev, corresponding member, USSR Academy of Sciences, who obtained encouraging results.

point of the medium is seemingly "interrogated" as to whether it is a scatterer and then, when all the points are interrogated, the results are mapped.

Figure 3 shows a section under the NORSAR seismic group constructed by P. A. Troitskiy on the basis of data from the registry of remote earthquakes for a frequency of 1.8 Hz. An unexpected result was obtained: columnar inhomogeneities passing through the entire lithosphere were detected. The method of seismoholographic investigations was tested and validated by ultrasonic modeling.

At the scale of seismic prospecting investigations in the field of seismic holography are being carried out at the Siberian Department, USSR Academy of Sciences, where convincing results have been obtained.

The seismoholography method can use microseismic oscillations. The idea is that each individual scatterer in the medium reradiates microseismic oscillations. This secondary radiation has an ordered spatial structure. Visualize that an object floats on the water surface. A random water wave is reradiated by this object and "rings" diverge from it. If the object became invisible, from these circles it would be possible to guess that it was present specifically in this place. Thus, microseismic random oscillations can be used on a par with oscillations from pulsed or harmonic sources for studying the structure of real media. Such a method requires observations by means of a dense system of stations over the investigated object, the processing of data from long-term registry. It was developed at the Institute of Physics of the Earth, tested using materials from the NORSAR group. The "section" obtained by this method for a depth of 100 km has a similarity to the "section" obtained using the already described holographic scheme.

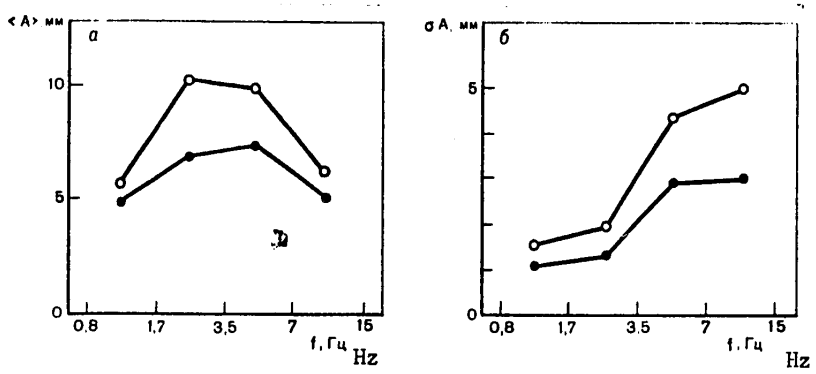

Fig. 4. Mean amplitudes of record of microseismic oscillations < A > -- a and mean fluctuations of amplitudes σ A -- b in four frequency bands. ● -- over deposit, o outside deposit.

The use of microseisms for visualizing inhomogeneities scattering seismic waves requires the processing of long samples of the record -- from several tens of minutes to several hours.

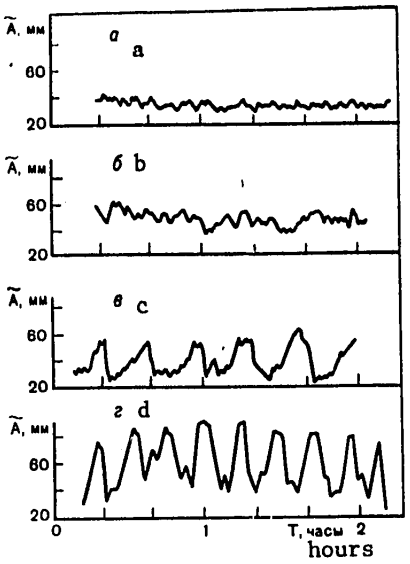

Fig. 5. Samples of envelope of record of microseismic noise Ã. Frequency band 30.9-31 Hz. a, b) records in "quiet" periods, c, d) records after strong earthquakes.

It can be anticipated that in the future seismoholography of microseismic oscillations will be used for reconnaissance observations in inaccessible regions and in those not having permanently operative seismic sources.

The structure of the field of microseismic oscillations is closely related to medium structure. In particular, the impoverishment of microseisms with high frequencies and a decrease in their intensity is observed in regions having increased absorption properties. The studies of the Institute of Physics of the Earth in the neighborhood of the Vostochno-Pervomayskoye petroleum deposit confirmed this. Figure 4 shows the averaged spectra of short-period microseisms and their fluctuations over deposits and outside deposits. The observed differences show that the region of the petroleum deposit is characterized by increased absorption of seismic waves.

Investigations of the structure of microseismic oscillations are being carried out in West Germany and in the United States for the purpose of finding zones of increased heating, sources of thermal energy which have strong absorption properties and thus serve as an outlet for microseisms. But a real medium, it appears, is not only an outlet, but also a source of microseisms: it has seismic emission.

Figure 5 shows records of the envelope of microseismic noise obtained at different times by the seismic observatory "Obninsk."*. The lower records clearly show a periodicity associated with the natural oscillations of the earth after strong earthquakes. The envelope spectrum contains all the main modes of the natural oscillations. The earth's natural oscillations modulate high-frequency microseisms in amplitude, and this means that the reason for microseisms is both external, exogenous sources, and also internal sources -- microfracturing constantly occurring in the medium. A detailed analysis makes it possible to detect fluctuations in the level of microseisms caused by lunar-solar tidal deformations.

The intensity of the emission is related to state of the medium and its fracturing at different scales; accordingly, the character of the emission carries information on these qualities of the medium. During recent years interest in this emission has been tied in to the prospects of using this phenomenon for earthquake prediction. A study is now being made of the possibility of using seismic emission in the exploration for minerals. For the time being

* Rykunov, L. N., Khavroshkin, O. B. and Tsyplakov, V. V., "Temporal Variation of High-Frequency Seismic Noise," IZV. AN SSSR: FIZIKA ZEMLI (News of the USSR Academy of Sciences: Physics of the Earth), No 1, 1979.

It is unclear whether a deposit of petroleum or gas is an adequately intensive source of microseisms and to what extent the anomaly of this quality is expressed relative to the surrounding rocks. There is indirect evidence that ore bodies should be sources of high-frequency microseisms.

Seismic emission makes a significant contribution to the field of high-frequency -- 10's of Hz -- microseismic oscillations. Accordingly, the spatial anomalies of the statistical characteristics of high-frequency microseisms are related not only to peculiarities of structure of the upper part of the medium, but also to the spatial distribution of microseismic activity, which can serve as a direct indication of presence of a deposit.

It has been established that vibrational oscillations stimulate seismic emission. This circumstance makes possible a substantial broadening of the possibility of investigating a new phenomenon and quality of real media -- the capability to "shed" microseismic oscillations, "to clarify themselves."

It has been established by recent investigations of structure of the seismic wave field near vibrational sources carried out by the Institute of Physics of the Earth and the Scientific Research Institute of Radiophysical Measurements that in sedimentary rocks, such as sandy loam and clayey loam, considerable nonlinear effects can appear even when there are insignificant deformations (10^{-5}-10^{-6}). The nonlinearity coefficient

$$K = v(dv/dp)$$

(ρ is density, v is the velocity of a longitudinal wave, p is pressure) determines the degree of the nonlinear effect of an elastic medium. In unconsolidated ground it attains values 10^4 and possibly greater; in consolidated monolithic rocks it is about several tens. The K parameter is an important physical characteristic of the medium and therefore it is extremely desirable to learn how to determine it in the upper part of the section -- to a depth of 5-10 km.

As is well known, heterogeneous triphase media have strong nonlinear properties and therefore there is every basis for assuming that petroleum deposits constitute clear anomalies of the nonlinearity coefficient.

A number of effects are related to nonlinear elasticity: interaction of seismic waves, characteristic distortions of harmonic signals. The interaction is expressed, for example, in the development of low-frequency waves with the interference of high-frequency waves with close frequencies. In this process beats arise at a low frequency, oscillations are detected (are nonlinearly distorted) by the medium, as a result of which a low-frequency wave is formed.

Another effect is distortion of a harmonic wave as it propagates in a nonlinearly elastic medium. The wave in this case acquires the form of a relatively complex periodic oscillation. This means that a part of the seismic energy passes into the higher harmonics. The development of high-frequency oscillations at multiple frequencies can be used for detecting volumes of the medium having anomalously high values of the nonlinearity coefficient. For example,

it is possible to irradiate a definite region of the medium by harmonic seismic oscillations at some fundamental frequency, with the registry in this case of waves of multiple frequencies. Using areal reception systems, it is possible to find the directions to the sources of high-frequency seismic oscillations -- the regions of anomalously strong nonlinear properties. Low-frequency seismic waves will develop in these same regions if they are irradiated by high-frequency harmonic signals close in frequency.

The described effects indicate ways to detect the volumes of the medium having anomalously strong absorbing properties. It is important that nonlinear elasticity is also present in other phenomena -- temporal changes in the velocities of propagation of waves associated with a change in the field of stresses.

Finally, although this problem is beyond the framework of seismology, it is impossible not to note that the model of the medium in the form of a system of rock entities (blocks), in addition to a close approach to a real medium from the point of view of a description of its mechanical properties, has still another highly important quality. The natural assumption that there is an interblock space (slits between entities), filled with gas or fluid, immediately makes it possible to find the reason for numerous electromagnetic processes observable during rock deformation. Seismoelectric effects have long been known, but until now have not been used in detecting and studying the nonlinear properties of rock.

In connection with the problem of earthquake prediction, during the last decade great interest has been shown in temporal changes in the velocities of seismic waves. It has been established that prior to strong earthquakes there is a decrease in the ratio of the velocities of longitudinal and transverse waves in the focal region and both velocities decrease. After an earthquake the velocities are restored.

The change in the velocities of elastic waves is associated with a change in the stressed state of the medium, the concentration of stresses before an earthquake in the focal region. The effects of a change in velocities attain several percent.

In seismically passive regions the change in the stressed state of the medium is associated primarily with tidal deformations. Although these deformations are only 10^{-8}-10^{-9}, the relative change in the velocities of seismic waves in the upper part of the earth's crust in this case attains 10^{-4}. It can be seen that the effect is not great but it can be detected and used in determining the nonlinearity coefficient.

The clearly expressed anomalies of nonlinear effects associated with a deposit of petroleum or gas should give stronger effects, which makes it possible to detect them despite the relatively small (kilometers) spatial dimension.

A study of the temporal changes in the medium requires use of systematic probings using sources having a high operational stability. Systematic probings can be coordinated with a study of the medium using remote sources. Taking into account that source-instrument distances of hundreds and a few

thousand kilometers will be overcome by seismic probings in the very near future, we arrive at the conclusion that it is feasible to combine programs for investigations in the field of seismic prospecting, on the one hand, and in the field of earthquake prediction, on the other, since both tasks can be solved using a single network of stationary seismic sources.

The problems involved in seismic prospecting and earthquake prediction, despite the difference, have much in common: both are directed to detecting a spatial inhomogeneity on the basis of a combination of geophysical fields, both constant and variable with time. The focal region is characterized by relatively rapid temporal changes in elastic properties: in its development an inhomogeneity undergoes a number of phases and then, after a strong earthquake, virtually disappears. A deposit is an almost time-invariable formation, but at the same time reversible changes occur in it, caused by the effect of tidal deformations.

The ideas of the new prospecting methods mentioned above were developed in seismology in connection with the problems of earthquake prediction. Thus, investigations for the prediction of earthquakes seemingly became model experiments relative to the problems encountered in seismic prospecting. Taking into account the internal similarity of the problems, it can be assumed that other methods of earthquake prediction can be used in the reconnaissance and exploration of mineral deposits. In particular, precise geodetic measurements, study of the variation of tilts and deformations caused by lunar-solar tides should also reveal anomalies associated with the deposit.

It should be noted that in the solution of problems in seismic prospecting and earthquake prediction the instrumentation and methods for field observations, the procedures for the interpretation of data obtained by individual methods and multisided interpretation are the same. The bringing together of the efforts of scientists for solution of these problems will considerably enhance the effectiveness of scientific research and design work.

There is still another aspect of the discussed problems. For the time being new seismic prospecting methods are in the earliest stage in their development. Regardless of how effective they may prove to be in the future, they will not completely replace traditional methods because they are oriented on obtaining qualitatively different information on the medium. In addition, a deep study of the physical phenomena associated with wave propagation in real media will make it possible to improve the theory and method for the interpretation of traditional seismic prospecting methods.

Investigations of the new physical principles for seismic prospecting were initiated very recently, but even now it is clear that the seismic prospecting method has great possibilities for development in new directions, which will determine its scientific and technical progress after 5-10 years.

5303 - END -
CSO: 1865/156